Summer 2017

Lignin Contribution to the Global Carbon Pool: Investigating the Abiotic Modification of Lignin by Reactive Oxygen Species

Derek Charles Waggoner
Old Dominion University

LIGNIN CONTRIBUTION TO THE GLOBAL CARBON POOL: INVESTIGATING THE ABIOTIC MODIFICATION OF LIGNIN BY REACTIVE OXYGEN SPECIES

by

Derek Charles Waggoner
B.S. Biochemistry, May 2009, Old Dominion University

A Dissertation Submitted to the Faculty of
Old Dominion University in Partial Fulfillment of the
Requirement for the Degree of

DOCTOR OF PHILOSPHY

CHEMISTRY

OLD DOMINION UNIVERSITY
August 2017

Approved By:

Patrick G. Hatcher (Director)

James W. Lee (Member)

Bala Ramjee (Member)

Sandeep Kumar (Member)

ABSTRACT

LIGNIN CONTRIBUTION TO THE GLOBAL CARBON POOL: INVESTIGATING THE ABIOTIC MODIFICATION OF LIGNIN BY REACTIVE OXYGEN SPECIES

Derek Charles Waggoner
Old Dominion University, 2017
Director: Dr. Patrick G. Hatcher

Evidence suggests that reactive oxygen species (ROS), largely generated through photochemical processes, are important in transforming the chemical composition of the large pool of terrestrially-derived dissolved organic matter (DOM) exported from land to water annually. However, due to the challenges inherent in isolating the effects of individual ROS on DOM composition, the role of ROS in the photochemical alteration of DOM remains poorly characterized. The main focus of the studies within this dissertation aim to more thoroughly characterize the alterations to lignin, used as an analog for terrestrial DOM, resulting from reactions with ROS.

To investigate the possibility that the alteration of lignin, through reactions involving ROS, could lead to the production of compounds not recognized as having terrestrial origin, lignin-derived DOM was prepared from a sample of Atlantic white cedar (*Chamaecyparis thyoides*) and used for a number of studies. Lignin-derived DOM was independently exposed to hydroxyl radical ($^{\bullet}OH$) generated by Fenton reaction, singlet oxygen ($^1O_2$) produced using the photosensitizer Rose Bengal, and superoxide ($O_2^{-\bullet}$) via stable potassium superoxide solution, under controlled laboratory conditions to accentuate how each ROS is responsible for the alteration of lignin. Advanced analytical techniques including high performance liquid chromatography (HPLC), nuclear magnetic resonance (NMR), and Fourier transform ion cyclotron resonance mass

spectrometry (FTICR-MS), were employed to characterize alteration to lignin taking place following various ROS treatments.

Results of these studies have shown distinct differences in the types of new compounds observed from exposure to each ROS as well as ROS reactivity. The alteration of lignin to compounds not typically associated with terrestrial DOM has been demonstrated upon exposure to ROS. It is also suggested that ROS could selectively react with different fractions of lignin like compounds based largely on oxygen content. Additionally, results indicate that partially oxidized lignin could react further with ROS to generate compounds resembling condensed aromatic-like compounds, previously believed to be primarily pyrogenic in origin, as well as alicyclic compounds commonly observed in marine DOM.

This dissertation is dedicated to coffee, you were always there for me

ACKNOWLEDGEMENTS

There are a number of people I would like to acknowledge and thank, each of whom greatly influenced my time at ODU. First and foremost I want to thank my advisor Dr. Patrick Hatcher for giving me the opportunity to join his group all those years ago, and for all the guidance, support, and encouragement that followed. The group writing retreats, outings, sampling trips, and conferences have made my time in graduate school unforgettable, and I truly cannot thank him enough. I would additionally like to thank Dr. Andrew Wozniak and Dr. Rachel Sleighter for the countless discussions, advice, and friendship. Both of you were always there when I needed help with my research, and more importantly when I needed a break from research. I would also like to acknowledge the other members of my committee, Dr. Ramjee, Dr. Lee, and Dr. Kumar, all of whom provided valuable discussions and were instrumental in my success, thank you all.

I have to thank all the members of the Hatcher group. This research group has really turned into my family, and I am fortunate enough to have been a part of it. I wouldn't trade my time with you all for anything. There are a few group members I want to mention in particular. Sarah Gurganus, my "lab wife" and the person who pushed me to succeed and never give up; Isaiah Ruhl, for always being there for me during the frustrating times; Dr. Albert Kamga, for all the conversations and fun memories; Dr. Wassim Obeid, one of the best scientists and friends anyone could ask for…"it is known"; Dr. Amanda Willoughby, for being the kindest, most inspiring person I know, and the person I can always count on; and Dr. Blaine Hartman, for always being honest, providing constant motivation, and general awesomeness. You all have made my time at ODU truly amazing, and I really could not have done this without you.

NOMENCLATURE

AI_{mod}	modified aromaticity index
(Ad/Al)v	carboxylic acid to aldehyde ratio of vanillyl compounds
BC	black carbon
C	carbon
CBB	Chesapeake Bay bridge
CDOM	chromophoric dissolved organic matter
CO_2	carbon dioxide
COO	carboxyl group
CRAM	carboxyl rich alicyclic molecules
DBE	double bond equivalents
DHP	dehydrogenase polymer
DMSO	dimethyl sulfoxide
DOC	dissolved organic carbon
DOM	dissolved organic matter
DS	Dismal Swamp
ESI	electrospray ionization
ESI-FTICR-MS	electrospray ionization Fourier transform ion cyclotron resonance mass spectrometry
Fe	iron
$FeSO_4$	iron sulfate
FFA	furfurly alcohol

FID	free induction decay
FTICR-MS	Fourier transform ion cyclotron resonance mass spectrometry
GB	Great Bridge
GC-MS	gas chromatography mass spectrometry
GC x GC-MS	two dimensional gas chromatography mass spectrometry
H	hydrogen
H_2O_2	hydrogen peroxide
HCl	hydrochloric acid
HMW	high molecular weight
HPLC	high performance liquid chromatography
ICR	ion cyclotron resonance
KMD	Kendrick mass defect
KO_2	potassium superoxide
LC-MS	liquid chromatography-mass spectrometry
LMW	low molecular weight
m/z	mass to charge
MeOH	methanol
N	nitrogen
NaOH	sodium hydroxide
NH_4OH	ammonium hydroxide
NMR	nuclear magnetic resonance
O	oxygen
OH	hydroxyl

$^{\bullet}OH$	hydroxyl radical
$^{1}O_2$	singlet oxygen
$[^{1}O_2]_{ss}$	singlet oxygen steady state concentration
$O_2^{-\bullet}$	superoxide
OM	organic matter
OSC	offshore coastal
P	phosphorus
PDA	photodiode array
POC	particulate organic carbon
POM	particulate organic matter
ppm	parts per million
ROS	reactive oxygen species
RP-HPLC	reverse phase high performance liquid chromatography
S	sulfur
S/N	signal to noise
S/V	syringyl to vanillyl phenol ratio
T	tesla
tDOM	terrestrial dissolved organic matter
TMAH	tetramethylammonium hydroxide
TOF	time of flight
TP	Town Point
UV	ultraviolet

TABLE OF CONTENTS

Page

LIST OF TABLES

LIST OF FIGURES

Figure Page

Figure Page

CHAPTER I

INTRODUCTION

Lignin, a phenolic biopolymer giving structural support to woody and vascular plants, is believed to account for ca. 20% of the organic matter input to the biosphere. Globally it is estimated that there is $3x10^{14}$ kg of lignin present in biomass on Earth (Thevenot et al., 2010), with $1.1x10^{13}$ kg produced annually (Field et al., 1998). Lignin is therefore second only to cellulose in terms of natural abundance and as such, a significant contributor to the global C cycle. There are a variety of suggested degradation pathways for lignin (Stevenson, 1994), however, the fate of lignin in the environment is not well understood. The work presented here aims to show that lignin may contribute significantly to the dissolved organic matter (DOM) pool, as well as play a larger role in the humification of soils than previously believed.

As lignin is exported from terrestrial systems it becomes incorporated into the complex mixture of natural DOM, representing a dynamic pool of carbon on Earth (Hedges, 1992). Rivers worldwide transport an estimated 0.4×10^{15} g of terrestrial dissolved organic carbon (DOC) and approximately 0.2×10^{15} g of particulate organic carbon (POC) annually to the oceans (Bianchi, 2011; Jaffe et al., 2013; Schlesinger and Melack, 1981), roughly equivalent to the annual turnover of marine DOC (Williams and Druffel, 1987). Despite the large contribution, the physical and chemical changes that terrestrial organic matter undergoes during its transport from rivers to the oceans are yet to be fully understood.

This dissertation is formatted based on the journal *Organic Geochemistry*

Unique analytical challenges exist due to the complexity of terrestrial DOM, and it is currently believed to disappear in the oceans as determined by carbon isotopic analysis (Bauer, 2002), lignin-phenol biomarkers (Opsahl and Benner, 1997, 1998) and optical measurements (Blough and Del Vecchio, 2002). To explain the disappearance, previous studies have primarily focused on photochemical mineralization, microbial oxidation, and salinity induced flocculation, as these are believed to be the three major removal processes of terrestrial DOM. Photochemical oxidation occurring in freshwater and marine systems are estimated to mineralize approximately 10-15% of DOM present to CO_2 and CO,(Miller and Zepp, 1995) with biological usage of labile photo-produced components roughly doubling that percentage (Mopper and Kieber, 2002). This suggests that photodegradation is responsible for removing ~20-30% of terrestrial DOM in aquatic systems. Flocculation resulting from mixing along a salinity gradient (0-25) has been shown to cause a DOC decrease of only 2-5%,(Sholkovitz, 1976; Søndergaard et al., 2003) while another study concluded that salinity induced flocculation could not account for the DOC removed based on estuarine transects and end member mixing experiments (Fox, 1983). This in turn leaves a large portion of the terrestrial DOM, thought to be removed, unaccounted for.

This work will focus primarily on photochemical processes to explain how lignin could potentially be altered to forms no longer recognizable as terrestrial organic matter. Lignin phenols and other light absorbing, chromophoric components of terrestrial DOM (CDOM), account for a substantial portion of the total DOM (up to 50%), and are highly susceptible to photodegradation, believed to be the major process impacting CDOM (Guo et al., 2007). For example, terrestrial CDOM subjected to solar radiation has been shown to preferentially lose ^{13}C depleted compounds over time, thereby shifting the isotopic signature closer to that of oceanic DOM (Lalonde et al., 2014). Photoreactions are also believed to be responsible for an observed decrease in the average

molecular weight of DOM during the photobleaching process, where a portion of the DOC is mineralized to CO_2 and other small molecules. The remaining non-mineralized components of terrestrial DOM have optical properties similar to those of aquatic derived DOM and are therefore indistinguishable using current optical analysis techniques (Blough and Del Vecchio, 2002; Helms et al., 2008; Spencer et al., 2009).

Lignin phenols, the commonly used biomarkers for terrestrial DOM, have additionally been shown to be removed or degraded following solar irradiation. The composition of lignin can provide insight into the origin of DOM and can be broadly grouped into low molecular weight (LMW) (<1,000 Dalton) and high molecular weight (HMW) (>1,000 Dalton) fractions. In riverine systems the ratio of vanillic acid to vanillin (Ad/Al)v are not substantially different between the LMW (~10% of dissolved lignin) and HMW(~90% of dissolved lignin) fractions. Following photo irradiation, the (Ad/Al)v of the LMW fraction (~79% of dissolved lignin) is significantly increased, indicating a high degree of oxidation has occurred, whereas the HMW fraction(~21% of dissolved lignin) experiences a decrease in the (Ad/Al)v when compared to the starting DOM. Dissolved lignin from the open ocean has been shown to be resistant to further photo degradation, with no appreciable changes to (Ad/Al)v or syringyl to vanillyl phenols (S/V). The high (Ad/Al)v and low S/V of open ocean DOM when compared to riverine samples would indicate that lignin experiences oxidative degradation during export from riverine systems to the open ocean (Opsahl and Benner, 1998). Based on photo irradiation of riverine samples, the majority of dissolved lignin transported to the open ocean has been altered from HMW fraction to a LMW fraction that is not able to be isolated using ultrafiltration, likely resulting in an underestimate of terrestrial DOM present in the open oceans (Opsahl and Benner, 1998). This suggests that the oceanic DOM could have a much larger contribution from terrestrial DOM than previously thought. Calculations of

global refractory, non-labile, pools of terrestrial DOM entering the oceans annually (0.034 to 0.128 x 10^{15} g C yr^{-1}) (Lalonde et al., 2014) are roughly equivalent to the annual turnover of DOC (0.1 x 10^{15} g C yr^{-1}) in the oceans (Williams and Druffel, 1987).

Motivation for this study partially originated with work by Chen et al. (2014) showing that DOM from the Great Dismal Swamp, an ombrotrophic blackwater swamp exporting terrestrial DOM to the Chesapeake Bay and to the North Atlantic Ocean, when subjected to photochemical degradation for extended periods of time (30-60 d) was substantially chemically transformed. A portion of the DOM was altered to an organic material that precipitated (photoflocculated), a similar phenomenon observed previously by others (Helms et al., 2013; von Wachenfeldt et al., 2008). This material was subjected to negative ion electrospray ionization coupled to Fourier transform ion cyclotron resonance mass spectrometry (ESI-FTICR-MS). The resulting molecular formulas for this photoflocculated material indicate that a significant proportion was composed of condensed aromatic molecules, not present in the initial DOM, referred to as photoBC as they resembled black carbon like molecules. Moreover, the condensed aromatic molecules formed were gradually consumed with increasing irradiation, perhaps as a result of containing photo-reactive chromophores that were further decomposed. The remainder of the photoflocculated material was comprised of formulas that were aliphatic in nature and resemble molecules referred to by Hertkorn et al. (2006) as carboxyl-rich alicyclic molecules (CRAM). The newly produced molecules were not initially present in the DOM prior to photoirradiation suggesting that the photoBC and "photoCRAM" molecules were generated by photodegradation. While the CRAM-like molecules partly precipitated to contribute to the particulate organic matter (POM), a large fraction remained soluble to contribute substantially to the DOM, becoming the dominant components of DOM at increased photoirradiation times. This is consistent with recent studies on oceanic DOM showing

that CRAM-like molecules are ubiquitous in the oceans as well as estuarine systems (Hertkorn et al., 2006; Lam et al., 2007; Sleighter and Hatcher, 2008; Stubbins et al., 2010). The way in which photodegradation of DOM resulted in the formation of these newly observed molecules, as well as what compounds present within the DOM were modified to form them; however, was not determined.

A number of studies have implied that photodegradation of organic matter occurs mainly through the action of reactive oxygen species (ROS) such as hydroxyl radical ($^{\bullet}OH$), singlet oxygen ($^1O_2$), superoxide ($O_2^{-\bullet}$), and photoactivated DOM complexes, often assisted by Fe that acts as an electron shuttler (Kopáček et al., 2006; Page et al., 2013; Porcal et al., 2013). One of the goals of this work is therefore to determine the contribution and types of modification each ROS might be responsible for during the photodegradation of DOM in sunlit surface waters.

While not well characterized in complex mixtures such as DOM, each ROS may exhibit different reactivity with DOM, or interact with different classes of compounds within DOM. Singlet oxygen, for example, acting as an electrophile, can undergo cycloaddition with dienes, and olefins abundantly present in DOM to form cyclic peroxides (Kearns, 1971). Non-cyclic allylic hydroperoxides can form upon $^1O_2$ reaction with olefins, as well as carbonyl containing compounds following olefin cleavage (Kearns, 1971). Hydroxyl radicals primarily react with DOM through addition to olefins or aromatic compounds, H abstraction, and electron transfer reactions (Walling, 1975; Wenk et al., 2011). Direct addition of $^{\bullet}OH$ has been shown to result in both hydroxylation, and cleavage of side chain groups from compounds, with low molecular weight acids frequently observed following reaction of DOM with $^{\bullet}OH$ (Goldstone et al., 2002; Walling, 1975). Electron transfer reactions associated with $^{\bullet}OH$, while rare, are believed to yield organic radical cation species, which can then undergo dimerization reactions to generate new

products (Walling, 1975). Superoxide, through nucleophilic substitution reactions, is capable of producing carboxylic acid anions from esters, as well as dicarboxylic acids from unsaturated cyclic compounds following ring cleavage (Lee-Ruff et al., 1976; Sawyer and Valentine, 1981). One electron reduction of organic compounds is commonly observed with $O_2^{-\bullet}$, and reactions with catechol like compounds, frequently present in DOM, result in radical anions that can undergo ring cleavage and polymerization (Lee-Ruff et al., 1976; Sawyer and Valentine, 1981).

In an effort to determine a potential pathway of photodegradation leading to the formation of new compounds, common degradation pathways for lignin were used as models. It is well known that lignin can be degraded by microorganisms (fungi and bacteria) through the action of oxidative enzymes that involve singlet oxygen, hydrogen peroxide and/or associated hydroxyl radicals (Crawford, 1981; Higuchi, 2004). It is suggested then, that oxidative degradation occurs by microbial processes, chemical oxidation reactions, and low-temperature condensation reactions. For example, certain fungi excrete a variety of oxidative enzymes (e.g., peroxidases) that act to generate OH radicals whose main purpose is to oxidize the lignin in wood, resulting in degradation products and cellulosic products that are more readily available for their metabolism. It is also known that bacteria can attack lignin aromatic structures by first inserting an oxygen and then rupture the aromatic ring of the resulting catechol-like structures to produce muconic acid-like structures that are conjugated di-unsaturated aliphatic carboxylic acids (Crawford, 1981). While microbial-based processes are largely believed to result in the complete mineralization of lignin, I hypothesize that it may be possible for a portion of lignin to be modified to a different endpoint when degraded via a photodegradation pathway.

The aim of the work presented here is therefore to further our understanding of how the reaction of lignin with ROS results in potential alteration, rather than mineralization, as it is

transported from terrestrial to aqueous environments. Chapter II begins to address this by using the whole alkaline extract of brown-rot degraded wood from the Dismal Swamp, and subjecting it to hydroxyl radical degradation by treatment with hydrogen peroxide in the presence of $FeSO_4$ (Fenton reaction). The products were then taken up and examined by ESI-FTICR-MS along with nuclear magnetic resonance (NMR). The van Krevelen plots for the wood extract before, and after hydroxyl radical treatment showed that hydroxyl radical greatly changed the distribution of formulas, resulting in the production of many new peaks emerging in the mass spectrum, including potential alicyclic and condensed aromatic-like formulas. Chapter IV further investigates the alteration of lignin by hydroxyl radical by separating a lignin extract according to its physiochemical properties prior to degradation using high performance liquid chromatography (HPLC), in an attempt to ascertain the origin of new formulas of interest generated upon exposure to hydroxyl radical. In order to get a more complete picture of how ROS are able to alter lignin, superoxide as well as singlet oxygen were also investigated.

CHAPTER II

FORMATION OF BLACK CARBON-LIKE AND ALICYCLIC ALIPHATIC COMPOUNDS BY HYDROXYL RADICAL INITIATED DEGRADATION OF LIGNIN

PREFACE

The content of this chapter was published in 2015 in Organic Geochemistry, and below is the full citation. See Appendix A for the copyright permission.

Waggoner, D.C., Chen, H., Willoughby, A.S. and Hatcher, P.G. (2015) Formation of black carbon-like and alicyclic aliphatic compounds by hydroxyl radical initiated degradation of lignin. *Organic Geochemistry.* **82**, 69-76.

1. INTRODUCTION

Lignin, a phenolic polymer, accounts for ca. 20% of the organic matter (OM) input to soil. It is estimated that it comprises 20-30 g kg^{-1} of woody and vascular plant material, for a global equivalent on the order of 3 x 10^{14} kg of lignin (Thevenot et al., 2010). On an annual basis 1.1 x 10^{13} kg of lignin is produced globally (Field et al., 1998), representing a substantial input to the global carbon cycle. The potential significance lignin has in the formation of soil organic matter and carbon cycling has resulted in a growing interest in determining the degradation pathways and ultimately the fate of lignin in the environment, especially since lignin is implicated as a major contributor to some models of humification in soil (Stevenson, 1994).

Compared with many plant biopolymers, lignin is substantially more resistant to microbial degradation; however, certain microorganisms are capable of degrading it. Various white rot fungi

are able to cleave lignin aliphatic side chains, as well as the aromatic rings during enzymatic degradation (Higuchi, 2004). Evidence suggests that the microbial degradation of lignin occurs by a series of radical intermediates generated by fungal enzymes. Microbial degradation is thought to completely mineralize lignin to small molecules which are able to be used as food sources for various organisms, and that lignin does not contribute significantly to soil humic material (Crawford, 1981).

In aquatic systems, lignin present in dissolved OM (DOM) is susceptible to photodegradation, either directly by UV irradiation or indirectly through reaction with hydroxyl radicals (Goldstone et al., 2002; Pullin et al., 2004; Stubbins et al., 2010). Previously believed to require sunlight for their generation, there is growing evidence that hydroxyl radicals can be produced in a variety of systems in the absence of sunlight (Aeschbacher et al., 2009; Maurer et al., 2010; Page et al., 2011). Humic substances, ubiquitously present in soils, peats, and aqueous environments, have been shown to generate hydroxyl radical species through reactions involving oxygen and redox-active hydroquinone-type compounds (Maurer et al., 2010). In addition, the Fe^{2+} naturally present in sediments, and subsequently water systems, can undergo oxidation in the presence of O_2 to generate hydroxyl radicals through Fenton chemistry (Vermilyea and Voelker, 2009; Walling, 1975). Hydroxyl radicals generated through any of these processes have been shown to rapidly react with DOM to produce low molecular weight acids, or mineralize completely to CO_2 along with oxidized organic compounds (Heitmann et al., 2007; Page et al., 2013). Because lignin has the potential to account for a significant portion of DOM and terrestrial humic material, it is important to fully understand how hydroxyl radicals may degrade lignin and what the end result of those degradation products may be.

Studies interested in the fate of lignin in sediments, rivers, and oceans typically monitor the amounts of lignin phenol biomarkers present, as an indicator of lignin's contribution to a sample (Opsahl and Benner, 1997; Spencer et al., 2009). As lignin is exported from terrestrial to riverine systems and eventually the open ocean, lignin phenols undergo substantial modification, believed mainly to be oxidative degradation, and can therefore no longer be recognized as having a lignin origin (Opsahl and Benner, 1998). Once the biomarkers used to monitor lignin have been degraded, it is substantially more difficult for indicator methods to track further alterations to lignin's structure, therefore the fate of degraded lignin products in both soil and aqueous systems is not well known.

A recent study by Chen et al. (2014) attempted to better understand the role photodegradation plays in aquatic systems by photoirradiating a DOM sample, primarily composed of lignin, for up to 60 days and investigating the molecular level alterations taking place using Fourier transform ion cyclotron resonance MS (FTICR-MS). Chen et al. (2014) showed the formation of both alicyclic/aliphatic and condensed aromatic compounds; these were not present in the initial DOM sample. The presence of such compounds in natural samples has previously been attributed to biological or anthropogenic activity, and therefore the formation of these compounds in an abiotic system is a significant new finding.

In the study by Chen et al. (2014), it is apparent that hydroxyl radicals generated during photoirradiation are responsible for part of the alterations to the DOM observed. Furthermore, as the DOM sample used by Chen et al. had a strong contribution from lignin, the condensed aromatic formulas generated as a result of photoirradiation could be originating from the aromatic components associated with dissolved lignin. To investigate if lignin subjected to non-

photochemical hydroxyl radicals can produce a similar suite of products as observed by Chen et al. (2014), we subjected a lignin-rich extract of brown rotted wood to hydroxyl radicals generated using Fenton chemistry in the absence of sunlight. We employed both proton nuclear magnetic resonance spectroscopy (^{1}H NMR) and ultrahigh resolution mass spectrometry (MS) to characterize the bulk and molecular level changes to lignin following exposure to hydroxyl radicals.

2. MATERIALS AND METHODS

Lignin from the Great Dismal Swamp in Virginia was isolated from a wood sample, Atlantic white cedar (*Chamaecyparis thyoides*), which had been shown to have been degraded by brown rot fungi, which removes cellulose (Liu et al., 2011). The extraction was carried out by grinding the sample to a powder before stirring into 0.01 M NaOH for 24 hours. The resulting solution was then filtered through a 0.7µm glass fiber filter to remove any undissolved species. The extract was adjusted to pH 3 using 1.0 M HCl and subjected to a Fenton reaction, which generates hydroxyl radicals in solution via oxidation of Fe^{2+} by H_2O_2. To perform the experiments, 18 mL of pH adjusted lignin extract was transferred to 30 mL vials, to which varying amounts (0.1-4.0mg) of $FeSO_4$ heptahydrate was added (1-40 ppm Fe^{2+} final concentration). To initiate the Fenton reaction 2 mL of 30% H_2O_2 (3.25 M final concentration) was added to each vial, at which point a black precipitate was produced (in the high iron concentration samples), and was removed by filtration. The particles generated were then redissolved using NH_4OH (pH = 9) and diluted 2-fold with LC-MS grade MeOH before instrumental analysis. Inorganic salts that interfere with instrumental analysis were removed from the filtrate (i.e. DOM) using cation exchange resin. Both the flocculated material (black particles that were redissolved in the NH_4OH) and the DOM

following the Fenton reaction were subjected to MS using a Bruker 12 T FTICR-MS instrument, operated in the negative electrospray ionization (ESI) mode, as described by Sleighter and Hatcher (2011). Spectral details were compared to those obtained for base-extracted lignin (i.e., not reacted with hydroxyl radicals). Peaks were assigned unique molecular formulas using a MATLAB script written in house at Old Dominion University according to previously published criteria (Stubbins et al., 2010). ^{1}H NMR spectra were obtained for the flocculated material, DOM, and initial lignin in H_2O/D_2O (90:10), using a Bruker Biospin Avance III 400 MHz NMR equipped with a broadband inverse solution state probe. All samples were analyzed directly using an optimized version of the WATERGATE pulse sequence of Lam and Simpson (2008).

3. RESULTS AND DISCUSSION

Fig. 1 is a van Krevelen plot showing the molecular details of the CHO formulas found in the initial base-extracted wood, and both the dissolved and precipitated material following exposure to hydroxyl radicals. The corresponding NMR spectra for each sample are also displayed alongside for comparison. The initial extract shows NMR characteristics typically observed for lignin (Ralph et al., 1999), attesting to the fact that brown rot fungi minimally alter lignin during wood degradation. The van Krevelen plot of elemental formulas for the initial extract (Fig. 1a) displays formulas that plot in the region typically associated with lignin (H/C= 0.6-1.7, O/C= 0.1-0.6) (Hockaday et al., 2009; Sleighter and Hatcher, 2008). Following the Fenton reaction, we observe major transformations in the molecular composition shown by substantial alteration of the OM detected in the ^{1}H NMR spectra (Fig. 1f-g) and the creation of a significant number (50%) of new formulas (1646/3289) which fall into several notable regions of the van Krevelen plot (Fig. 1d). A number of newly created formulas plot in the aliphatic region, having a molar H/C ratio

>1.5 (Hockaday et al., 2009); however, several formulas in this region were also present in the initial extracted wood, suggesting that not all compounds in this region are present due to hydroxyl radical oxidation, or that the initial brown rot degradation was responsible for the initial formulas in this region.

Most surprising are the compounds that plot in the region commonly associated with condensed aromatic structures, having modified aromaticity index (AI) values greater than 0.67 (Koch and Dittmar, 2006), which are often considered to be like those of black carbon (BC). The use of AI is suggested to provide a more conservative estimate of condensed aromatic content when compared to double bound equivalents to carbon ratio (DBE/C) based assignments, as AI takes into consideration the unsaturations of heteroatoms present. Lastly, there was an abundance of formulas that emerged at higher O/C but had the same H/C as aromatic components of lignin in the sample; these likely represent oxidized lignin. The results generated in this study are in agreement with those observed in the photodegradation study by Chen et al. (2014), where 42% of the aliphatic formulas and 25% of the aromatic formulas identified match exactly the formulas produced following hydroxyl radical degradation of lignin. The large number of formulas consistent between studies suggests that similar processes are occurring in both the photoirradiation experiment and hydroxyl radical degradation by Fenton chemistry. Chen et al. (2014) also showed that the new formulas created upon photochemical degradation were similar to formulas obtained from extracts of natural samples related to the DOM used in lab irradiations, suggesting that there was a good correspondence between lab simulations and natural samples.

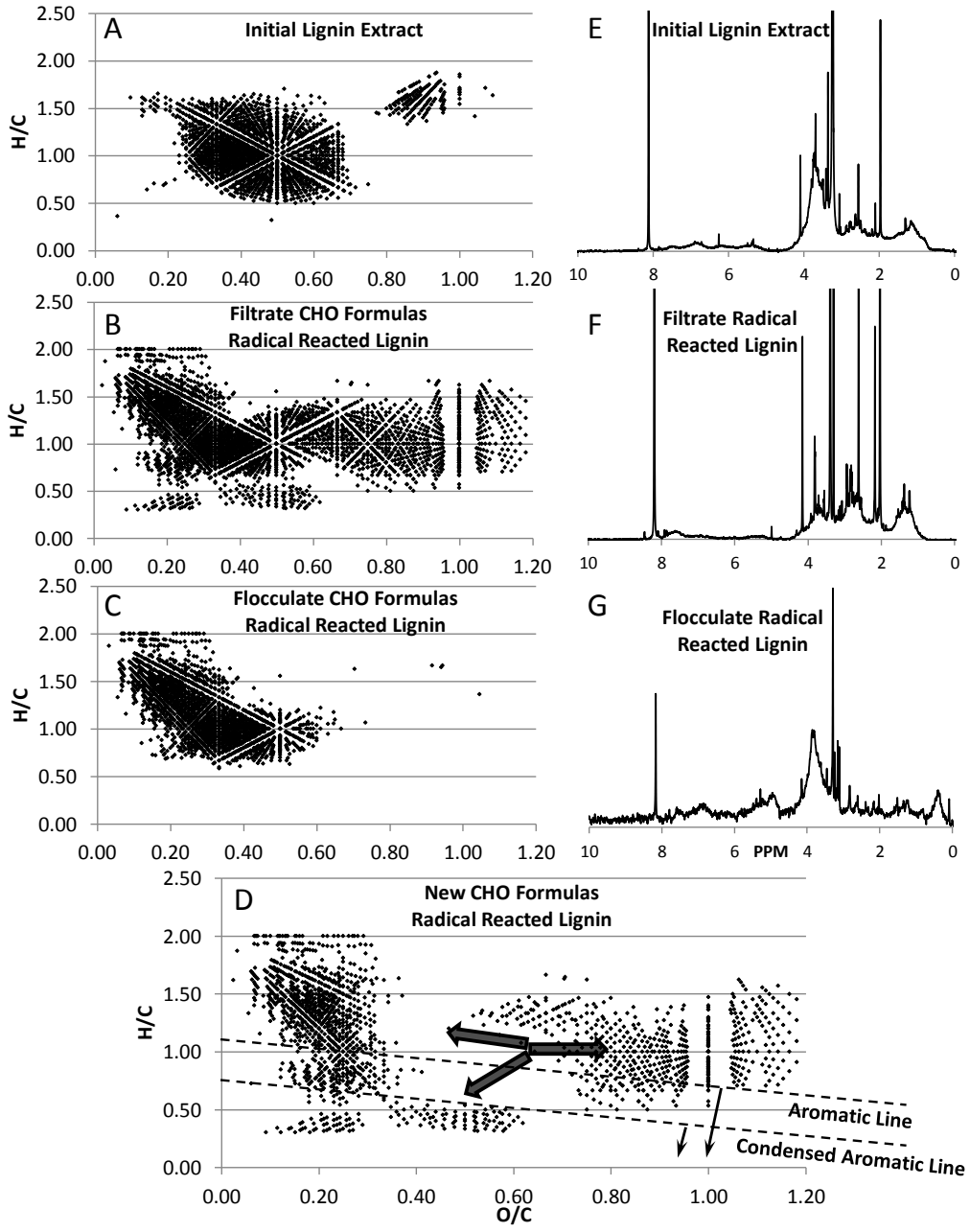

Fig. 1. Van Krevelen plots of CHO formulas from FTICR mass spectra of lignin extracted from Dismal Swamp wood (a-d), alongside the corresponding ^{1}H NMR spectra (e-g). From top to bottom: A), the initial base extract of lignin; B), hydroxyl radical reacted filtrate; C), hydroxyl radical reacted flocculate; and D), a plot of the newly formed CHO formulas. Arrows on the newly

formed formulas plot indicate the shifts observed vs. the initial lignin extract along with dashed lines indicating the aromatic (AI>0.5) and condensed aromatic (AI>0.67) cut-offs.

Higuchi (2004) , in an extensive review, summarized the well known observation that lignin oxidation by enzymatic hydroxyl radicals involves ring hydroxylation and ring opening to produce unsaturated aliphatic and hydroxylated carboxylic acids (*cis,cis*-muconic acids) and hydroxylated muconic acids (Higuchi, 1990; Higuchi, 1993; Umezawa and Higuchi, 1987; Umezawa et al., 1983). Fungi, mainly the white rot type, accomplish this by promoting hydroxyl radical decomposition of the lignin to access the sugars in wood. We propose that a similar set of reactions take place in our experiments and that some of the major alterations observed, namely the trend towards increasing O/C, are consistent with oxidative ring opening to unsaturated aliphatic and hydroxylated carboxylic acids as shown in Fig. 2. The ^{1}H NMR spectra in Fig. 1e-g are consistent with this suggestion as a significant reduction in aromaticity (6.8-7.8 ppm) was observed from the initial lignin base-extract to the dissolved phase following hydroxyl radical treatment. The shift in molecular formulas in the van Krevelen diagram to higher O/C (Fig. 1d) is also consistent with unsaturated aliphatic and hydroxylated carboxylic acid formation described in several studies (Higuchi, 2004; Leonowicz et al., 2001; Stenson et al., 2003).

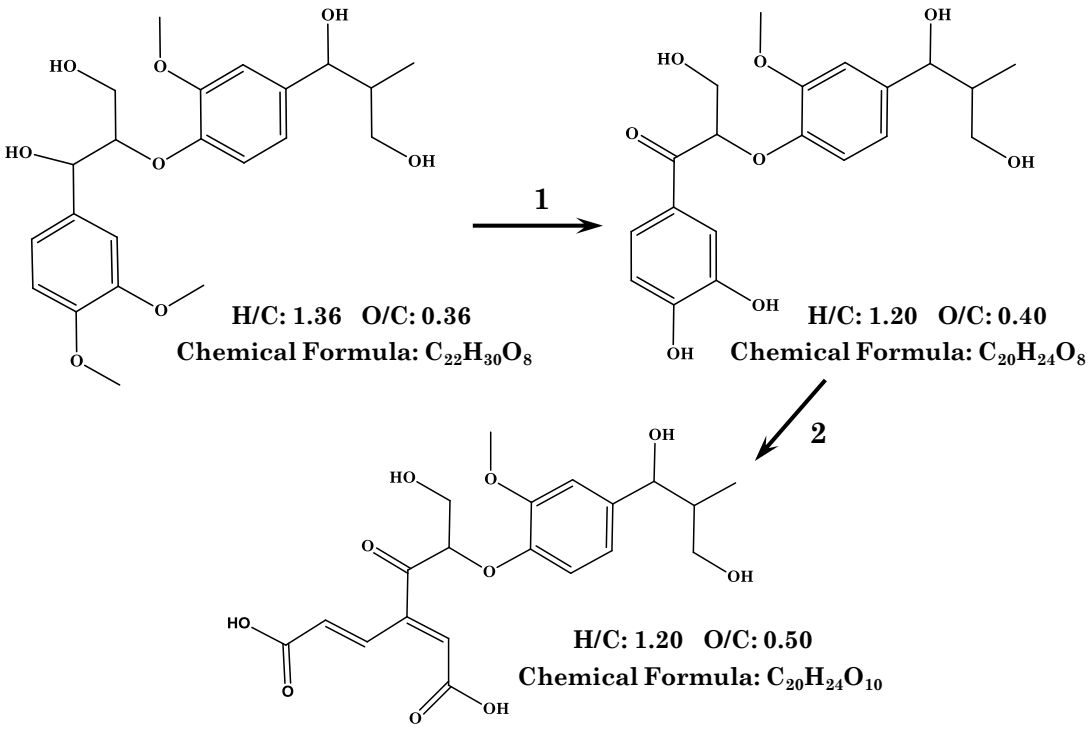

Fig. 2. Scheme depicting (1) side chain oxidation, depolymerization, demethylation and (2) ring opening of lignin resulting in unsaturated aliphatic and hydroxylated carboxylic acid containing structure. Adapted from Stenson et al. (2003)

The ultrahigh resolution MS data show additional changes not expected from ring opening/carboxylation/hydroxylation. Fig. 1d, showing only the new formulas formed in both the flocculate and filtrate, indicates that several clusters of new formulas emerge other than those shifted to higher O/C. One cluster is towards a higher H/C and lower O/C ratio, defining compounds that are more aliphatic in nature, but which still have significant oxygen functionality, likely from carboxyl and hydroxyl groups, as will be shown below. This is consistent with hydroxyl radical reacted products having an increased level of aliphatic resonances (2 - 3 ppm) over the initial base-extracted lignin as observed in the ^{1}H NMR data (Fig. 1 e-g). The unsaturated

aliphatic carboxylic acids resulting from lignin modification (ring opening) described in Fig. 2 could play a key role in the formation of these compounds. For example, several studies have shown that unsaturated aliphatic acids can undergo polymerization via radical processes to generate long chain aliphatic molecules with associated carboxyl groups as displayed in Fig. 3 (Matsumoto et al., 1996; Matsumoto et al., 1998). We suggest that subsequent loss of carboxyl groups from these chains would result in compounds like those observed in the aliphatic region of Fig. 1d.

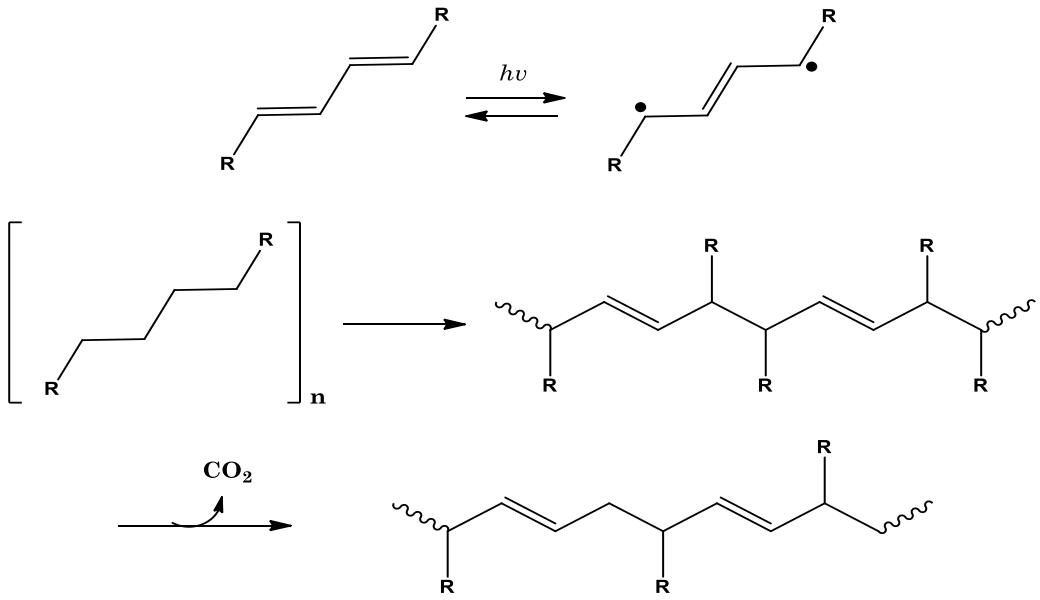

Fig. 3. Proposed scheme displaying the formation of compounds present in aliphatic region through a radical polymerization process followed by loss of carboxyl groups. R groups here indicate carboxyl groups. Modified from Matsumoto et al. (1998)

Additionally, a number of compounds with a molar H/C < 1.5 yet still aliphatic in nature (~ 200 formulas) have molecular formulas consistent with carboxyl rich alicyclic molecules (CRAM), as described by Hertkorn et al. (2006) having (Double Bond Equivalents)DBE/C = 0.30-0.68; DBE/H = 0.20-0.95; DBE/O = 0.77-1.75. These alicyclic compounds could also be formed through radical polymerization similar to that described in Fig. 3, or through another process (cyclization). It is well known that conjugated unsaturated (hydroxylated) acids can undergo cyclization (Devine and Oh, 1992; Diels and Alder, 1928; Martin and Hill, 1961). It may then be possible to produce aliphatic/alicyclic acids (Harris and Wamser, 1976) via electrocyclic reactions as depicted in Fig. 4. All these types of compounds would reasonably plot in the range of H/C and O/C space (i.e., O/C < 0.3, and H/C > 1.0) shown for newly produced aliphatic formulas in Fig. 1d.

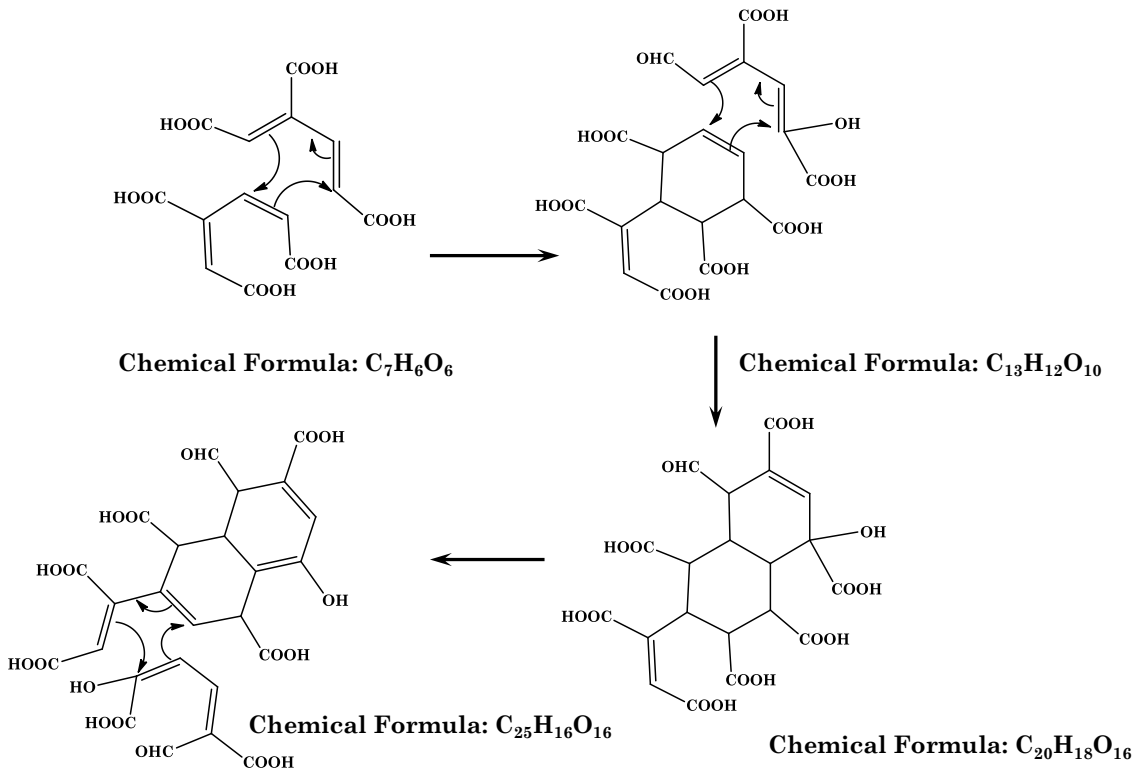

Fig. 4. Proposed electrocyclization scheme to convert lignin-derived unsaturated aliphatic and hydroxylated carboxylic acids to condensed aromatic and CRAM.

The last group of newly created compounds plot in the area associated with condensed aromatic formulas on the van Krevelen diagram, having H/C ratios < 0.6 and O/C values similar to or slightly lower than the original lignin. There appear to be two clusters of condensed aromatic formulas differing mainly in their O/C ratios. Condensed aromatic structures do not yield intense NMR resonances, but the peak at 7.7 ppm is characteristic of protons associated with multi-ring systems. Fig. 5 depicts several possible structures for the newly generated formulas assigned to compounds in the condensed aromatic region. Formulas associated with pyrogenic black carbon

typically have an O/C value < 0.3, however data in Fig. 1 shows additional peaks with formulas having an O/C ratio between 0.3-0.6. When examining the formulas associated with peaks from the cluster of condensed aromatic having the higher O/C, they have an average of 14 fewer carbon atoms than the cluster at lower O/C. We suggest that the smaller molecules may be reacting further to form the larger condensed structures present.

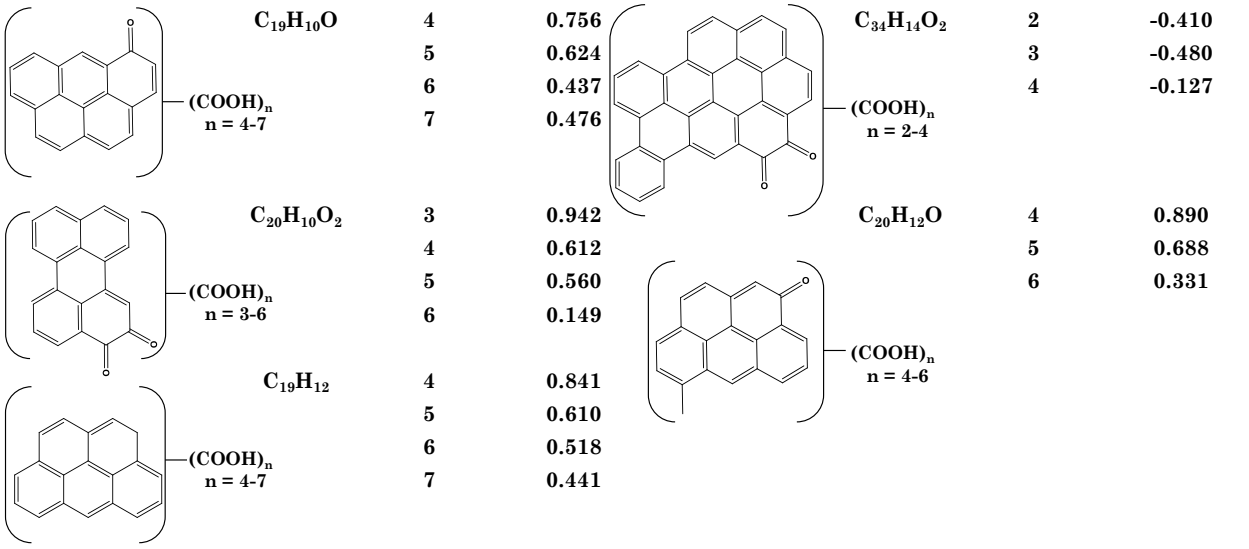

Fig. 5. Proposed condensed aromatic structures for molecular formulas assigned to lignin extract following reaction with hydroxyl radical. The error represents the difference, in ppm, between the observed and theoretical masses for each formula.

If unsaturated and hydroxylated aliphatic carboxylic acids are the first step in lignin oxidation, transforming the resulting compounds to those with a lower O/C ratio requires loss of oxygen atoms from the structures, and a loss of CO_2 would satisfy this need. Considering that wood chemists have proposed that fungal degradation involves loss of CO_2 from muconic acids through decarboxylation, it is reasonable to expect decarboxylation to be part of the process observed here. Kendrick mass defect (KMD) analysis of the aromatic and aliphatic compounds (Fig. 6), based on COO group formulation (Ikeya et al., 2013) yields a series of points horizontally aligned on a KMD plot indicating that they belong to a homologous series. Formulas having the same KMD value differ only by the mass of carboxylic acid groups in Fig. 6. This illustrates that carboxylic acid groups are the main criterion separating homologous series in both of these datasets. The presence of a large number of series differing by a carboxylic acid group (*m/z* 44) suggests that most of the molecules are carboxyl-substituted and that decarboxylation is most likely responsible for the shift to lower O/C observed in Fig. 1.

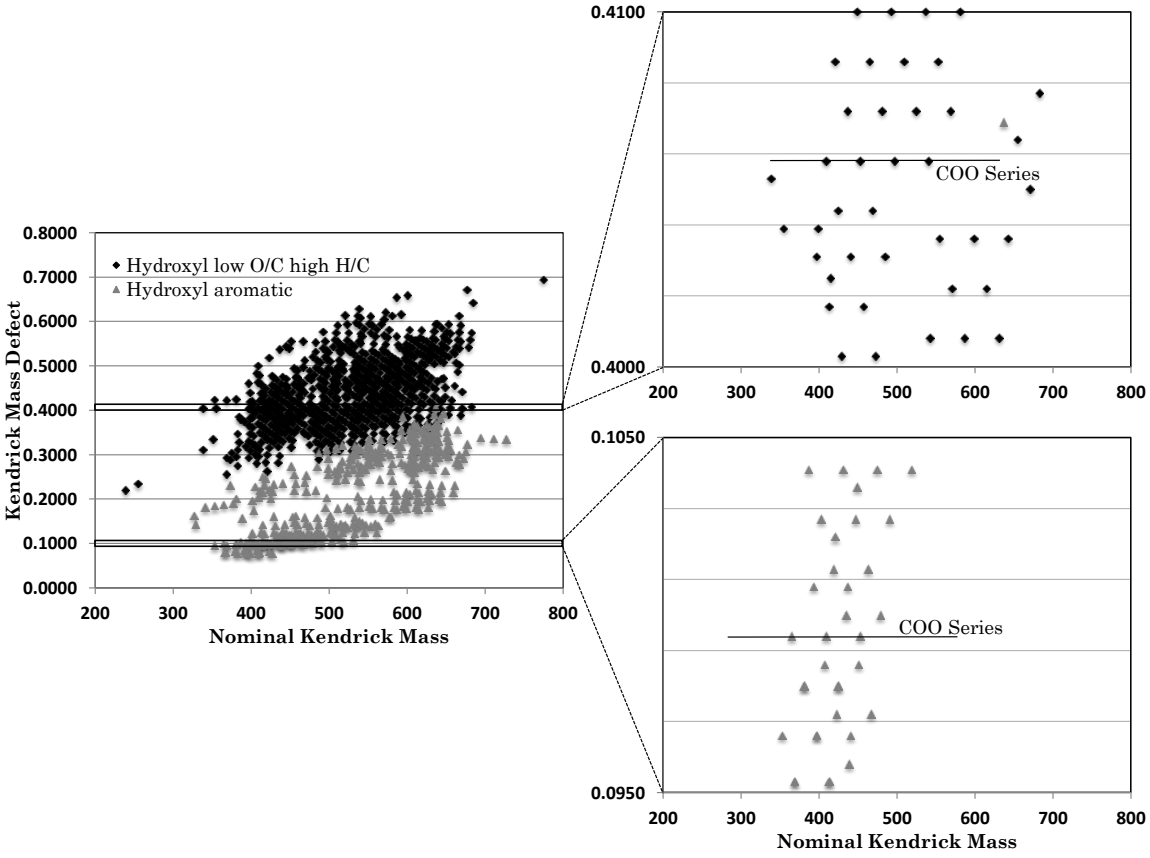

Fig. 6. Kendrick mass defect plot of aromatic and aliphatic formulas after hydroxyl radical reaction calculated from COO KMD analysis.

Loss of carboxyl groups is insufficient to explain the divergent clustering towards both a higher H/C ratio in the case of the aliphatic formulas and a lower H/C ratio in the case of condensed aromatic formulas. We suggest that this divergence can be explained if the loss of carboxyl groups propagates organic radicals, a process noted in several studies (Candeias et al., 1996; Higuchi, 2004; Jovanovic and Steenken, 1992). Some radicals would be hydrogen scavengers leading to the production of aliphatic structures, in this case alicyclic structures. Other radicals would sacrifice hydrogen and undergo aromatization and condensation to form condensed aromatic structures as

shown in Fig. 7. It is possible that these transformations occur in a concerted fashion. Additionally, while this study was aimed at investigating the fate of lignin, it is important to note that this process could potentially be occurring with other aromatic biopolymers such as tannins as well, and that lignin was used as it contributes more substantially to soil organic matter.

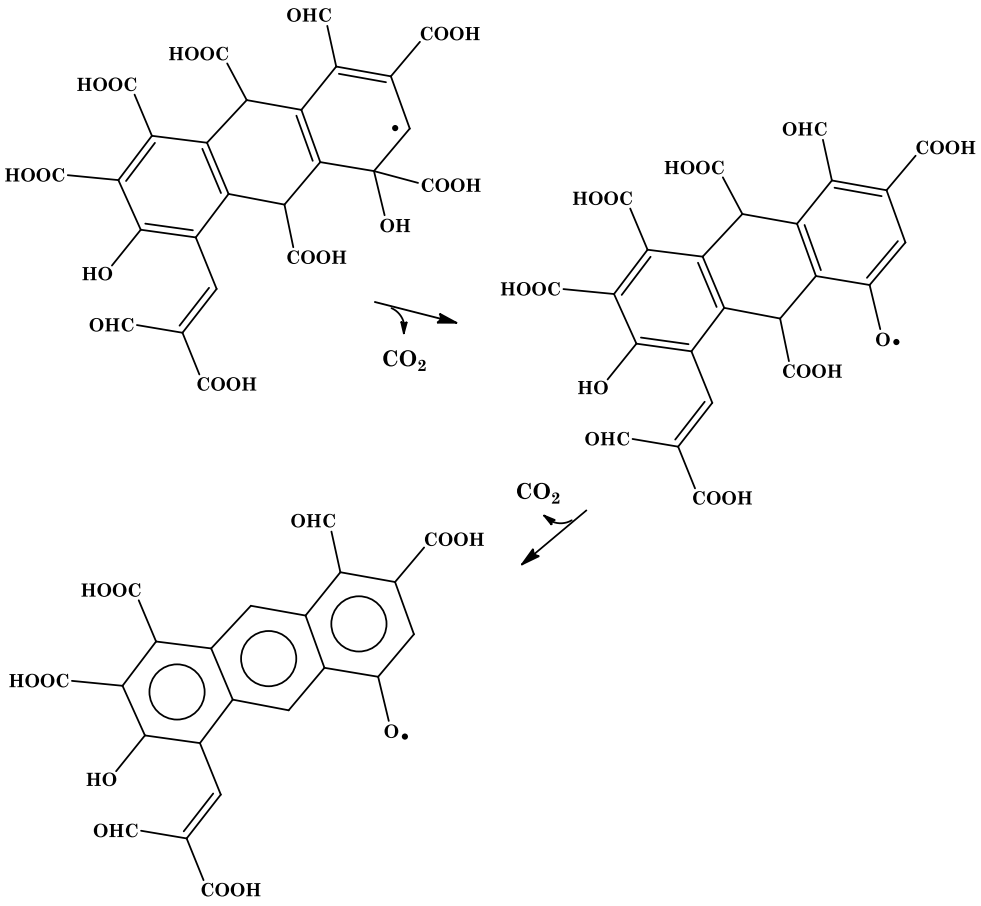

Fig. 7. Proposed aromatization of radical containing alicyclic compounds to produced condensed aromatic structures following loss of carboxyl groups and hydrogen abstraction.

The implications of our findings are significant for understanding the fate of lignin in oxic systems. We can expect that the common loss of lignin during export of terrestrial OM from points of deposition in soil to DOM in natural waters can be partially explained by these suggested transformations. Moreover, the creation of compounds that are polycondensed and carboxyl substituted suggests that a non-pyrogenic mechanism can yield compounds resembling BC. At the same time, our findings provide a pathway for the concerted formation of aliphatic structures that also contain attached carboxyl and hydroxyl groups. Such compounds have been observed in natural waters and termed CRAM. The evidence presented here suggests that lignin could be responsible for at least a portion of the BC and CRAM observed in soil and peat, and that this portion in fact occurs by way of hydroxyl radical initiated oxidation.

CHAPTER III

THE ROLE OF REACTIVE OXYGEN SPECIES IN THE DEGRADATION OF LIGNIN DERIVED DISSOLVED ORGANIC MATTER

PREFACE

The contents of this Chapter was published in 2017 in Geochimica et Cosmochimica Acta, and below is the full citation. See Appendix A for copyright permission.

Waggoner, D.C., Wozniak, A.S., Cory, R.M., and Hatcher, P.G. (2017). The role of reactive oxygen species in the degradation of lignin derived dissolved organic matter. *Geochimica et Cosmochimica*, 208, 171-184.

1. INTRODUCTION

Natural dissolved organic matter (DOM) is a dynamic pool of carbon on Earth (Hedges, 1992), and is a critical intermediate in the global C cycle (Cole et al., 2007). Rivers worldwide transport an estimated 0.4×10^{15} g of terrestrial dissolved organic carbon (DOC) and approximately 0.2×10^{15} g of particulate organic carbon (POC) annually to the oceans (Bianchi, 2011; Jaffe et al., 2013; Schlesinger and Melack, 1981), roughly equivalent to the annual turnover of marine DOC (Williams and Druffel, 1987). Studies of DOM carbon isotopes (Bauer, 2002; Lalonde et al., 2014), optical properties (Blough and Del Vecchio, 2002) and lignin-phenol biomarkers (Opsahl and Benner, 1997, 1998) have suggested that terrestrial DOM disappears quickly once in oceans. However, current understanding from rates of photochemical

mineralization, bacterial respiration, and salinity induced flocculation (Fox, 1983; Sholkovitz, 1976; Søndergaard et al., 2003), suggest that these three major removal processes for terrestrial DOM likely cannot account for all loss of this DOM in estuaries. Recent work suggests that upwards of 50% of terrestrially-derived DOM may be partially oxidized or chemically altered by sunlight during transit from land to coastal waters (i.e., partial degradation) (Cory et al., 2014; Spencer et al., 2009), thereby masking identification of the origin of this C using conventional isotopes and biomarker proxies (Blough and Del Vecchio, 2002; Helms et al., 2008; Spencer et al., 2009; Waggoner et al., 2015).

Consistent with these recent studies showing that rates of photochemical transformations are sufficient to process a large fraction of DOM export from land to water, others have shown that photochemical alteration of terrestrial DOM results in compounds resembling those found in marine waters (Chen et al., 2014; Cory et al., 2010). Pathways for the photochemical alteration of terrestrial DOM may involve reactive oxygen species (ROS) such as singlet oxygen ($^1O_2$), hydroxyl radical ($^{\bullet}OH$), and superoxide ($O_2^{-\bullet}$), along with photo-activated DOM complexes (McNally et al., 2005; Page et al., 2013; Porcal et al., 2013; Scully et al., 2003; Ward et al., 2014). Photo-excited chromophoric DOM interacts with dissolved oxygen or water to produce reactive transient ROS and organic radicals, which in turn break down both the chromophoric DOM as well as the uncolored pool of DOM not accessible to direct photochemical degradation (Cory et al., 2009; Cory et al., 2010; Goldstone et al., 2002; Pullin et al., 2004; Scully et al., 2003). For example, it is well-established that DOM can react with $^1O_2$ (Cory et al., 2010) and $^{\bullet}OH$ in natural waters (Page et al., 2014). Furthermore, when DOM reacts with $^1O_2$ and $^{\bullet}OH$, evidence suggests that the primary products may be photochemically-modified DOM (i.e., partial photo-oxidation; (Cory et al., 2010; Cory et al., 2014; Waggoner et al., 2015), and not complete photo-oxidation of

DOM to CO_2 (i.e., photo-mineralization, (Cory et al., 2010; Page et al., 2014; Southworth and Voelker, 2003). Further evidence in support of partial photo-oxidation of terrestrially-derived DOM by ROS includes the relatively high ratio of photochemical oxygen consumption to CO_2 production by DOM. Specifically, studies have shown that the molar ratio of photochemical O_2 consumption per CO_2 production by DOM is > 1; (Andrews et al., 2000; Cory et al., 2014; Miles and Brezonik, 1981; Ward and Cory, 2016), suggesting substantial oxygen incorporation into DOM. The role of ROS partial photo-oxidation of DOM is not well known due to the difficulty of isolating individual ROS and their reactions with DOM (Cory et al. 2009, 2010). At present, each ROS is expected to vary substantially in its reactivity with DOM.

For example, while $^1O_2$ is a fairly short-lived and selective oxidant, photochemical transformation of DOM by $^1O_2$ may be more important than other ROS due to higher $^1O_2$ concentrations in the hydrophobic interior of DOM (Grandbois et al., 2008; Latch and McNeill, 2006). Electrophilic $^1O_2$ can undergo cycloaddition with dienes and olefins abundant in DOM to form cyclic peroxides (Kearns, 1971). Non-cyclic allylic hydroperoxides can form upon $^1O_2$ reaction with olefins, as well as carbonyl containing compounds following olefin cleavage (Kearns, 1971). Previous work showed that alteration of DOM by $^1O_2$ led to production of O-containing aliphatic formulas (Cory et al. 2010).

Hydroxyl radical is an unselective oxidant and reacts at near diffusion rates with organic compounds and thus is expected to be an important oxidant of DOM (Goldstone et al., 2002). Hydroxyl radicals primarily react with DOM through addition to olefins or aromatic compounds, H abstraction, and electron transfer reactions (Walling, 1975; Wenk et al., 2011). Direct addition of $^{\bullet}OH$ has been shown to result in both hydroxylation, and cleavage of side chain groups from compounds, with low molecular weight acids frequently observed following reaction of DOM with

$^{\bullet}$OH (Goldstone et al., 2002; Walling, 1975). Electron transfer reactions associated with $^{\bullet}$OH, while rare, are believed to yield organic radical cation species, which can then undergo dimerization reactions to generate new products (Walling, 1975). Consistent with the rapid and unselective oxidation of organics by $^{\bullet}$OH, substantial alteration of lignin derived DOM upon exposure to $^{\bullet}$OH has been shown under laboratory conditions, resulting in the formation of condensed aromatics and molecules classified as carboxyl rich alicyclic molecules (CRAM) (Waggoner et al., 2015).

In contrast to $^1O_2$ and $^{\bullet}$OH, $O_2^{-\bullet}$ is relatively long-lived, which may allow it to react with a range of moieties within the DOM pool (Rose et al., 2010). Superoxide, through nucleophilic substitution reactions, is capable of producing carboxylic acid anions from esters, as well as dicarboxylic acids from unsaturated cyclic compounds following ring cleavage (Lee-Ruff et al., 1976; Sawyer and Valentine, 1981). One electron reduction of organic compounds is commonly observed with $O_2^{-\bullet}$, and reactions with catechol like compounds, frequently present in DOM, result in radical anions that can undergo ring cleavage and polymerization (Lee-Ruff et al., 1976; Sawyer and Valentine, 1981). No study has investigated the effects of $O_2^{-\bullet}$ on DOM composition, but given known reactions of organics with $O_2^{-\bullet}$ this ROS may contribute to oxidation and oxygen incorporation into DOM.

Thus, despite strong evidence for the importance of ROS in transforming DOM composition in sunlit surface waters, including much knowledge on the potential reactivity of ROS with model compounds, few studies have characterized the effects of individual ROS exposure on DOM composition. To address this knowledge gap, we exposed lignin-derived DOM to $^1O_2$, and $O_2^{-\bullet}$ to isolate the molecular level alterations specific to each ROS and then track those alterations using Fourier transform ion cyclotron resonance mass spectrometry (FTICR-MS). By selectively exposing lignin to each ROS under controlled conditions in the laboratory, we amplify the

reactions of interest to isolate their potential pathways for alteration of DOM. We combined this new information with data obtained previously for $^{\bullet}OH$ (Waggoner et al., 2015) to understand the potential classes of terrestrial DOM that may be transformed by ROS, and to identity potential products of these ROS-mediated transformations of DOM..

2. MATERIALS AND METHODS

2.1 Lignin extraction

Alkali-soluble lignin, representing terrestrial DOM, was isolated from a brown rot fungal degraded wood sample, Atlantic white cedar (*Chamaecyparis thyoides*), collected from the Great Dismal Swamp in Virginia as previously described (Liu et al., 2011; Waggoner et al., 2015). The sample of wood was dried and ground to a fine powder prior to 24 hour stirring in 0.01 M NaOH. The resulting base extract was then filtered through a 0.7 µm glass fiber filter to remove any undissolved solids. This stock solution of lignin, approximately 400 ppm C, was subsequently used directly for treatment by $^1O_2$. For $O_2^{-\bullet}$ treatment, the base extract was cation exchanged with extensively washed Dowex 50Wx8 (H-form) to remove sodium prior to lyophilization.

2.2 Reaction with singlet oxygen

Singlet oxygen reactions were carried out in duplicate 500ml quartz round bottom flasks by adding the photosensitizer Rose Bengal (disodium salt, final concentration $1x10^{-5}$ M) to the base extracted lignin (pH 10) and bubbling with O_2 for approximately 20 minutes (Miller, 2005). The pH chosen was suggested to be more efficient for $^1O_2$ generation by Rose Bengal based on reaction rate kinetics when compared to reactions at neutral or slightly acidic pH, which show lignin and lignin model compounds preferentially react with excited state sensitizer over $^1O_2$ in non-basic conditions (Latch et al., 2003; McNally et al., 2005; Miller, 2005). A light control (no

Rose Bengal photosensitizer) and dark control (foil wrapped) were also prepared for comparison. All solutions were placed in a Percival growth chamber equipped with T8 fluorescent lights (Philips F17T8/TL841), held at 25 °C and 100% light intensity for 48 hours of photoirradiation. Light intensity was measured at 180 μM M^{-2} s^{-1} (400-700nm) using an LI-250A light meter over the duration of the experiment. Following irradiation, all samples were passed through cation exchange resin to remove salts that interfere with instrumental analysis. The resin was additionally rinsed with liquid chromatography-MS (LC-MS) grade methanol to elute any analyte sorbed to the resin.

The absorbance of the lignin + Rose Bengal solution was 1.6 times greater at 550 nm (peak absorbance of Rose Bengal) compared to the light control (lignin only; Fig. 8). Thus, in the lignin +Rose Bengal solution, there was more absorbance of the visible light by Rose Bengal than by lignin. In addition, the apparent quantum yield for $^1O_2$ by Rose Bengal at 550 nm (visible light) is ~ 0.7 (Haag et al., 1984), much higher than apparent quantum yields for ROS by lignin estimated at ~0.27 using model compounds (McNally et al., 2005). Together, these reaction conditions support selective reaction of lignin with $^1O_2$ because in the +Rose Bengal solution, the photochemical production of $^1O_2$ by Rose Bengal was likely much greater than photochemical production of other $^1O_2$ or other ROS by lignin. In addition, we verified photochemical production of $^1O_2$ from solutions containing only Rose Bengal and exposed to the same light as the lignin solution with and without Rose Bengal. Singlet oxygen was quantified from separate flasks containing Rose Bengal (at the same experimental concentration of $1x10^{-5}$ M) and furfuryl alcohol (FFA; a probe for $^1O_2$). FFA concentration was added at $2x10^{-4}$ M. Sub-samples for FFA degradation were collected at time points to verify photochemical production of $^1O_2$ from solutions of Rose Bengal exposed to the fluorescent bulbs used in the experiments (Haag and Hoigne, 1986).

The $[^1O_2]_{ss}$ for the experiment was determined to be 1 $x10^{-11}$ M. The concentration of $^1O_2$ was not measured in the lignin + Rose Bengal solutions because $^1O_2$ concentrations as measured by probes such as FFA may be influenced by reaction with and quenching by lignin, as demonstrated for lignin (Bentivenga et al., 1999; Bonini et al., 1998; McNally et al., 2005) and lignin model compounds (Crestini and D'Auria, 1997; Crestini and DÁuria, 1996). Further, it is difficult to speculate on differences in $[^1O_2]$ss in the lignin+ Rose Bengal solutions used in this study to the concentrations of $[^1O_2]$ss that terrestrial DOM may encounter in sunlit surface waters where DOM is the photochemical sensitizer for $^1O_2$ (i.e., in all sunlit surface waters (Andrews et al., 2000; Peterson et al., 2012)). This is because $^1O_2$ concentrations may vary several orders of magnitude from the hydrophobic interior of DOM to the more hydrophilic exterior (Latch and McNeill, 2006). Currently, there is no approach to selectively reproduce natural photochemical production of $^1O_2$ by DOM (or lignin) without introduction of other photochemically produced reactive oxygen species and intermediates by DOM. Thus, the goal of our experimental set-up was to maximize conditions for oxidation of lignin by $^1O_2$ by using Rose Bengal as the source of $^1O_2$ so that compared to controls, we may evaluate the potential effects of $^1O_2$ on lignin composition.

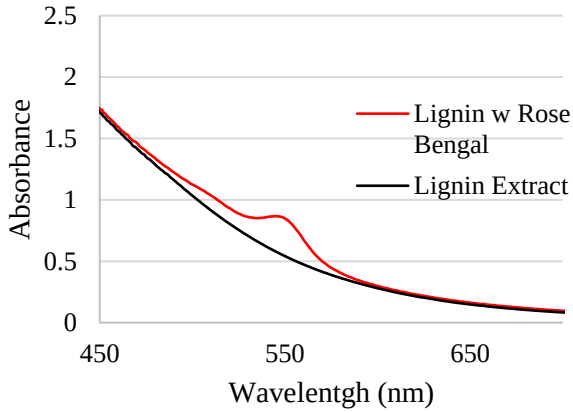

Fig. 8. UV-Vis absorbance for lignin sample amended with (Red) and without (Black) the photosensitizer Rose Bengal, demonstrating prevalent absorbance by Rose Bengal in the visible light range.

2.3 Reaction with $O_2^{-\bullet}$

A stable $O_2^{-\bullet}$ solution was prepared following (Valentine and Curtis, 1975). Briefly, 0.30M dicyclohexyl-18-crown-6 was used to solubilize 0.15M KO_2 in dry DMSO. The concentration of $O_2^{-\bullet}$ has been demonstrated to be roughly equivalent to the concentration of KO_2 in solution (Valentine and Curtis, 1975). A lignin solution was prepared by dissolving 2.0 mg of lyophilized lignin extract in 8 ml of Milli-Q water. The reaction was carried out by adding 2.0 ml of 0.15M $O_2^{-\bullet}$ solution over the course of 30 minutes to 4 ml of lignin solution with rapid stirring. Freeze dried samples of base extracted lignin were also added to DMSO and exposed to the $O_2^{-\bullet}$ solution for a comparison of solvent effects on the reaction. Samples in which solid KO_2 was added directly to the lignin solution and a DMSO solution saturated with analyte were also analyzed as an additional control. Samples were passed through cation exchange resin as described above to

remove inorganic salts that interfere with mass spec analysis, followed by a methanol rinse of the resin to recover sorbed analytes. This rinse was added to the aqueous/DMSO reaction medium.

2.4 TMAH thermochemolysis

All samples (+ ROS and controls) were subjected to tetramethylammonium hydroxide (TMAH) thermochemolysis to evaluate the state of lignin degradation compared to the initial lignin extract. Lignin phenol biomarkers, i.e., vanillic and syringic acids, were measured after TMAH thermochemolysis to assess the level of oxidative degradation following exposure to singlet oxygen. It is expected that as the level of organic matter oxidation increases, the amount of acidic lignin phenols (vanillic and syringic acids) will increase relative to the corresponding aldehydes (vanillin and syringealdehyde) (Hedges and Ertel, 1982; Opsahl and Benner, 1998). Samples were dried and small amounts were placed in custom glass reaction tubes with TMAH (25% wt. in MeOH) as described by Filley et al. (2002). Briefly, methanol was removed under vacuum and all tubes were flame sealed prior to heating at 250 °C for 30 minutes. After returning to room temperature, the tubes were placed in liquid nitrogen to condense any gases formed before opening and extracting with ethyl acetate for GC-MS analysis.

2.5 FTICR-MS Analysis

Following $^{1}O_2$ and $O_2^{-\bullet}$ treatment, all samples were analyzed using a Bruker 12T Apex Qe FTICR-MS, housed in the College of Sciences Major Instrumentation Cluster at Old Dominion University, operated in negative electrospray ionization (ESI) mode. Samples were continualy infused into an Apollo II ESI ion source at a rate of 120 µL hr^{-1} using a syringe pump. ESI voltages were optimized for each sample to generate a stable ESI spray, with spray shield and capillary currents of 180-230 nA and 20-35 nA respectively. Ions were accumulated for 0.5-1.0s in a

hexapole prior to being transferred to the ICR cell, where 300 transients were collected using a 4 MWord time domain and co-added. The resulting FID was zero-filled once and Sine-Bell apodized before undergoing fast Fourier transformation and a magnitude calculation using Bruker Daltonics Data Analysis software. Each sample was externally calibrated using a polyethylene glycol standard, and internally calibrated using fatty acids, dicarboxylic acids, and natural compounds belonging to CH_2 homologous series based on Sleighter and Hatcher (2008) prior to analysis. It is important to point out that FTICR-MS analysis performed only observes molecules that charge in the negative ion electrospray mode. Such molecules would need to possess ionizable functional groups, such as oxygen containing functional groups commonly found in lignin. Any molecules lacking such groups would not be observed; however, it is likely that they would also not be part of the sample extract due to limited or no solubility.

Unique molecular formulas were assigned to peaks having a signal to noise (S/N) threshold of 3, using a MATLAB script written in house at Old Dominion University according to the criteria $^{1}H_{5\text{-}100}\ ^{16}O_{1\text{-}30}\ ^{14}N_{0\text{-}6}\ ^{32}S_{0\text{-}2}\ ^{34}P_{0\text{-}2}$, with subscripts denoting the range of atoms allowed for a single formula. Formulas were screened based on the rules described by Stubbins et al. (2010) for natural organic matter, and Kendrick mass defect homologous series (CH_2, H_2, CO_2, and O_2) were used to select ambiguously assigned formulas (Kujawinski and Behn, 2006). All formulas assigned are within 1 ppm error of the measured m/z, with 94% of formulas having 0.5 ppm or lower error.

2.6 GC x GC TOF-MS Analysis

Lignin phenol biomarker analysis was performed using a LECO Pegasus 4D GC x GC TOF-MS following reaction with TMAH. Analyses were carried out with an autosampler (CTC Analytics) integrated to the GC system (Agilent Technologies, 6890N) fitted with a thermal modulation assembly. The columns used were a 30 m x 0.25 mm i.d. RTX-5 first dimension

column, and 1 m x 0.1 mm i.d. RXI-17 second dimension column. Helium was used as a carrier gas and adjusted for constant flow throughout the run. The injector was operated in splitless mode and held at a constant 280°C throughout the run. The temperature program used consisted of an initial temperature of 40°C for 2 minutes then ramping to 280°C at 10°C min^{-1} and holding for 10 min after a 1 µL sample injection. A total modulation time of 4 seconds was used for the second dimension column consisting of a 1.30 second hot pulse and 0.70 second cold pulse. Peak areas were measured by the Pegasus software and identification of the products was via mass spectral comparisons to NIST library spectra.

3. RESULTS

3.1 Chemical composition of Dismal Swamp lignin extract and dissolved organic matter

The molecular characteristics (elemental formulas from ESI-FTICR-MS data) of the alkali-soluble lignin extract are shown in Figure 9 as points on a van Krevelen diagram, generated by plotting the atomic H/C vs O/C ratios for the assigned formulas. Also depicted in Figure 9 is a van Krevelen diagram of dissolved organic matter from the Dismal Swamp for comparison to the lignin extract. Regions typically associated with lignin-like, carbohydrate-like, and tannin-like compounds have been added to van Krevelen diagrams, along with cutoff lines depicting where aromatic and condensed aromatic compounds are predicted to fall within the plot (Chen et al., 2014; Sleighter and Hatcher, 2008). For both the lignin extract and DOM from the Dismal Swamp, all formulas cluster within the region characteristic of lignin (Sleighter and Hatcher, 2007). Of the multitude of elemental formulas in the DOM (total number excluding isotopologues = 1873) approximately 58% correspond exactly to those observed in the lignin extract. One difference is the presence of formulas in the carbohydrate-like region for the lignin extract, formulas not

observed in the DOM. This is most likely attributable to the more elevated levels of partly degraded cellulosic components in the wood as shown in solid-state ^{13}C NMR data (not shown).

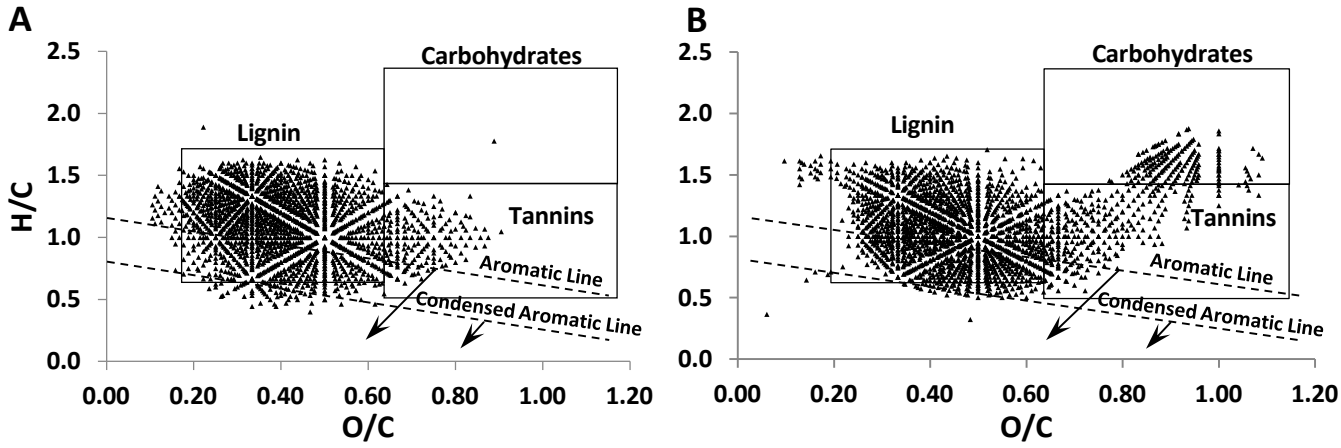

Fig. 9. Van Krevelen plots of CHO formulas for initial Dismal swamp DOM (A) and Dismal swamp lignin extract (B). Common regions associated with lignin, carbohydrates, and tannins are displayed. Lines showing the cutoffs for aromatic compounds ($AI_{mod} \geq 0.5$) and condensed aromatic compounds ($AI_{mod} \geq 0.67$) are additionally shown.

3.2 Reaction with $^1O_2$

There were significant differences between $^1O_2$-reacted vs. control samples in lignin phenols expected to be indicators of organic matter oxidation, as measured by TMAH thermochemolysis (i.e., vanillic and syringic acids; Fig. 10). Lignin extract exposed to elevated concentrations of $^1O_2$ (i.e., the + Rose Bengal treatment) showed substantially elevated (Ad/Al)v ratio values compared to dark and light controls (i.e, no Rose Bengal). This result indicates greater degradation of lignin when exposed to $^1O_2$ (via addition of Rose Bengal) compared to the controls,

given the expectation that oxidation of organic matter by $^1O_2$ increases the aldehyde to acid ratio of vanillyl compounds (Hedges and Ertel, 1982; Opsahl and Benner, 1998).There was no significant difference in the (Ad/Al)v between the dark and light controls, providing further evidence for the Rose Bengal treatment as having substantially greater $^1O_2$ concentrations compared to the controls, and thus greater alteration of the lignin (Fig. 10).

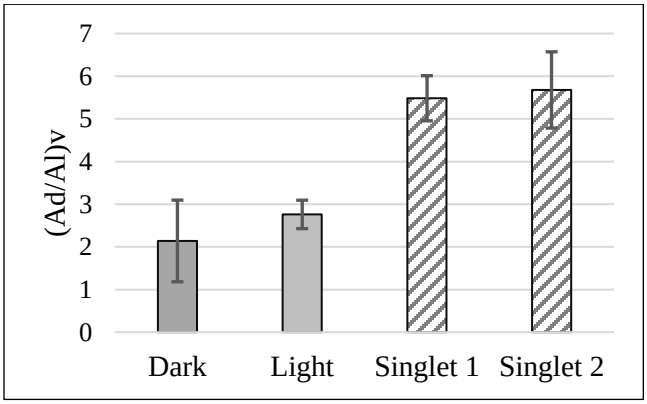

Fig. 10. Ratio of vanillic acid to vanillin (Ad/Al)v, in dark control, light control, and replicate $^1O_2$ exposed lignin DOM samples. TMAH thermochemolysis was performed in triplicate for all samples with error bars indicating standard deviation of measurements.

The molecular formulas generated from FTICR-MS analysis of the $^1O_2$ exposed lignin extract resulted in 2617 assigned molecular formulas, 2297 being comprised of only C, H, and O atoms (~88%), as shown in the van Krevelen diagram (Fig. 11). Assigned formulas center around the region typically associated with lignin, with half of the newly produced formulas trending toward a higher O/C ratio, and plotting in an area commonly associated with tannin like compounds. The remaining new formulas largely plot in the higher H/C ratio portion of the lignin

region, with a few formulas plotting in areas associated with aromatic compounds. A small decrease (9%) in the modified aromaticity index (AI_{mod}) for the CHO formulas in the lignin extract occurred as a result of $^1O_2$ treatment, suggesting a slight decrease in the unsaturated formulas present.

Formulas assigned following $^1O_2$ exposure were also used to investigate the potential pathways of organic matter alterations by $^1O_2$ that might be occurring. A series of Kendrick mass defect analyses were performed on $^1O_2$ exposed samples and controls using the following equations:

$$KM\ (COO) = IUPAC\ mass_{measured}[44.0000/43.98983] \quad (1)$$

$$KM\ (O_2) = IUPAC\ mass_{measured}[32.0000/31.98983] \quad (2)$$

$$KMD = [NM - KM] \quad (3)$$

where KM=Kendrick mass, NM= nominal mass, IUPAC mass = the measured exact mass of the peak based on the assigned formula. Kendrick mass defect plots are based on comparison of functional groups or atoms, such as COOH or O_2, vs. the nominal Kendrick mass. These plots identify the series of formulas differing by a selected mass corresponding to a monoatomic or diatomic atom or to functional group. For example, Kendrick mass defect plots showing a series of formulas differing from each other only by the number of oxygen atoms are distinguished by differences in m/z 32 corresponding to the mass of O or O_2. Likewise, formulas differing only in mass of m/z 44 corresponding to the mass of COOH functional group. Other trends, such as the addition of OH groups, characterized by a mass offset of m/z 18, can also be observed within the O_2 KMD plot. As shown in Figure 12 for the Kendrick mass defect plots for series of formulas differing in the number of O_2 or COOH groups, the plots define formulas separated horizontally

with a slope of 0 to be part of a homologous series of formulas differing in the number of O atoms or COOH groups. The KMD series for O_2 shows a general increase in nominal mass over the starting base extract with an increase in the average number of formulas falling into a series (Fig. 12). This result is consistent with the addition of oxygen to the formulas present in the lignin extract prior to exposure to $^1O_2$ resulting in an increase of overall nominal mass. The KMD for COOH also shows an increase in the average number of formulas per series. Furthermore, these formulas plot at the higher mass end of series, suggesting that additional carboxyl groups are being formed due to the oxidation of organic matter by $^1O_2$. The increase in nominal mass observed for new compounds following $^1O_2$ exposure does not apply to the bulk lignin extract, which shows negligible change in the magnitude weighted average molecular mass.

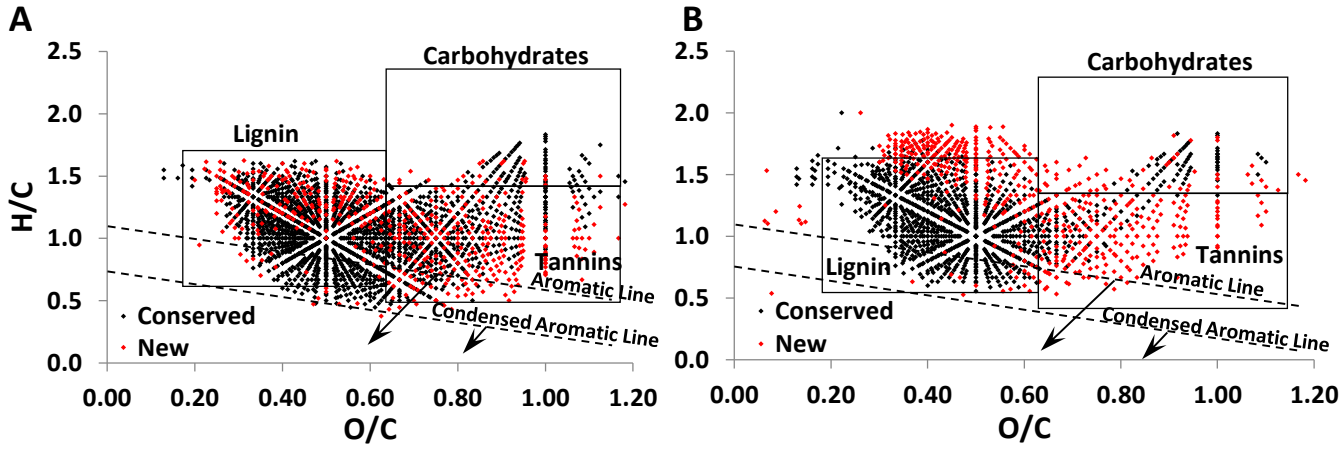

Fig. 11. Van Krevelen plots of CHO formulas produced following Dismal Swamp degraded lignin exposure to $^1O_2$ (A), and $O_2^{-\bullet}$ (B), with newly created formulas displayed in red and conserved formulas in black.

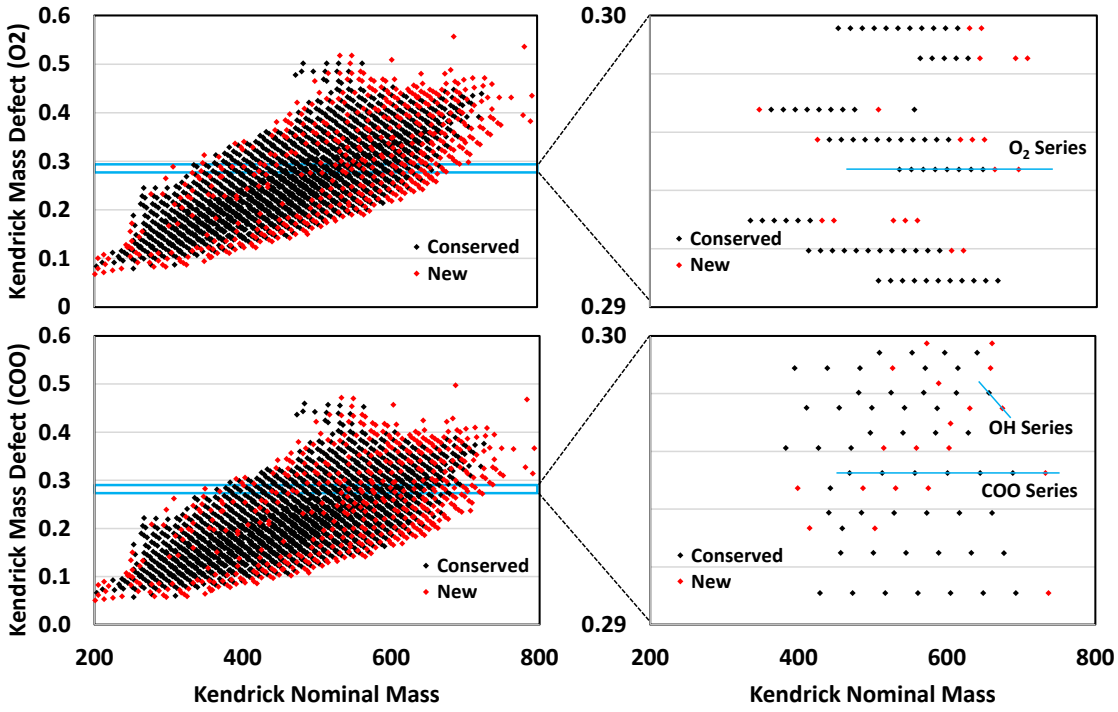

Fig. 12. Kendrick mass defect plots for lignin following reaction with $^1O_2$ with the top plot showing KMD for oxygen series and the bottom COO series. Newly formed formulas are shown in red while conserved are black.

3.3 Reaction with $O_2^{-\bullet}$

Similar to the $^1O_2$ experiments, TMAH thermochemolysis was used to investigate the oxidative degradation effect $O_2^{-\bullet}$ exposure had on the lignin phenol biomarker signature. The control extract lignin exhibited a low (Ad/Al)v ratio consistent with a minimally degraded lignin sample (Fig. 13, cation base extract). The $O_2^{-\bullet}$ exposed lignin showed no significant difference in (Ad/Al)v compared to the controls (Fig. 13). Solid potassium $O_2^{-\bullet}$ showed a much larger (Ad/Al)v ratio compared to + $O_2^{-\bullet}$ treatment and the control lignin extract (Fig. 13)

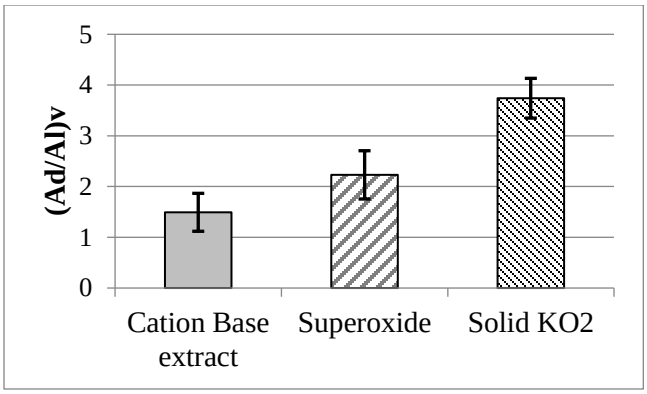

Fig. 13. Ratio of vanillic acid to vanillin (Ad/Al)v, in initial base extract, solid potassium $O_2^{-\bullet}$, and 0.15M $O_2^{-\bullet}$ exposed lignin DOM samples. TMAH thermochemolysis was performed in triplicate for all samples with error bars indicating standard deviation of measurements.

Of the 1927 total formulas assigned, 1595 of the formulas in the + $O_2^{-\bullet}$ treatment contained only C, H, and O atoms (~83%). A number of new CHO containing formulas, 525, were produced from $O_2^{-\bullet}$ exposure, with 247 falling into the area located directly above the region typically associated with lignin type compounds. These new formulas have an H/C value greater than 1.5, suggesting that they possess more aliphatic characteristics than the un-reacted control extract of lignin. The generation of new aliphatic formulas is also evident in the 41% decrease in the AI_{mod} value for CHO formulas (AI_{mod} 0.18), indicating a trend toward more saturated formulas in $O_2^{-\bullet}$ treated lignin. To investigate further differences between the new formulas vs. those present in the controls, Kendrick mass defect plots were analyzed for COOH, O_2, and H_2 series for the $O_2^{-\bullet}$ experiments (Fig. 14).

The KMD analysis for COOH (Fig. 14) shows that, when new formulas are present in series with conserved formulas, new formulas differing in mass by COOH typically plot at higher nominal masses. This result suggests addition of COOH groups by $O_2^{-\bullet}$ to an existing compound,

which would increase the mass relative to formulas present initially, rather than removal of COOH from some formulas present initially which would decrease the mass relative to initial formulas. KMD plots for oxygen show a similar trend, with new points in the series falling at higher masses indicating the addition of oxygen following exposure to $O_2^{-\bullet}$, rather than loss from formulas already present. The H_2 series (Fig. 14); however, shows that newly produced formulas result from both the addition and removal of hydrogen, with new formulas plotting at the upper and lower mass ranges of the KMD series. Despite the addition of oxygen to existing formulas, the whole lignin extract following $O_2^{-\bullet}$ treatment shows an 18% decrease in average molecular mass for the CHO formulas.

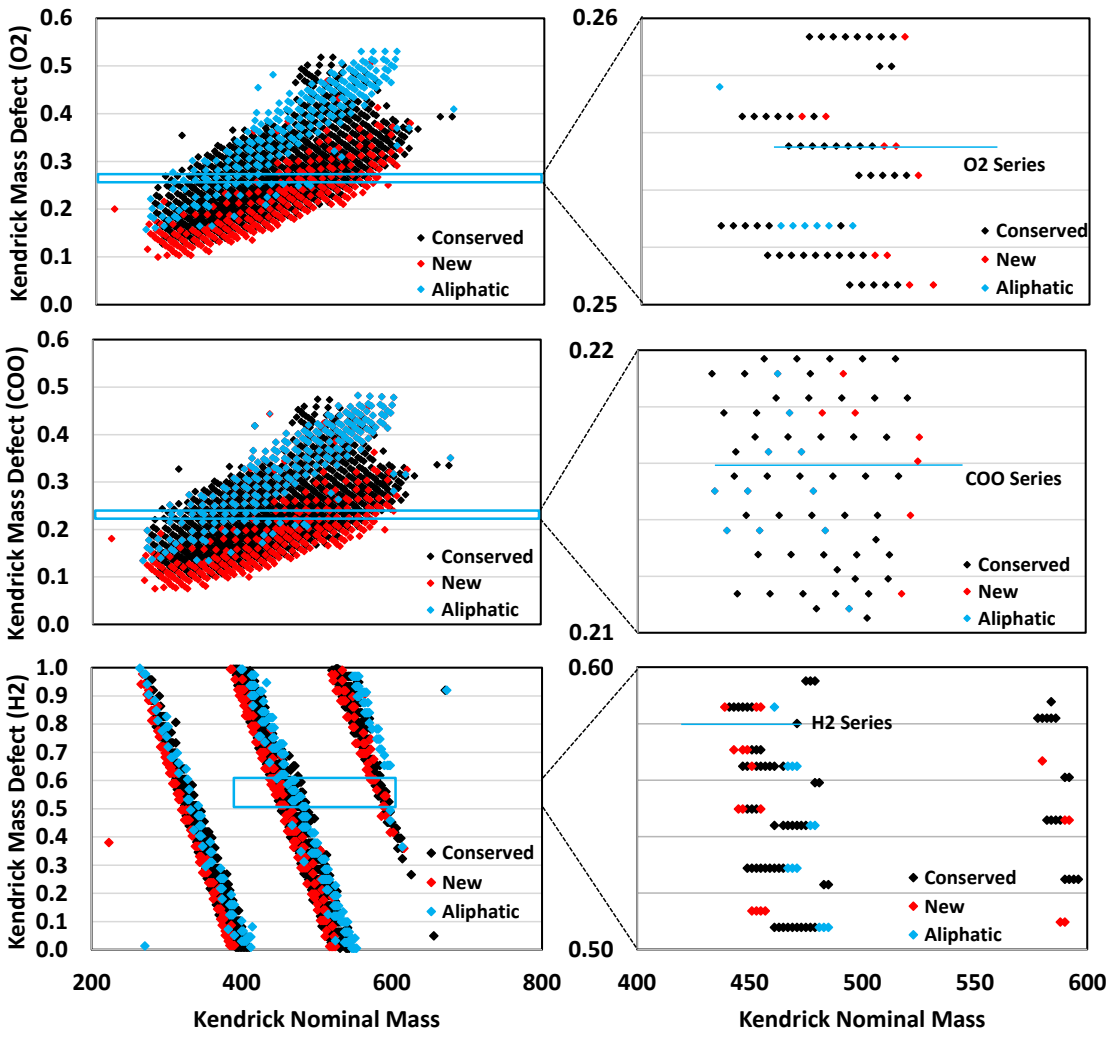

Fig. 14. Kendrick mass defect plots for lignin following reaction with $O_2^{-\bullet}$ with the top plot showing KMD for O_2 series, the middle COO series, and the bottom H_2 series. Conserved formulas (black) are displayed alongside new formulas (red) and new aliphatic formulas having H/C > 1.5 (blue).

3.4 ROS reactivity with lignin

The relative reactivity of each ROS toward lignin derived DOM may be inferred from the FTICR-MS data by comparing formulas from each experiment that were completely removed by the treatment selective for each ROS: $^1O_2$, $O_2^{-\bullet}$ (this study) and $^\bullet OH$ (Waggoner et al., 2015). Formulas displayed in the van Krevelen diagram represent the CHO containing formulas from each ROS treatment that were present in the initial samples and completely removed following exposure to the ROS tested (Fig. 15). There were strong differences in the formulas removed from lignin between ROS treatments, e.g., between $^1O_2$, $O_2^{-\bullet}$ and $^\bullet OH$ (Fig. 15). Singlet oxygen exposure resulted in removal of 442 formulas. These formulas lost had an average mass of 513 m/z and O/C value of 0.48. Exposure to $O_2^{-\bullet}$ removed 631 formulas characterized by an average mass of 460 m/z and O/C value of 0.29. Reaction of organic matter with $^\bullet OH$ resulted in loss of 1042 formulas characterized by an average mass of 585 m/z and O/C ratio of 0.54. These results show that $^\bullet OH$ removed larger, more oxidized formulas compared to $^1O_2$ and $O_2^{-\bullet}$, which tended to remove smaller and less oxidized (more saturated) formulas (Fig. 15).

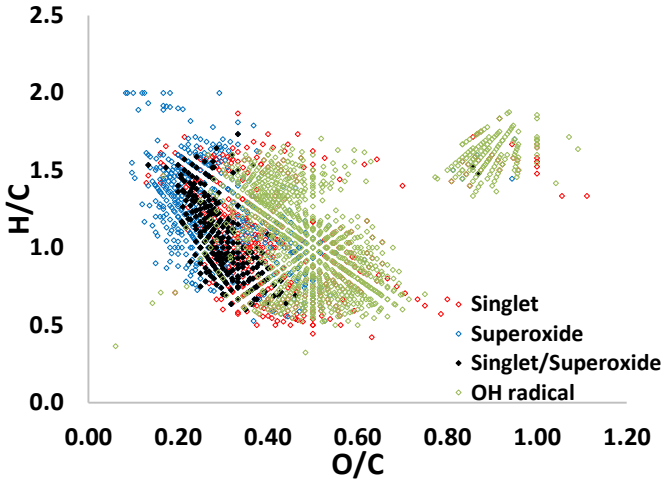

Fig. 15. Van Krevelen plot of CHO containing formulas lost from Dismal Swamp lignin extract after $^1O_2$ (red), $O_2^{-\bullet}$ (blue), and $^\bullet OH$ (green) exposure. Lost formulas common to both $^1O_2$ and $O_2^{-\bullet}$ are shown in black.

4. DISCUSSION

4.1 Lignin extract from Dismal Swamp is representative of terrestrially-derived dissolved organic matter

The abundance of formulas common to the lignin extract and to DOM from Dismal demonstrate that both are enriched in organic matter associated with lignin and lignin breakdown products. This is consistent with the source of DOM in the Dismal Swamp, Virginia. In this system, DOM is derived mainly from the decaying vegetation in an ombrotrophic peat (Hartman et al., 2015). Rain water permeates through the peat, comprised mostly of woody plant remains, and extracts organic matter with characteristics similar to the organic matter in the peat. Because most of this decaying vegetation in the peat is wood, there is a substantial component of the DOM in Dismal Swamp derived from lignin (Sleighter and Hatcher, 2008). The lignin extract therefore

is representative of organic matter prior to dissolution of decaying woody debris and export to sunlit surface waters where DOM may be altered by ROS.

4.2 Alteration of lignin extract by $^1O_2$

Upon exposure to $^1O_2$ generated by Rose Bengal, the base extracted lignin changed in composition in a manner consistent with oxidative degradation as measured by both FTICR-MS and GCxGC-TOF-MS following TMAH thermochemolysis compared to the dark and light controls (Fig. 10). One of the largest changes in composition was a change in the phenol biomarkers vanillic acid and vanillin, commonly designated as G6 and G4, respectively (McKinney et al., 1995). The much greater (Ad/Al)v ratio in the replicate $^1O_2$ treated lignin (Fig. 9) compared to dark and light controls was consistent with photo-oxidized lignin (Opsahl and Benner, 1998). Previous work demonstrated that with increasing organic matter oxidation the amount of the more oxidized acidic lignin phenol components (vanillic and syringic acids) increases relative to the corresponding less oxidized aldehydes (vanillin and syringealdehyde) (Hedges and Ertel, 1982; Opsahl and Benner, 1998). Consistent with the results of the TMAH analysis, many new formulas were identified via FTICR-MS in the +Rose Bengal treatment compared to the dark and light controls suggesting oxidation of lignin phenolic units.

The new formulas produced in the +Rose Bengal treatment identified by FTICR-MS are predominantly grouping in the tannin-like region and in the upper H/C portion of the lignin region (Fig. 11). The tannin-like formulas observed following exposure to $^1O_2$ in the +Rose Bengal treatment were not abundant in the initial lignin, suggesting that these formulas are most likely oxidized lignin compounds. Consistently, previous work demonstrated that $^1O_2$-oxidation of terrestrially-derived DOM resulted in production of formulas plotting in the same high H/C region of the lignin-like compounds as the new formulas identified here (Cory et al. (2010). While the

new formulas in this study plotting in the lignin-like region are in good agreement with products of $^1O_2$-oxidation of terrestrially-derived DOM identified by Cory et al. (2010), no tannin-like compounds were observed at higher O/C values in their study due to quenching of these formulas by the presence of high concentrations of Rose Bengal used to selectively react DOM with $^1O_2$.

Additionally, the KMD analyses consistently showed new formulas produced indicative of additions of oxygen and carboxyl groups (Fig. 12). Because addition of oxygen atoms alone would not add to COOH series, the generation of a greater number of COOH groups suggests possible opening of the aromatic ring associated with lignin (Fig. 16). This potential ring-opening scheme shows the depolymerization and demethylation of lignin followed by cleavage of the aromatic ring, resulting in carboxylic acid containing compounds as suggested in previous work involving $^{\bullet}OH$ (Waggoner et al., 2015). Loss of these carboxyl groups and subsequent condensation could also be responsible for the new formulas observed in the aromatic portion of the tannin-like region that were not observed in the starting lignin extract (Waggoner et al., 2015).

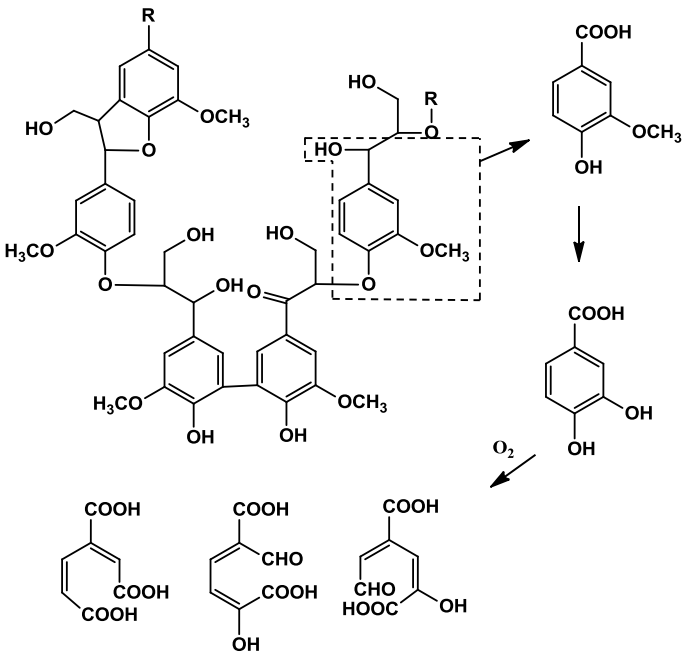

Fig. 16. Reactions of lignin induced by radical-initiated enzymatic processes in soils. The main reactions are those described by Crawford and Crawford (1980).

It is possible that oxygenated peaks may have been present to some degree in the lignin prior to the $^1O_2$ exposure (i.e., prior to treatment with Rose Bengal). Differences in oxygenated peaks between dark or light control and $^1O_2$ exposed lignin could be due to lower ionization efficiencies or quenching by compounds in the control (unreacted) lignin compared to $^1O_2$ exposed lignin. However, increased oxygen functionality should yield compounds with greater ionization efficiencies, due to charge site availability. Therefore the presence of new formulas in the $^1O_2$-exposed lignin is consistent with formulas produced by reaction with $^1O_2$. Experimental replicates further support the presence of these new formulas, as well as the reproducibility of the analysis, with lignin extracts exhibiting 90 percent formula similarity between replicates (Sleighter et al., 2012).

The TMAH and FTICR results suggest that the alteration of the lignin extract was primarily due to reaction with $^1O_2$ as opposed to reaction of the lignin extract with other ROS. While the lignin extract likely produces ROS upon exposure to light (Appiani and McNeill, 2015; Grandbois et al., 2008; Latch and McNeill, 2006), light controls (containing no Rose Bengal) showed no changes in composition compared to dark controls. This result suggests no detectable alteration of the lignin extract from ROS generated by the lignin or from direct photo-degradation of the lignin extract. Little alteration was expected to result from the photochemical reactions initiated by the lignin extract because (1) absorbance by Rose Bengal was greater than the lignin extract in the region of maximum output of the light source used (400-700 nm), and (2) ROS production from the lignin extract was expected to be less than the production of $^1O_2$ by Rose Bengal, given that yields of photochemical production of ROS from terrestrially-derived DOM are highest in the UV (Mopper and Kieber, 2000) where output from the light source was relatively low. Consistent with the expectation that alteration of lignin extract should be highest in the +Rose Bengal treatment compared to the dark or light control, there was no significant differences in the (Ad/Al)v ratios between dark and light controls. Because no ROS would be expected to be produced by lignin in the dark control, this result indicates no detectable alteration of the lignin extract during the 48-hour light exposure from production of ROS by the lignin extract in the light control (Fig. 10).

4.3 Alteration of lignin extract by $O_2^{-\bullet}$

Exposure of the lignin extract to $O_2^{-\bullet}$ altered the composition of the lignin in different ways compared to $^1O_2$ exposure. The (Ad/Al)v ratio following $O_2^{-\bullet}$ exposure was less than half that of the $^1O_2$ –exposed lignin (Figures 2, 5), suggesting that $O_2^{-\bullet}$ exposure resulted in less oxidative degradation as measured by TMAH thermochemolysis. The (Ad/Al)v values obtained from the direct addition of solid potassium superoxide to the lignin extract were much higher than the $O_2^{-\bullet}$

treatment in DMSO, suggesting oxidative degradation similar to exposure to $^1O_2$. This observation is consistent with evidence in the literature that $^1O_2$ is likely generated when potassium superoxide is added directly to aqueous solution (Khan, 1981) and demonstrates the value of the $O_2^{-\bullet}$ in DMSO treatment as an approach to isolate the effects of $O_2^{-\bullet}$ and $^1O_2$.

As was found for the $^1O_2$ –exposed lignin, $O_2^{-\bullet}$ exposed lignin shows new formulas plotting in the higher O/C ratio region of the van Krevelen plot typically associated with tannin-like compounds (Fig. 11). While the (Ad/Al)v ratio obtained for the $^1O_2$ exposed lignin suggests addition of oxygen to the lignin structure consistent with these higher O/C formulas, the much lower (Ad/Al)v ratio in the $O_2^{-\bullet}$ exposed lignin suggests that oxidative degradation may not be the only mechanism of alteration of lignin by $O_2^{-\bullet}$. In addition to oxidation, $O_2^{-\bullet}$ mediated reactions with lignin may lead to loss of the methoxyl group from lignin via demethylation reactions to form catechol-like structures (Crawford, 1981). Catechols and their derivatives can undergo ring opening and carboxylation upon reaction with $O_2^{-\bullet}$, (Lee-Ruff et al., 1976), consistent with the production of high O/C formulas in the $O_2^{-\bullet}$ treatment.

A prominent alteration of lignin after $O_2^{-\bullet}$ exposure was that roughly 50% of the new formulas plot at a higher H/C ratio (H/C >1.40) in an area directly above the region associated with lignin. These new formulas have a substantially decreased DBE (5 down from 10) when compared to the conserved formulas (i.e., those common to treated and control lignin), and a modified aromaticity index (AI_{mod}) (Koch and Dittmar, 2006, 2016) value of 0.02. This result suggests substantially more aliphatic compounds containing oxygen functional groups in the $O_2^{-\bullet}$ exposed lignin compared to the control (Fig. 11). These finding are in good agreement with previous work suggesting that photo-degradation of terrestrially-derived DOM transforms unsaturated aromatics to more saturated compounds (Gonsior et al., 2009; Tremblay et al., 2007).

Production of O-containing aliphatics after exposure to $O_2^{-\bullet}$ is consistent with a small increase in the acid/aldehyde ratio compared to the controls (Fig. 13) because newly produced aliphatic formulas may no longer contain the methoxy phenol required for the (Ad/Al)v assessment of lignin degradation.

The KMD analysis indicates a high degree of oxygenation for $O_2^{-\bullet}$ exposed lignin compared to the control. For example, KMD analysis of oxygen shows numerous homologous series comprised of many formulas, with new formulas generally plotting at higher nominal masses within these series. This finding indicates that incorporation of oxygen into lignin formulas from $O_2^{-\bullet}$ exposure has little detectable effect on the (Ad/Al)v of the lignin. This result may be explained by the fact that many of the formulas contributing to the long oxygen series are those of the newly formed aliphatic formulas, and would therefore not influence the lignin phenol based (Ad/Al)v measurement. KMD analyses also provided evidence for the addition of carboxyl groups to lignin from $O_2^{-\bullet}$ exposure. Formation of carboxyl groups is consistent with reactions of $O_2^{-\bullet}$ with catechol-like compounds resulting in ring opening discussed above (Lee-Ruff et al., 1976). Closer examination of the KMD results also show that a large number of the new formulas in the carboxyl plot belong to series not observed in the initial lignin extract, suggesting that the structures of these formulas are not a simple transformation of pre-existing formulas by addition or removal of carboxyl or oxygen groups, but rather undergo multiple alteration steps.

The KMD for H_2 series demonstrates another possible alteration of lignin by $O_2^{-\bullet}$, where the addition of H_2 to conserved formulas results in new, more aliphatic, formulas with a lower DBE (Fig. 14). The plot shows that in some cases loss of H_2 from a conserved formula can also generate new non-aliphatic formulas (Fig. 14), suggesting that $O_2^{-\bullet}$ exposure may result in both hydrogenation as well as proton abstraction from lignin. Superoxide has been proposed to serve

as a proton-coupled electron shuttle in biological systems, typically involving trace metals (Afanas'ev, 1991; Miller et al., 2003); however, it may be possible that a similar mechanism is occurring in lignin extracts (Lee-Ruff et al., 1976; Sawyer and Valentine, 1981). If $O_2^{-\bullet}$ were acting as a proton shuttle capable of reacting with dienes, little production of condensed aromatic formulas would be expected. Previous work observed production of condensed aromatics from $^{\bullet}OH$ reaction with lignin derived DOM (Waggoner et al., 2015) and suggested that these formulas form through a Diels-Alder type cyclization mechanism (Waggoner et al., 2015). This mechanism could be quenched if the dienes required were protonated by $O_2^{-\bullet}$. The subsequently formed cation could then react with $O_2^{-\bullet}$ anion producing more aliphatic formulas observed with higher O/C ratios (Fig. 11).

4.4 Assessment of organic matter oxidation by ROS in natural waters

The findings from this and previous studies suggest that $^1O_2$, $O_2^{-\bullet}$, and $^{\bullet}OH$ interact with different classes of terrestrially-derived organic matter (Fig. 15). Superoxide appears to react with, and eliminates formulas having the lowest O/C ratios and lowest average mass (460 m/z), followed by $^1O_2$ (513 m/z) and $^{\bullet}OH$ (585 m/z). The mass trend could suggest that sterical considerations play some part in the reactivity; however, closer inspection of the formulas likely selectively transformed by each ROS indicate that differences in the number of oxygen atoms in the formulas account for most of the selectivity, with carbon contents remaining relatively constant (26-28 carbons) for the formulas removed. Previous work also suggests that the reactivity of ROS with DOM may depend on oxygen content (Cory et al., 2010).These findings may suggest that compounds containing fewer oxygen atoms are most activated toward reaction with $O_2^{-\bullet}$, allowing for the addition of O_2, carboxylation, and ring opening. The formulas removed by $^1O_2$ are characterized as having a greater number of oxygen atoms, and higher DBE relative to those

removed by $O_2^{-\bullet}$, suggesting that $^1O_2$ is reacting with the more oxygen substituted components present in the lignin extract. A greater reactivity of $^1O_2$ toward oxygenated aromatics is also supported by the increased (Ad/Al)v ratio observed following TMAH when compared to $O_2^{-\bullet}$ (Figures 2, 6). Lastly, data obtained from previous work (Waggoner et al., 2015) indicates that $^{\bullet}OH$ is reacting with and removing formulas with the greatest overall mass, greatest number of oxygen atoms, and roughly equivalent DBE to those removed by $^1O_2$. An increase in oxygen functionality, particularly hydroxyl group substitution on aromatic systems, has been demonstrated to increase $^{\bullet}OH$ scavenging in certain types of compounds (Cao et al., 1997; Wang et al., 1997). We suggest that compounds present within the lignin extract also show an increase in radical scavenging ability as the amount of oxygen functionality increases. These findings are in good agreement with previous work showing the antioxidant properties of humic acids (Aeschbacher et al., 2012), as well as soil permafrost DOM (Ward and Cory, 2016). It is also possible that the increased oxygen functionality from exposure to $^1O_2$ and $O_2^{-\bullet}$ may in turn enable further reaction with $^{\bullet}OH$ and the generation of condensed aromatics and CRAM-like molecules.

4.5 Comparison to alteration of DOM in natural waters

Many studies have concluded that a substantial fraction of the large quantity of terrestrial DOM annually exported to the oceans (0.4×10^{15} g of C) must be altered during transport from rivers to coastal and open marine waters (Andrews et al., 2000; Cory et al., 2014). As DOM is transported from rivers to coastal waters, DOM composition shifts from higher molecular weight, more aromatic compounds, into lower molecular weight aliphatic compounds (Opsahl and Benner, 1998; Tremblay et al., 2007). Findings from this study on the effects of ROS on lignin are generally consistent with observed modification of terrestrially-derived DOM composition along the river

to marine transect. For example, net changes in lignin composition from reactions with all ROS are a decrease in molecular weight ($O_2^{-\bullet}$ and $^{\bullet}OH$) and a shift to more aliphatic formulas (all ROS).

Further evidence for the role of ROS in transforming terrestrially-derived DOM during export from land to water is that many formulas produced by reaction of lignin with each ROS have been detected in riverine DOM draining the Dismal Swamp (Sleighter et al., 2010). For example, 78 % of the formulas produced by reaction of lignin with $O_2^{-\bullet}$ were also identified in riverine DOM. For $^1O_2$ and $^{\bullet}OH$, 45 % and 20 % of formulas generated by reaction of lignin with these ROS, respectively, matched formulas in riverine DOM. However, it is important to note that formula match only identifies potential products of ROS in riverine DOM given that there likely exist multiple pathways that produce the same formulas. In addition, there may be large structural differences between these formulas, as it is possible to have many isomers for a given formula (Sleighter and Hatcher, 2011).

These findings may also have implications for use of proxies to detect contributions from lignin in marine DOM. For example, ca.18% of the total CHO formulas in coastal or offshore marine DOM match those produced by exposing lignin to either $O_2^{-\bullet}$ or $^1O_2$. These matching formulas in the coastal or offshore marine DOM, predominantly aliphatic in nature, are not typically attributed to terrestrially-derived organic matter because they differ in composition from formulas associated with lignin (Figure 17). Our results suggest that some biomarker proxies for lignin may under-estimate contributions from inputs of terrestrially-derived DOM that has been altered by ROS.

While results of this study provide information on potential transformations of terrestrially-derived DOM by ROS, it is not possible to relate these findings to the relative importance of each ROS in transforming DOM in natural waters. For example, photochemical

transformations of DOM by each ROS depend on the apparent quantum yield for production of each ROS (which can vary by at least an order of magnitude for most ROS (Andrews et al., 2000; Page et al., 2014; Peterson et al., 2012; Powers and Miller, 2014; Vaughan and Blough, 1998). In addition, at present it is difficult to quantitatively evaluate the relative importance of each ROS studied here on DOM composition due to potential heterogeneous concentrations of ROS within DOM (Latch and McNeill, 2006), as well as presence of quenchers such as salts or carbonates that may influence reactions of ROS with DOM along the riverine to marine transect (Burns et al., 2010).

Table 1. Percentage of new formulas from each ROS experiment found at various sampling locations along a transect spanning from the Elizabeth River to off the coast of VA. Data used for comparison based on Sleighter et. al. (2010).

	% New Formulas Matching		
Transect Location	$O_2^{-\bullet}$	$^1O_2$	$^\bullet OH$
Dismal Swamp (DS)	48.6	34.4	11.9
Great Bridge (GB)	46.3	21.8	9.8
Town Point (TP)	60.6	26.5	9.4
Chesapeake Bay (CBB)	33.0	17.7	5.5
Offshore Coastal (OSC)	14.7	9.9	1.1
No Match	21.9	54.9	79.7

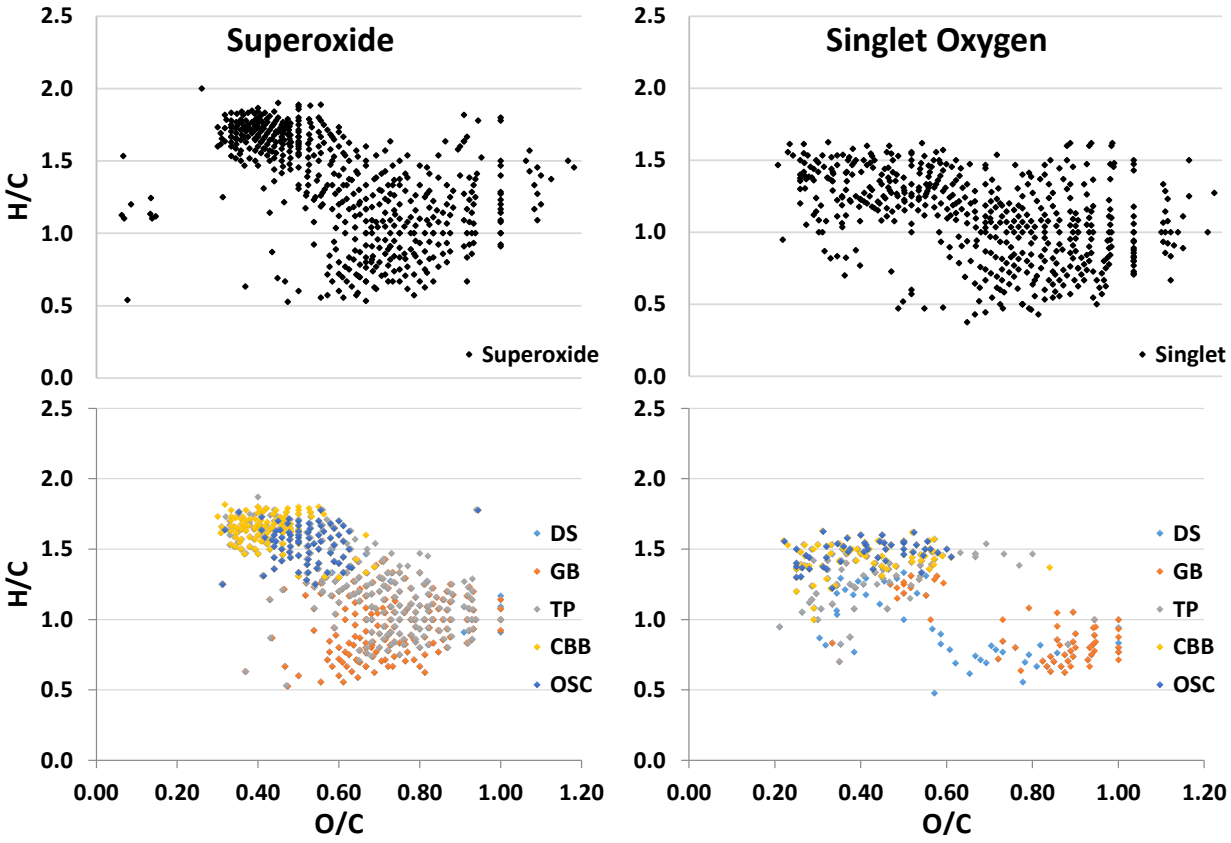

Fig. 17. Superoxide newly produced CHO formulas (Top left) with matching formulas from transect study (Lower left), along with new CHO formulas from singlet oxygen (Top right) and corresponding matches to transect data (Lower right). Transect data is displayed from inland at the Dismal Swamp (DS) to Virginia off shore coastal (OSC).

5. CONCLUSIONS

The work described here demonstrates potential molecular level alteration of lignin by the primary ROS encountered upon export from terrigenous systems. Each ROS studied here, or in previous work, is produced both in the light and in the dark by DOM in natural waters (Appiani and McNeill, 2015; Cory et al., 2010; Diaz et al., 2013; Garg et al., 2011; Page et al., 2013; Page

et al., 2014). Findings from this study suggest that each ROS may selectively transform lignin, and indicate that differences in the number of oxygen atoms in the formulas account for most of the selectivity between ROS with lignin. Substantial matches in formulas between ROS-transformed lignin with riverine and marine DOM are consistent with prior work concluding that ROS are important in altering terrestrially-derived DOM composition during riverine export (Andrews et al., 2000; Cory et al., 2009; Cory et al., 2010; Cory et al., 2014; Page et al., 2014; Peterson et al., 2012; Ward and Cory, 2016), resulting in DOM that is of lower molecular weight and more aliphatic compared to lignin. Overall, our study provides insight into the modification of DOM by the dominant ROS, and how the input of terrestrial DOM to coastal waters may be masked by such modification.

CHAPTER IV

HYDROXYL RADICAL ALTERATION OF HPLC FRACTIONATED LIGNIN: FORMATION OF NEW COMPOUNDS FROM TERRESTRIAL ORGANIC MATTER

PREFACE

The content of this chapter has been submitted to Organic Geochemistry

1. INTRODUCTION

Terrigenous organic matter is typically viewed as an assemblage of organic biomolecules from plant remains at various stages of decomposition, and includes carbohydrates, proteins, lignin, tannins, and plant cuticular substances. While the plant biopolymer lignin accounts for roughly 25% of all terrigenous biomass, and is viewed as the most refractory marker for terrigenous organic matter, the phenolic biomarkers used to ascertain the presence of lignin are often lost rapidly in soils (Thevenot et al., 2010), sediments (Hedges and Keil, 1995; Hedges et al., 1997), and dissolved organic matter (DOM) (Opsahl and Benner, 1997). Previous studies have highlighted photochemical and biogeochemical transformations as major removal pathways of tDOM, and particulate organic matter (POM), as it is transported to the oceans from the continents (Bianchi (2011) and references therein). The principal analytical techniques used to quantitatively evaluate the presence of lignin biomarkers are based on oxidative/pyrolytic methods that break down the lignin polymeric structure to monomers and dimers that are readily analyzed chromatographically (Hatcher et al., 1995). Loss of these lignin-derived monomers is frequently interpreted to mean that lignin is oxidized, or more often, completely mineralized. It has recently been suggested that a significant portion of the lignin is not lost via complete mineralization, but

is transformed by reactive oxygen species (ROS) in concert with transition metals, such as Fe, to organic matter unrecognizable as having terrestrial origins, becoming integrated into DOM (Chen et al., 2014) and sedimentary organic matter (Koch and Dittmar, 2016). We hypothesize that this process occurs during tDOM and POM transit through sunlit rivers, estuaries, and coastal waters, and significantly influences the identification of terrestrial organic matter in these systems.

In recent work by Waggoner et al. (2015), part of a larger effort to understand the impact that molecular reorganization has on the export of terrestrial carbon to the oceans, it is proposed that lignin may be transformed via oxidation reactions, through ring-opening and condensation reactions, to molecules that no longer resemble lignin. Formulas characteristic of condensed aromatic like, and alicyclic like compounds have been observed upon exposing a lignin extract to hydroxyl radical ($^{\bullet}OH$) (Waggoner et al., 2015), as well as a DOM photoirradiation study, where new formulas were largely attributed to ROS-induced alteration (Chen et al., 2014). While these studies demonstrated the formation of new compounds in complex mixtures following ROS exposure, the specific types of compounds being altered into condensed aromatic and alicyclic formulas were not determined. By examining the molecular characteristics of DOM produced from lignin that has undergone decomposition in a terrestrial environment by brown rot fungi, some of the complexity associated with analysis of whole DOM is partially avoided. These fungi, partially through the action of ROS, degrade wood and plant tissues by selectively decomposing the cellulosic components associated with biomass, while minimally altering the lignin (Hatcher, 1987). Processes affecting the alteration of lignin contained within DOM may prove to be similar in nature to those that impact the larger pool of terrigenous DOM. For example, Grinhut et al. (2011) recently showed, using ultrahigh resolution mass spectrometry, that wood degrading organisms employing ROS can oxidize natural organic matter (in the form of humic substances)

in much the same way as they degrade lignin, through oxidation, ring-opening, and depolymerization resulting in a loss of average molecular weight.

The highly complex nature of DOM, however, makes it difficult to determine what properties within lignin-derived organic matter may contribute to its alteration to compounds no longer recognizable as having lignin origins. To improve characterization of DOM, past studies have utilized reverse phase high performance liquid chromatography (RP-HPLC) to separate DOM components with differing physiochemical properties prior to characterization by ultrahigh resolution Fourier transform ion cyclotron resonance mass spectrometry (FTICR-MS) analysis (Aeschbacher et al., 2012; Liu et al., 2011; Ward and Cory, 2016). The current study will adopt this combined HPLC, FTICR-MS approach to fractionate and characterize lignin derived DOM, with the goal of determining the origin of new compounds observed in previous laboratory studies (Waggoner et al., 2015) where whole lignin extracts were subjected to $^{\bullet}$OH attack.

Hydroxyl radical is an unselective oxidant known to react with DOM through a number of mechanisms, including addition to olefins and aromatic components, H abstraction, and electron transfer reactions (Goldstone et al., 2002; Walling, 1975; Wenk et al., 2011). Addition of $^{\bullet}$OH directly to organic matter has been shown to not only hydroxylate compounds, but also cleave side chain groups resulting in low molecular weight acids being commonly observed following DOM reaction with $^{\bullet}$OH (Goldstone et al., 2002; Walling, 1975). While not commonly observed, electron transfer reactions involving $^{\bullet}$OH are believed to result in organic radical cations capable of generating new products through dimerization reactions (Walling, 1975). Under laboratory conditions, $^{\bullet}$OH has additionally been shown to cause significant alteration of lignin derived DOM, generating a suite of compounds not typically associated with terrigenous organic matter including alicyclic and condensed aromatic-like compounds (Waggoner et al., 2015).

Although there exist a number of studies emphasizing the importance of ROS, including •OH, in transforming DOM in environmental systems, there is limited information on how individual ROS alter DOM composition, and to what extent components having different physiochemical properties within DOM are modified. In an effort to further our understanding of •OH alteration of tDOM, lignin-derived DOM was separated into fractions based on polarity by RP-HPLC, and were then individually exposed to •OH under controlled laboratory conditions. The molecular level alterations specific to each fraction were then tracked using FTICR-MS to better understand the properties mediating DOM transformation by •OH.

2. MATERIALS AND METHODS

2.1 Lignin extraction

A lignin extract, representing tDOM, was prepared from a brown rot fungal degraded wood, Atlantic white cedar (*Chamaecyparis thyoides)*, collected from the Great Dismal Swamp in Virginia as described by Liu et al. (2011); Waggoner et al. (2015). Briefly, the sample was freeze dried and ground to a fine powder before 24 hour extraction in 0.01M NaOH. The lignin extract was then filtered through a 0.7 μm glass fiber filter to remove all solids prior to reverse-phase HPLC separation.

2.2 Reverse-phase HPLC Separation of lignin extract

Separation of the alkali-soluble lignin extract was carried out using a Shimadzu Prominence 20 series HPLC. The lignin extract, approximately 400ppm C, was injected onto a C_{18} column (5 μm, 250 x 4.6 mm, Alltima). Water (MilliQ) and Methanol (HPLC grade, Fisher Scientific) were used as the binary mobile phase, with a constant flow rate of 1mL/min and an oven temperature of 40°C. The gradient consisted of 5% methanol from 0-5 minutes, ramping to

30% from 5-6 min, held at 30% 6-8 min, ramping to 50% from 8-9 min, held at 50% 9-13 min, ramping to 100% methanol 13-16 min and holding at 100% 16-25 min. The gradient was then ramped back to 5% methanol from 25-28 minutes and held at 5% until the next injection for a total run time of 35 minutes. Peaks were detected using a Shimadzu SPD-M20A photodiode array (PDA) detector and collected via automated fraction collector. Peak areas for multiple-wavelengths (210-410 nm) were calculated using Shimadzu LCsolutions software, and used to estimate the percentage of the total lignin extract represented by each fraction, assuming similar molar absorptivity for all fractions. Approximately 6 mL of lignin extract was processed through the HPLC, collecting 8 fractions for analysis. Following collection, the fractions (80-100 mL) were frozen and freeze dried.

2.3 Lignin extract reaction with ˙OH

Freeze dried samples of each HPLC fraction were weighed out (0.32-0.52 mg) and dissolved in 0.5 mL MQ water. A 200 μL aliquot of each solution was taken to characterize the initial fractions prior to hydroxyl radical exposure. Each solution was passed through a small amount of extensively washed Dowex 50Wx8 (H-form) cation exchange resin to remove any salts remaining from the extraction. An additional 250 μL of liquid chromatography-MS (LC-MS) grade methanol was eluted through the resin and added to each fraction, resulting in a roughly 50:50 water:methanol (v/v) used for FTICR-MS analysis.

The remaining solution (300 μL) for each fraction was then exposed to ˙OH generated via Fenton chemistry. Each fraction was adjusted to pH 3 using HCl to which a 100 μL solution of $FeSO_4$ was added, giving a final iron (II) concentration of 40 ppm. The addition of 30% hydrogen peroxide (50 μL) initiated the reaction. After 1 hour, all samples were passed through cation resin

as described above. To aid in detection, all •OH exposed samples were freeze dried and redissolved in 200 μL LC-MS grade methanol.

2.4 FTICR-MS analysis

Initial fractions, along with •OH treated fractions, were analyzed using a Bruker 12T Apex Qe FTICR-MS, housed in the College of Sciences Major Instrument Cluster at Old Dominion University (Cosmic). All samples were continuously infused via syringe pump at a rate of 120 μL hr^{-1}, into an Apollo II electrospray ionization (ESI) source, operated in the negative ionization mode. ESI voltages were optimized for each sample to give spray shield and capillary currents between 180-220 nA and 18-45 nA respectively. Ions were accumulated for 0.5-1.0 s in a hexapole prior to transfer to the ICR cell for detection. For each sample, 300 transients were collected using a 4 MWord time domain and co-added. Using Bruker Daltonics Data Analysis software, the resulting free induction decays (FID) were zero-filled and Sine-Bell apodized before undergoing fast Fourier transform and magnitude calculations.

Following Sleighter and Hatcher (2008), each mass spectra was externally calibrated using polyethylene glycol (PEG), and internally calibrated using fatty acids, dicarboxylic acids, and CH_2 compounds belonging to homologous naturally present in the samples. An in house written MATLAB script was used to assign unique molecular formulas to peaks having a signal to noise (S/N) threshold of 3 based on (Sleighter et al., 2012), and according to the criteria $^{1}H_{5\text{-}100}$ $^{16}O_{1\text{-}30}$ $^{14}N_{0\text{-}6}$ $^{32}S_{0\text{-}2}$ $^{34}P_{0\text{-}2}$, with subscripts indicating the range of each atom allowed for a single formula. All formulas assigned must conform to rules outlined in Stubbins et al. (2010), and were screened by Kendrick mass defect series (CH_2, H_2, CO_2, and O_2) to select for ambiguously assigned

formulas (Kujawinski and Behn, 2006). The exact masses of all formulas assigned are within 1 ppm error of the measured m/z.

3. RESULTS

3.1 HPLC separation of lignin extract

The PDA detector shows the major absorbance peaks in the initial alkali-soluble lignin extract occur in the UV region between 190 and 410 nm, with Figure 18 depicting a representative PDA plot and HPLC chromatogram collected at an absorbance of 260 nm. The fraction collection intervals for the lignin extract (F1-F8), are additionally designated in Figure 18. Multiple injections of the lignin extract demonstrate a high reproducibility, with peak retention times across HPLC chromatograms showing very little variation. The relative polarity of the lignin extract peaks (Fig. 18) can be broadly categorized based on the elution solvent at the time of detection, with fraction 1 (F1) eluting in 95% water: 5% methanol, constituting the most polar/hydrophilic peak present in the lignin extract. The subsequent fractions, F2-F3, which eluted with 95% water: 5% methanol, decreasing to 70% water: 30% methanol are slightly less hydrophilic. An intermediate polarity set of peaks, F4-F6, were then eluted using equal parts water and methanol, followed by the most non-polar/ hydrophobic peaks F7-F8, eluting with 100% methanol.

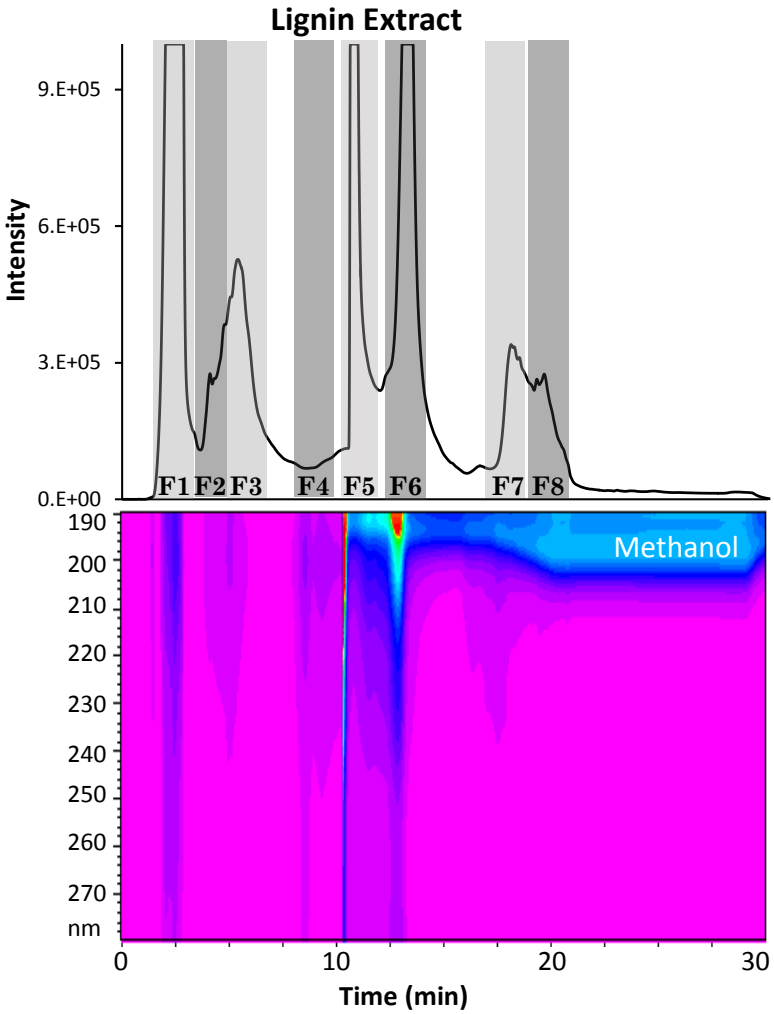

Fig. 18. HPLC chromatogram (UV at 260 nm) and PDA (190-450 nm) plot of Dismal swamp lignin extract, with fractions (F1-F8) displayed in gray.

To roughly estimate the percentage of the whole lignin extract represented by each fraction, the absorbance between 210-410 nm was calculated for each peak (F1-F8) and compared to the total absorbance for a given HPLC run. Figure 19 shows the percentage of total absorbance relative to the whole lignin extract for each fraction, with approximately 86% of the total absorbance accounted for by F1-F8. Roughly 50% of the total absorbance is from F5-F6, suggesting these

fractions may contribute more to the total sample, assuming there is similar molar absorptivity between lignin extract fractions. The first fraction (F1) accounts for an additional c.a. 12% of the total absorbance, and therefore likely represents a significant portion of the lignin extract as well. Fractions F2, and F8 combine for only c.a. 4% of the total absorbance, suggesting these are likely a relatively small component of the initial lignin extract.

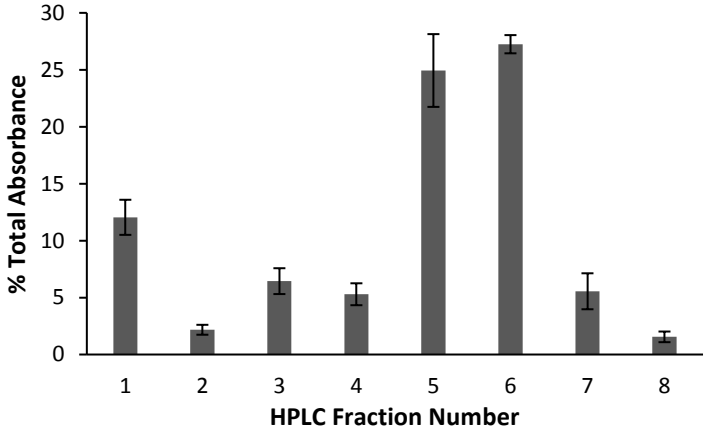

Fig. 19. Percentage of total absorbance for each fraction of the lignin extract. Values obtained based on total peak area between 210-410 nm, with error bars showing standard deviation for three injections.

3.2 FTICR-MS analysis of HPLC fractionated lignin extract

The elemental formulas generated from ESI-FTICR-MS data illustrate the molecular characteristics for each fraction of the lignin extract, displayed in Figure 20 as points on van Krevelen diagrams, by plotting the atomic H/C vs O/C ratios of the formulas assigned. Fractionation of the lignin extract resulted in the assignment of 4457 molecular formulas, 3554 of which contained only C, H, and O atoms (~80%), compared to the whole lignin extract, where ~87 % (2623) of the 3030 formulas assigned were comprised of only C, H, and O atoms. The region of the van Krevelen diagram typically associated with lignin-like formulas plots between H/C values of 0.5-1.5, and O/C values of 0.20-0.60 (Sleighter and Hatcher, 2008), and is well represented in each of the fractions collected.

Figure 20 shows that formulas assigned for the first HPLC fraction (F1), while partially plotting in the area of the van Krevelen diagram typical of lignin, largely trend toward high O/C values, consistent with being the most polar of the fractions collected. Fractions 2-3 were not well resolved by HPLC, and are therefore very similar in composition, having a number of formulas with O/C values greater than 0.60, the upper range associated with lignin, and relatively hydrophilic in character. The intermediate polarity lignin extract peaks, F4-F6, are centered within the lignin region of van Krevelen space. The remaining two fractions, F7-F8, shift to lower O/C values (< 0.20) and higher H/C values (>1.5) than is typically observed for lignin, suggesting more aliphatic characteristics and commensurate with being the most hydrophobic of the lignin extract fractions.

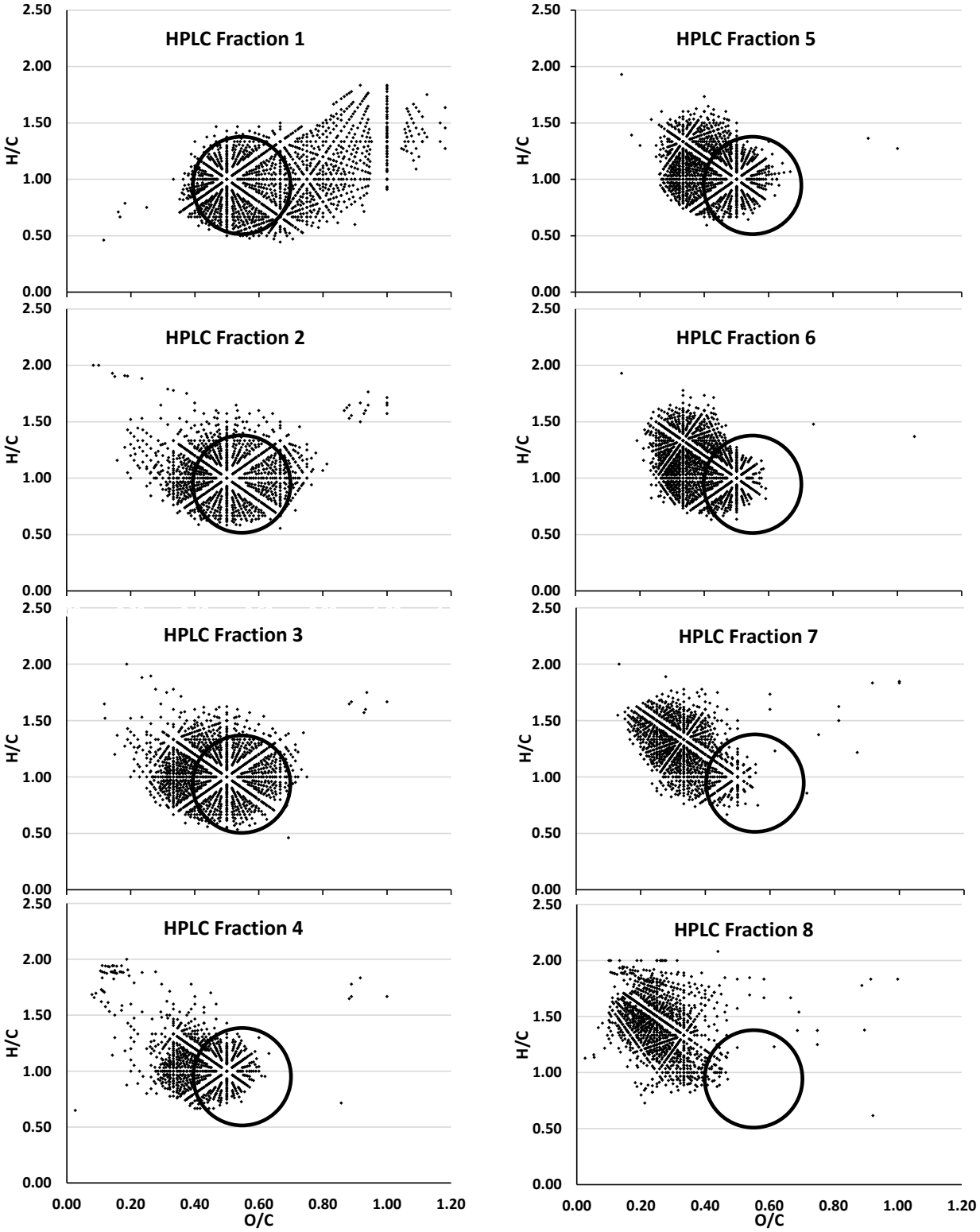

Fig. 20. Van Krevelen plots of CHO formulas for HPLC fractions 1-8 of the lignin extract. The black circle is a reference to visualize changes between fractions.

These trends can be further illustrated upon examination of the formulas assigned in both the whole lignin extract, and the individual HPLC fractions of the lignin extract. Displayed in Table 2 are the total numbers of assigned formulas for the whole lignin extract and HPLC fractions, along with their peak magnitude weighted average m/z, O/C, H/C, and modified aromaticity index (AI_{mod}) values (Aeschbacher et al., 2012; Sleighter and Hatcher, 2008). The initial lignin extract resulted in approximately 3000 assigned formulas, having magnitude-weighted m/z (471), and O/C values (0.55) that fall in the middle of values obtained for the HPLC fractions. Following HPLC separation, the highest weighted average m/z (552) was calculated for F6, with the lowest m/z (438) present in F8. Although no clear mass trend is observed for the lignin fractions, the magnitude-weighted O/C values show a steady decline from 0.66 in F1 to 0.24 in F8, consistent with a change from more hydrophilic to more hydrophobic properties with increasing fraction number. The H/C values remain relatively constant from F1-F6 (~1.08) before increasing to 1.66 in F8, suggesting an increase in the aliphatic characteristics in fractions F7-F8. The AI_{mod} shows a general increasing trend over F1-F6 (0.31-0.38) indicating an increase in aromaticity, before diminishing to 0.16 in F8, supporting the presence of formulas with more aliphatic characteristics. The decreasing O/C values and relatively constant H/C values for lignin fractions F1-F6 could suggest that oxygen substitution is the primary difference in these fractions. The inverse relationship of a decreasing O/C with an increasing AI_{mod} for F1-F6 could also indicate oxidation is largely occurring to olefinic components present within the lignin extract, as lower AI_{mod} values suggest the presence of fewer double bonds in a given formula (Koch and Dittmar, 2006). F7 and F8 do not display the same trend as F1-F6, having the lowest AI_{mod} and O/C values combined with the highest H/C values, indicating more saturated formulas with less oxygen substitution.

Table 2. FTICR-MS data for whole lignin extract (LE), HPLC fractionated LE (F), and hydroxyl radical (HR) reacted HPLC fractions. Values displayed are magnitude weighted with errors representing the standard deviation for all formulas assigned.

Fraction	Formulas	m/z	O/C	H/C	AI_{mod}
LE	3030	471 ± 108	0.55 ± 0.22	1.07 ± 0.33	0.34 ± 0.28
LE -F1	1673	490 ± 105	0.66 ± 0.19	1.07 ± 0.30	0.31 ± 0.22
LE -F2	1350	468 ± 104	0.50 ± 0.15	1.08 ± 0.30	0.35 ± 0.18
LE -F3	1600	485 ± 108	0.47 ± 0.14	1.08 ± 0.30	0.36 ± 0.18
LE -F4	1023	513 ± 104	0.41 ± 0.14	1.09 ± 0.29	0.37 ± 0.16
LE -F5	1505	538 ± 104	0.42 ± 0.13	1.07 ± 0.27	0.38 ± 0.17
LE -F6	1619	552 ± 109	0.39 ± 0.11	1.10 ± 0.28	0.36 ± 0.16
LE -F7	1267	499 ± 106	0.33 ± 0.10	1.27 ± 0.26	0.29 ± 0.15
LE -F8	1437	438 ± 123	0.24 ± 0.10	1.66 ± 0.31	0.16 ± 0.16
HR-F1	2437	574 ± 145	0.53 ± 0.33	0.74 ± 0.37	0.52 ± 0.31
HR-F2	1483	499 ± 126	0.65 ± 0.20	1.10 ± 0.33	0.28 ± 0.20
HR-F3	852	450 ± 127	0.55 ± 0.25	1.06 ± 0.38	0.38 ± 0.22
HR-F4	997	491 ± 115	0.60 ± 0.30	1.11 ± 0.44	0.31 ± 0.27
HR-F5	2825	521 ± 131	0.64 ± 0.19	1.02 ± 0.32	0.34 ± 0.23
HR-F6	2705	507 ± 138	0.57 ± 0.18	1.06 ± 0.32	0.34 ± 0.20
HR-F7	2562	478 ± 127	0.44 ± 0.17	1.28 ± 0.33	0.26± 0.22
HR-F8	1707	441 ± 112	0.38 ± 0.17	1.39 ± 0.32	0.22± 0.19

3.3 FTICR-MS analysis of •OH treated lignin extract fractions

Treatment of HPLC fractions F1-F8 with •OH resulted in 6632 total formulas being assigned, with 4643 (70%) containing only C, H, and O atoms. Figure 21 shows the molecular level alteration occurring to the CHO formulas for the individual + •OH treated fractions. The van Krevelen plot for F1 (Fig. 21), shows the removal of formulas having low O/C values (< 0.60) from the initial untreated lignin fraction, representing roughly 12% of the total absorbance (Fig.2), with the generation of new formulas plotting at higher O/C values, > 0.70, suggesting further addition of oxygen to the already polar formulas of F1. A second group of new formulas is also seen in F1, having H/C values less than 0.75, and O/C values less than 0.40, in an area commonly attributed to condensed aromatic-like formulas following •OH treatment. Using a conservative estimate for condensed aromatic formulas (AI_{mod} values > 0.67) (Koch and Dittmar, 2006, 2016), the low H/C, low O/C formulas in F1 show an average m/z of 680 (43 ± 5 C, 9 ± 4 O) compared to F1 m/z of 490 prior to •OH treatment (Table 2). The increase in m/z and AI_{mod} values observed in F1 can additionally be seen in Figure 22, showing formulas having an increase in carbon number and DBE, corresponding to an increase in AI_{mod} value, in the +•OH treated lignin extract vs. the initial fraction. While the magnitude weighted mass for the total •OH treated F1 fraction is comparatively lower (574 m/z) than the high AI_{mod} formulas, and likely has contributions from the addition of oxygen, the increase in mass to a value of 680 m/z for the formulas having AI_{mod} values >0.67 is not likely attributed to the addition of oxygen. It would be expected that addition of oxygen would occur at olefinic carbons, resulting in a decrease in DBE and increase in O/C value which is not observed for formulas having high AI_{mod} values. It has been suggested previously that the increased average molecular weight observed could also derive from cyclization reactions, resulting in the formation of condensed aromatic like formulas (Waggoner et al., 2015).

Hydroxyl radical treated fractions F2-F4 (Fig. 21) show similar trends as those observed in F1, with formulas having O/C values less than 0.60 being predominantly removed, with concurrent production of higher O/C formulas following exposure to •OH. While F2 has a number of initial formulas still present in the + •OH treated lignin extract, F3-F4, representing c.a. 12% of the lignin extracts total absorbance (Fig. 19), have few formulas remaining matching those of the untreated fractions (14% and 1% respectively). The nearly complete removal of CHO formulas initially present in the lignin extract suggests these fractions may be particularly susceptible to reaction with •OH. Of the new formulas observed in F3 (430 formulas) and F4 (675 formulas) following •OH treatment, c.a. 66% of those formulas in F3 and 57% in F4 match formulas present in other fractions of the lignin extract prior to •OH treatment.

Fractions F5 and F6, accounting for 25% and 27% of the total absorbance for the lignin extract, respectively (Fig. 19), did not show a large removal of formulas initially present for the + •OH treated lignin extract as observed in F3-F4, with greater than 60% of initial formulas still remaining. New formulas in the + •OH treated F5-F6 predominantly plot at higher O/C (>0.6), with a small subset in F5 having AI_{mod} values suggesting condensed aromatic-like formulas (>0.67), plotting at or below an H/C of 0.50 (Fig. 21). Formulas in F5 with high AI_{mod} values follow a similar trend to those in F1, having higher carbon number and DBE in the + •OH treated fraction that cannot be explained by the simple addition of oxygen (Fig. 22), but could potentially be attributable to cyclization/condensation reactions. Similar to F3-F4, a large percentage of new formulas generated following •OH treatment of F5 (863 formulas, 57%) and F6 (956 formulas, 66%) match those initially present in other fractions, indicating a possible origin for the high O/C formulas observed in the lignin extract.

The remaining two fractions F7-F8, represented the least polar components of the lignin extract, and accounted for c.a. 7% of the total absorbance observed (Fig. 19). Following treatment with •OH, F7 displayed the fewest number of initial formulas removed of any fraction tested (27%), suggesting F7 to be the most resistant fraction to modification by •OH (Fig. 21). Fraction F8 however, saw 60% removal of formulas initially present, predominantly oxygen poor (low O/C) and saturated (high H/C) formulas in the + •OH treated lignin extract. For new formulas produced in both F7 (1250 formulas) and F8 (705 formulas) following •OH exposure, 82% and 85% respectively match formulas present in other lignin extract fractions prior to •OH treatment.

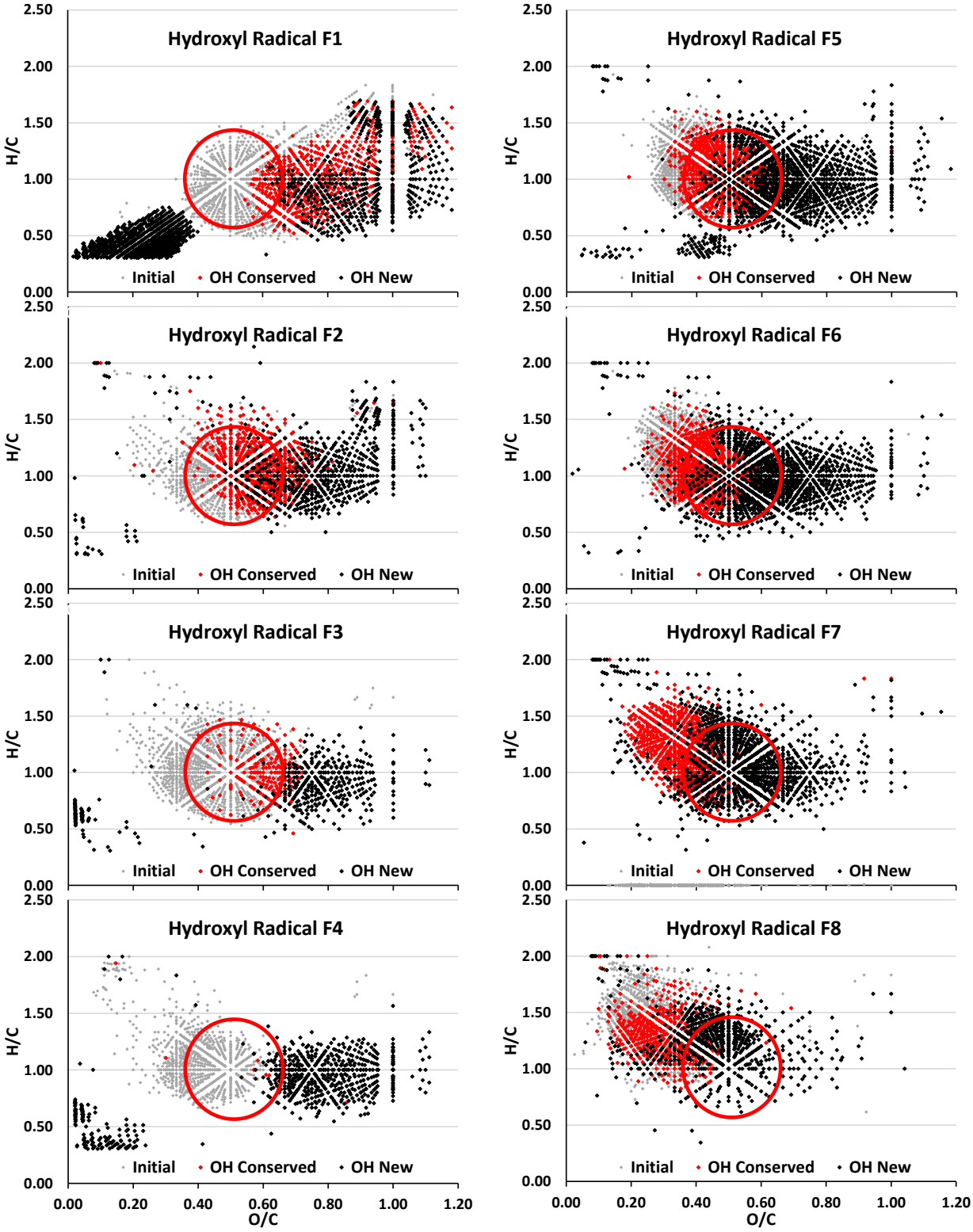

Fig. 21. Van Krevelen plots for Hydroxyl radical exposed HPLC fractions 1-8. Points shown are

CHO formulas for the initial fractions (grey), conserved (red), and newly produced (black), with the circle serving as a reference point for comparison.

The peak magnitude weighted average m/z, O/C, H/C, and AI_{mod} values for all + •OH treated lignin extracts are displayed in Table 2 for comparison to the initial lignin fractions. Following •OH exposure, most fractions (F3-F7) display a decrease in the magnitude weighted average m/z observed (3-7 %), while F1-F2 show an increase (7-13 %). With the exception of F1 that saw a c.a. 20% decrease in O/C values, all fractions displayed an increase in O/C values in + •OH treated fractions, ranging from c.a. 17% in F2 to 58% in F8. The observed increase in O/C can be attributed to both the addition of oxygen to initial formulas, as well as the removal of formulas with lower O/C values in + •OH treated lignin fractions. The H/C values for F2-F7 showed minimal change before and after •OH exposure (1-5 %), compared to F1 and F8 that were decreased by 31% and 17 % respectively. The decrease in H/C for F1 could largely be due to the presence of condensed aromatic-like formulas while F8 can be attributed to the removal of aliphatic formulas having H/C values > 1.5. Additionally an average decrease of 10% in AI_{mod} values was observed for F2-F7, suggesting a shift from more to less aromatic formulas in + •OH treated fractions. Fractions F1 and F8 however saw a 68% and 38% increase in AI_{mod} respectively, aligning with the removal of aliphatic formulas having low AI_{mod} values in F8, and the formation of condensed aromatic-like formulas in the case of F1. The observed trend of an increasing O/C combined with decreasing AI_{mod} could suggest addition of oxygen is primarily occurring on unsaturated carbons following •OH treatment. An increase in O/C could also be partially explained by the loss of small substituent groups from lignin formulas, consistent with the decrease in m/z and H/C observed in + •OH treated fractions.

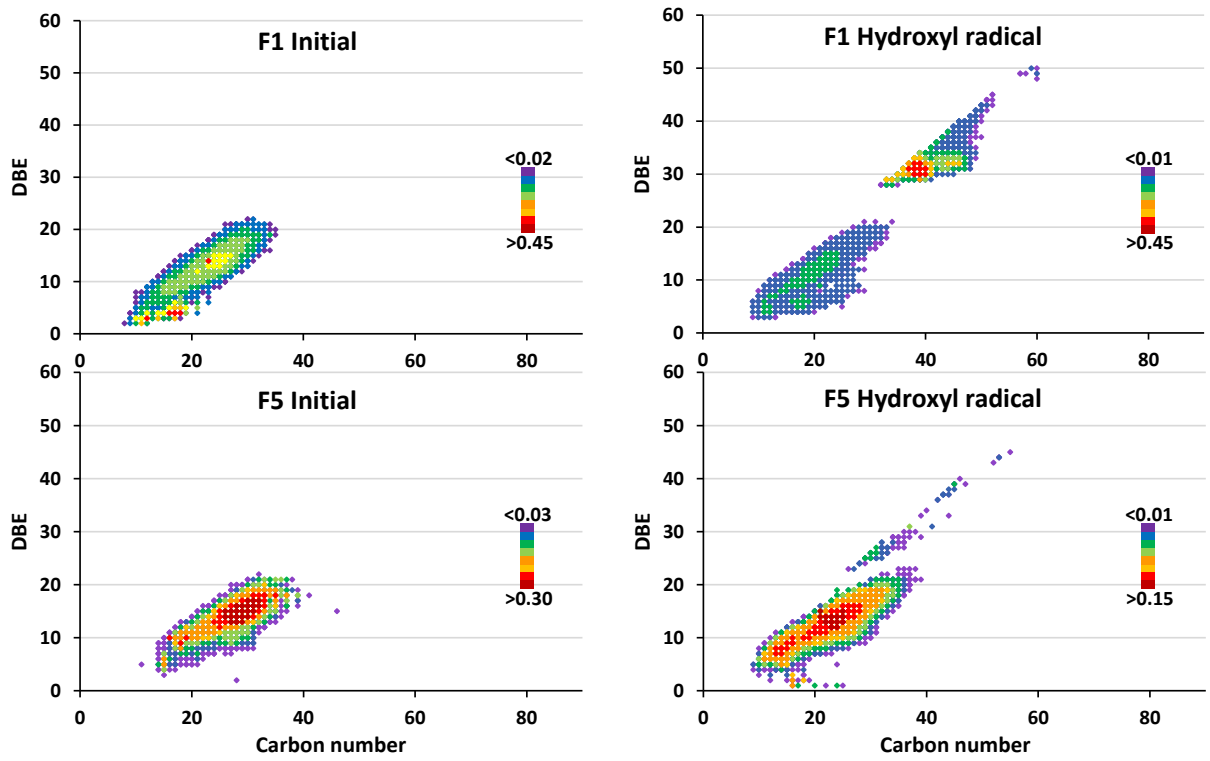

Fig. 22. Magnitude weighted double bond equivalent (DBE) vs. carbon number plots for the CHO containing formulas of fractions F1 (Top) and F5 (bottom) before (left) and after (right) ˙OH treatment.

3.4 Reactivity of ˙OH with lignin extract

The frequency at which formulas occur across all lignin extract fractions can additionally be used to gain insight into ˙OH mediated alteration of lignin. Figure 23 shows the number of fractions a formula was present in before and after ˙OH exposure. Data indicates that in the initial fractions, the most commonly occurring formulas were present in the lignin-like region centered at O/C 0.4 and H/C of 1.0 as expected. In the +˙OH treated fractions however, the most commonly occurring conserved formulas (those present in the initial fraction) are now centered at O/C 0.75 and H/C of 0.9 in an area typically associated with tannin-like formulas. This could suggest the

high O/C formulas initially observed are able to be generated from lignin formulas having a variety of physiochemical properties rather than from formulas attributed to a specific fraction. The frequency of new formulas formed in the +•OH treated fractions (Fig. 23) additionally suggest similar high O/C formulas can result from modification of all lignin fractions. Also displayed in Figure 23 is the frequency of formulas removed completely through reaction with •OH. Comparing to initial formulas present, formulas present in 3 or fewer fractions with O/C <0.6 were largely removed, whereas the most frequently present lignin-like formulas show incomplete removal.

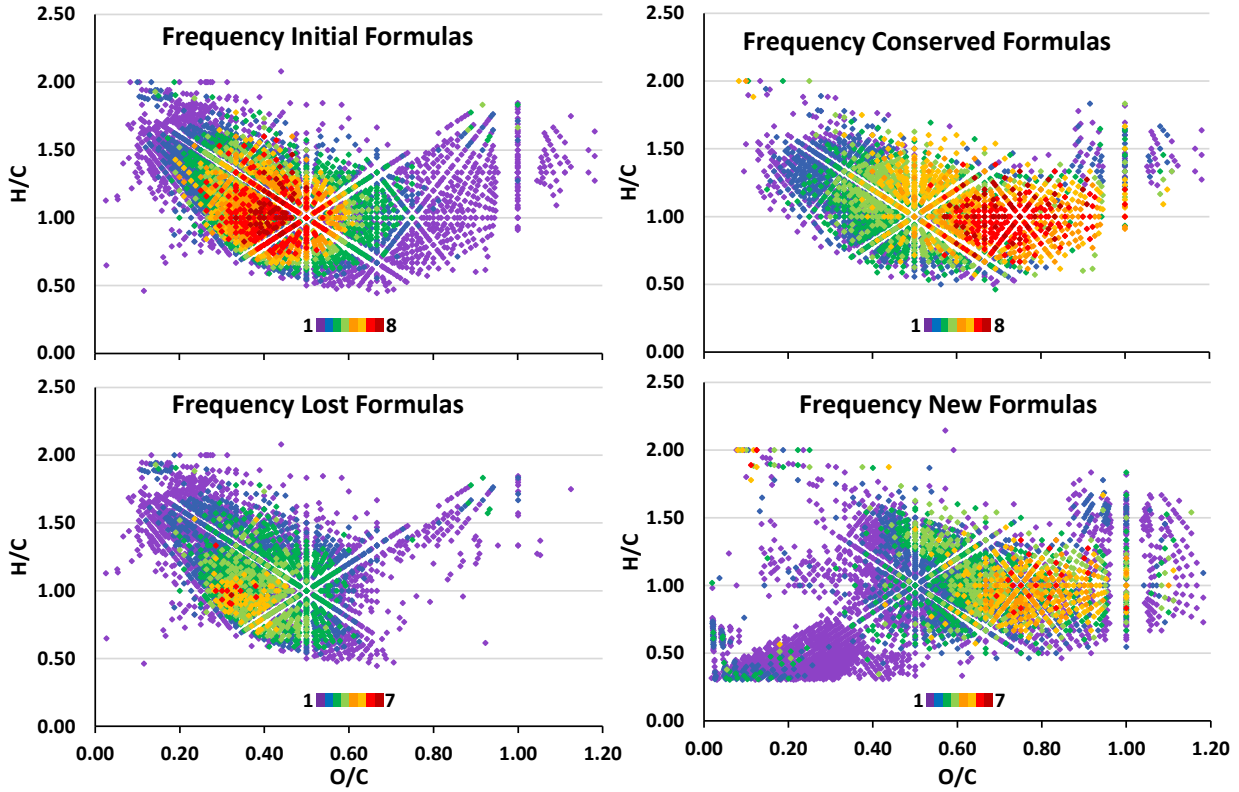

Fig. 23. Van Krevelen plots showing the frequency of CHO containing formulas in the initial lignin extract fractions F1-F8 (Top left). The frequency of conserved formulas following ˙OH treatment (Top right). Frequency of formulas removed in + ˙OH treated F1-F8 (Bottom left). Frequency of formulas new to F1-F8 following ˙OH treatment (Bottom right).

To further understand how ˙OH exposure alters lignin structurally, Kendrick mass defect (KMD) analyses were also performed using the formulas assigned in the initial fractions as well as the +˙OH fractions. Kendrick mass defect series were calculated for hydrogen (H_2), oxygen (O), and carboxyl groups (COO) according to the following equations:

$$KM\ (H_2) = IUPAC\ mass_{measured}[2.0000/2.01565] \quad (4)$$

$$KM\ (O) = IUPAC\ mass_{measured}[16.0000/15.99491] \quad (5)$$

$$KM\ (COO) = IUPAC\ mass_{measured}[44.0000/43.98983] \quad (6)$$

$$KMD = [NM - KM] \quad (7)$$

where KM = Kendrick mass, IUPAC mass = the exact peak mass measured based on the formula assigned, and NM = nominal mass. The plots displaying the Kendrick mass defect for H_2, O, and COO, vs. the nominal Kendrick mass (Fig. 24), identify formulas differing from one another by a selected mass. Due to the expected reactivity of ˙OH, Kendrick mass defect series were selected to show variations in the number of oxygen atoms, and carboxyl groups present, corresponding to differences in m/z of 16 and 44 respectively. Similarly, the addition, or removal of hydrogen (monatomic or diatomic) can be observed in formulas differing by an m/z of 2. Figure 24 shows representative H_2, O, and COO KMD series from F5, accounting for roughly 25% of the total absorbance for the lignin extract. The KMD series for oxygen and carboxyl groups show that new formulas in +˙OH treated lignin predominantly plot at higher nominal mass than the initial formulas present, consistent with the addition of oxygen functionality to existing formulas (Fig. 7). KMD analysis for H_2 series indicate the opposite to be occurring following ˙OH treatment, with the majority of newly produced formulas occurring at the lower mass range of series compared to formulas initially present in lignin fractions. The frequently observed loss of hydrogen from initial formulas suggests proton abstraction by ˙OH is widely occurring in all fractions, and is consistent with the decrease in H/C values in +˙OH fractions.

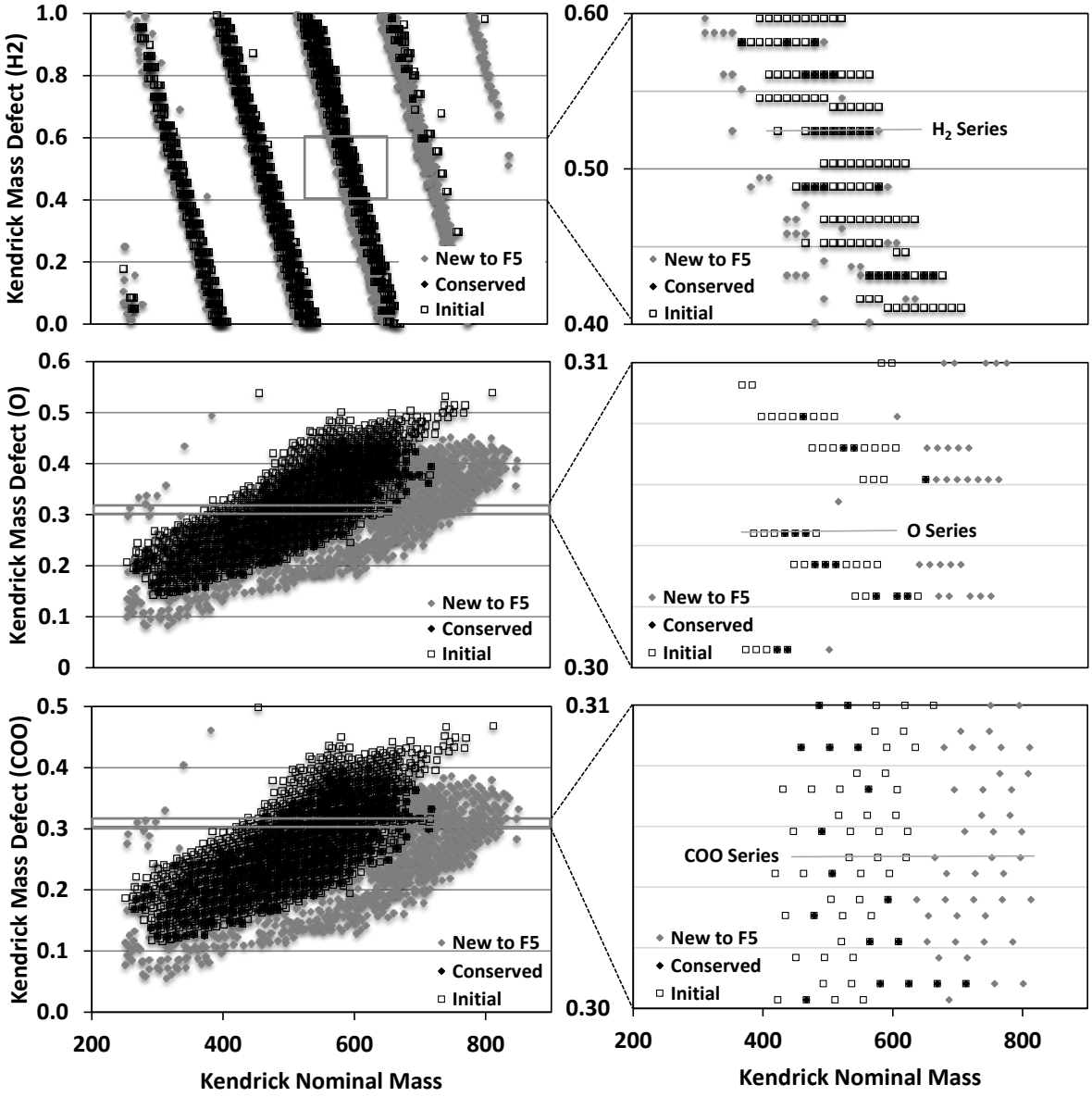

Fig. 24. Kendrick mass defect plots for representative lignin extract fraction (F5), with the top plot displaying KMD for hydrogen series, middle oxygen series, and the bottom COO series. New formulas formed in + •OH treated F5 are shown as grey diamonds. Conserved and initial formulas are indicated by black diamonds and squares respectively.

4. DISCUSSION

4.1 HPLC fractionation of brown rot lignin extract

Separation of brown rot lignin extract by RP-HPLC showed 6 observable peaks using a PDA detector, which were subsequently collected as 8 fractions (Fig. 18). The distribution of peaks indicates the presence of compounds within the lignin extract having a range of polarities from hydrophilic (F1-F3), to hydrophobic (F7-F8) based on elution solvent composition. The intermediate polarity peaks (F5-F6), accounting for the majority (52%) of the total absorbance observed, are most likely representative of the lignin extract that has been least modified by the brown rot fungi. The hydrophilic fractions (F1-F3) representing c.a. 20% of the total absorbance, are consistent with lignin that has been partially oxidized by brown rot fungi (Fig. 19)(Crawford, 1981). Hydrophobic peaks (F7-F8), accounting for c.a 7% of the absorbance of the lignin extract, are also observed and could indicate the presence of deoxgenated lignin degradation products, for example, brown rot removal of methoxy substituents from lignin, thereby decreasing the O/C value (Davis et al., 1994) or decarboxylation reactions as suggested by Waggoner et al. (2015). It is also possible that these formulas represent fungal residues.

4.2 FTICR-MS analysis of brown rot lignin HPLC fractions

Fractionation of the brown rot lignin extract resulted in a 47% increase in the number of assigned formulas when compared to the number of formulas assigned to the whole, unfractionated lignin extract using FTICR-MS. This can be attributed to the increased ionization efficiency afforded to individual fractions having lower complexity and less charge competition. The resulting formulas, when plotted on van Krevelen diagrams (Fig. 3), show clear differences in the fractional composition of the lignin extract, consistent with variations in polarity between

fractions. The formulas contributing to the majority of the total absorbance plot within the region of van Krevelen space typically associated with lignin-like compounds. Fractions containing high O/C (F1) and high H/C formulas (F7-F8), not typical of lignin, contribute a smaller percentage (19%) of the total lignin extract based on absorbance calculations (Fig. 19-20). The presence of these atypical formulas suggests the brown rot fungi have contributed to the partial modification of initial lignin formulas to produce the high O/C formulas observed.

Formulas assigned in fractions F2-F4, while plotting within the lignin-like region of the van Krevelen diagram (Fig. 3), and accounting for c.a. 14% of the absorbance observed, elute under more polar conditions on RP-HPLC than the dominant peaks observed (F5-F6), which accounted for over half (52%) of the total absorbance for the lignin extract. This increase in polarity, while still plotting within the lignin region, could suggest the presence of more readily accessible polar functional groups, such as acidic or hydroxyl substituent groups, in addition to the ester and methoxy functionality commonly associated with lignin-like compounds. Modification to lignin structure resulting in increased acidic and hydroxyl groups has been proposed in biological systems previously and therefore could be the result of brown rot fungi (Crawford, 1981), however it is also possible that such functionality exists naturally within the complex structure of lignin.

Results from HPLC and FTICR-MS suggest that fractions F5-F6 are the most representative of lignin, being both comprised of formulas characteristic of lignin-like compounds (Fig. 3), defined by previous studies (Liu et al., 2011), as well as accounting for the largest portions of the total absorbance observed for the lignin extract (Fig. 19). Fractions F5-F6 additionally constitute the highest magnitude weighted m/z of any fraction collected (Table 2), suggesting that the lignin-like formulas have not undergone extensive degradation processes such as de-

methylation or de-methoxylation to decrease molecular mass (Crawford, 1981). We do however recognize that some modification of the original lignin has occurred to render the molecules soluble in alkali extract.

The last fractions collected F7-F8, constituting the most hydrophobic portion of the lignin extract, indicate a decrease in the magnitude weighted O/C, AI_{mod}, and m/z values when compared to F5-F6 (Table 2), consistent with a change from more aromatic lignin-like structures, to compounds having more aliphatic characteristics. Shifts in composition from highly unsaturated aromatic compounds towards more saturated compounds has been observed in studies investigating the degradation of DOM (Gonsior et al., 2009; Tremblay et al., 2007), therefore the presence of aliphatic-like formulas not typically associated with lignin would further suggest these formulas are the result of degradation by brown rot fungi.

4.3 Modification of HPLC separated brown rot lignin by ˙OH

Following exposure to ˙OH generated by Fenton chemistry, the various fractions of the brown rot lignin extract underwent a number compositional changes as determined by FTICR-MS. The first group of new formulas in the + ˙OH treated lignin fractions largely trend toward higher O/C values when compared to the corresponding initial untreated fractions (Fig. 21). This ubiquitous shift to higher O/C values suggests oxidative degradation is occurring to all +˙OH treated fractions, and is consistent with observations from previous studies showing partial oxidation of DOM is readily achievable by ROS (Chen et al., 2014; Waggoner et al., 2015; Waggoner et al., 2017; Ward and Cory, 2016). The second group of new formulas observed in select +˙OH treated fractions, plot at lower H/C (<0.75), low O/C (<0.50), and have AI_{mod} values (>0.67) suggesting condensed aromatic-like compounds (Fig. 21). The condensed aromatic-like

formulas present in +•OH treated fractions are additionally consistent with formulas observed upon +•OH treatment of the whole lignin extract (Waggoner et al., 2015).

In addition to the production of high O/C formulas, loss of the lower O/C formulas present in each fraction was observed for the majority +•OH treated fractions (Fig. 21), similar to results from studies investigating the photochemical and bacterial degradation of DOM (Kujawinski et al., 2004). Formulas having O/C values <0.30 were not extensively removed from the more hydrophobic fractions (F5-F7), consistent with recent work suggesting •OH preferentially reacts with hydroxyl substituted aromatic compounds having O/C values between 0.30-0.60, capable of serving as radical scavengers (Waggoner et al., 2017). Fractionation of the lignin extract further substantiates •OH preferential reaction with lignin-like formulas falling within these O/C criteria, illustrated by the near complete removal of fractions that exclusively occupy this O/C range, F3-F4, following +•OH treatment. The more hydrophobic fractions (F5-F7) exhibit formulas that are largely conserved following •OH treatment, possibly indicating a lack of aromatic hydroxyl substitution in fractions F5-F7 (Fig. 21). An additional observation is the roughly 60% loss of initial formulas from the most hydrophobic fraction (F8), falling outside of the reactive O/C range, and predominantly plotting in the aliphatic region (H/C >1.5) (Fig. 21). Loss of these formulas could be attributed to the presence of aliphatic alcohols in F8, capable of reacting with •OH, and resulting in the generation of aliphatic radicals following proton abstraction (Alam et al., 2003).

4.4 Reactivity of •OH with lignin extract

The overall reactivity of •OH toward various lignin fractions can be further assessed by examining the frequency at which formulas occur between fractions, as well as investigating the types of common mass loss from formulas. Figure 23 displays a number of changes to the frequency of formula occurrences observed in initial lignin extracts compared to +•OH treated

lignin fractions. Following •OH treatment, the most frequently observed formulas plot in the tannin-like/oxidized lignin region (O/C >0.60), in contrast to the initial lignin fractions where the most frequently occurring formulas are centered in the lignin-like region (0.30> O/C <0.60). The frequency of formulas observed in the tannin-like/oxidized lignin region for +•OH treated fractions would suggest a common reaction pathway, independent of the initial polarity of the fraction. This could indicate that hydroxyl groups may be partially responsible for the difference in polarity observed by HPLC driving the fractionation/separation of the initial brown rot lignin extract. Additionally, the common endpoint of formulas, despite differences in the initial polarity between fractions ranging from hydrophilic to hydrophobic, could indicate a similar lignin core structure present in all fractions that is undergoing alteration. This further suggests that all fractions likely have a lignin origin, and do not likely have major contributions from other sources such as fungal biomass.

Figure 23 also displays the frequency of formulas most commonly lost from initial fractions, along with the frequency of new formulas present in each lignin fraction following •OH treatment. As expected, the highest frequency of formulas removed coincides with the highest frequency of initially present formulas. However, formulas appearing in 4 or fewer fractions with O/C values <0.60 are found to be more efficiently removed. These initial formulas occur at lower frequency and are largely accounted for by fractions other than F5-F6, representing the most substantial portion of the lignin extract based on absorbance (Fig. 19). The efficient removal of these formulas could therefore indicate that alteration of lignin-like formulas, e.g. addition of hydroxyl or acidic functionality, makes these formulas more susceptible to further alteration by •OH. The frequency of new formulas follows a similar trend to that seen with the conserved formulas (Fig. 23). The most commonly observed new formulas were those plotting in the tannin-

like/oxidized lignin region. Again, the ability of these high O/C formulas to be generated from lignin fractions, having a range of different polarities, suggests a common pathway for their formation.

New formulas present at low H/C values and having AI_{mod} values >0.67 are shown to be less frequent than the corresponding formulas in the tannin-like region. The most frequent of these condensed aromatic-like formulas formed following •OH treatment of the most polar lignin fractions (F1-F4), further suggesting the presence of hydroxyl and acidic functionality could result in additional alteration to lignin formulas, specifically to the formation of condensed aromatic-like formulas as observed in natural DOM (Chen et al., 2014).

Mass differences between the initial and •OH treated lignin fractions can additionally be used to gain some insight into potential reaction pathways through KMD analysis. The trends in the H_2, O, and COO KMD series shown for fraction F5 (Fig. 24) can be observed throughout the lignin fractions. KMD plots for O, and COO series show the prevalence of new formulas produced in +•OH treated lignin fraction plotting at higher m/z than the formulas initially present. For the O KMD series, this would suggest, and is consistent with, the direct addition of •OH to olefins or aromatic rings associated with lignin, resulting in the higher mass formulas observed (Goldstone et al., 2002; Walling, 1975). The direct addition of oxygen is also in good agreement with the general increase in magnitude weighted O/C values observed following •OH treatment (Table 2). The higher mass formulas present in the COO KMD series, however, cannot be attributed to simple addition of •OH. Addition of COO to initially present formulas, combined with an average 10% decrease in the AI_{mod} values across fractions F2-F8 (Table 2), suggests that •OH addition to the aromatic ring of lignin results in cleavage of the aromatic ring to form di-acids, similar to those observed in the microbial degradation of lignin (Crawford and Crawford, 1980). These high O/C

di-acids could also potentially explain the formation of the condensed aromatic-like formulas (AI_{mod} >0.67) observed following •OH treatment of polar fractions. It has been proposed previously that di-acids can undergo cyclization and condensations reactions to form condensed aromatic-like formulas observed in natural DOM, from lignin-like formulas (Waggoner et al., 2015). The DBE vs. C number plot shown in Figure 22 supports such a condensation/cyclization type pathway. Upon reaction with •OH, a new set of formulas is observed in fractions F1 and F5 (Fig. 22) having higher DBE, corresponding to the condensed aromatic aromatic-like formulas. These new formulas plot at higher carbon numbers than initially present formulas, and would therefore be consistent with the condensation/cyclization pathway proposed previously that results in higher DBE, higher carbon number formulas (Waggoner et al., 2015).

KMD analysis for H_2 shows new formulas present in hydrogen series plotting at lower m/z when compared to formulas from initial fractions (Fig. 24). Loss of hydrogen from formulas in +•OH treated lignin fractions indicate that •OH is not only adding to lignin formulas, but also abstracting protons. Proton abstraction by •OH would be consistent with the observed decrease in magnitude weighted H/C values observed (Table 2), as well as known reactions involving •OH (Goldstone et al., 2002; Walling, 1975).

5. CONCLUSIONS

The work presented here describes the possible alterations occurring to various polarity-separated fractions of lignin upon exposure to •OH. In the context of this study, lignin is meant to serve as an analog for tDOM, the fractionation of which allowed for the more thorough characterization of changes taking place following exposure to one of the dominant photochemically produced ROS encountered by tDOM upon export to aquatic systems. Results of this work indicate that oxygen content plays a key role in both the reactivity of lignin (tDOM)

toward •OH, in addition to the types of new formulas observed following reaction with •OH. Hydroxyl radical has been shown to readily alter lignin, spanning a range of polarities, to formulas resembling tannin-like compounds. Partially oxidized lignin-like formulas have additionally been suggested to be responsible for condensed aromatic-like formulas commonly observed in DOM samples. While the relative contribution •OH makes to the alteration of tDOM, compared to other ROS, cannot be fully assessed due to the complexity of reactions taking place in natural systems, this study attempts to provide information into the types of alterations that may be possible in various polarity components of a lignin extract, representing tDOM, upon exposure •OH. More importantly, the results presented herein suggest that ROS are able to alter the molecular structure of lignin, e.g. ring-opening and condensations reactions, resulting in molecules lacking lignin phenols that would identify them as being derived from lignin. This then suggests that the loss of lignin biomarkers is not the result of complete mineralization as previously suggested, but rather the result of lignin being molecularly altered into oxidized forms that no longer bear the lignin biomarker signature following attack by ROS (Cory et al., 2010; Page et al., 2014; Ward and Cory, 2016).

CHAPTER V

CONCLUSIONS AND FUTURE WORK

1. CONCLUSIONS

The studies presented in this dissertation set out to further our understanding of how reactive oxygen species (ROS), mainly generated through photochemical processes, could potentially alter the terrestrial biopolymer lignin into compounds no longer recognized as having lignin origins, and ultimately resulting in an underestimation of lignin's contribution to the vast pool of dissolved organic carbon (DOC) in the marine environment. Previous studies examining the presence of lignin biomarkers to determine the amount of lignin surviving export from rivers have suggested that less than 5% of oceanic DOC is attributed to lignin, with the majority of lignin being mineralized to CO_2 (Hedges et al., 1997; Opsahl and Benner, 1997). By investigating the dominant ROS encountered by lignin during its export to marine systems, simulated under controlled laboratory conditions, I demonstrated that lignin could be altered by ROS to molecular species commonly observed in dissolved organic matter (DOM) that are not typically associated as being derived from lignin. The findings from this work not only demonstrate that the molecular signature of lignin, e.g., lignin phenols, can be masked through reactions involving ROS, but also imply that the contribution of terrestrial organic matter, specifically lignin, to marine environments could be much greater than previously thought. With rivers worldwide exporting an estimated 0.2-0.4 Gt of terrestrial DOC annually to the oceans, alteration of lignin to molecules present in oceanic DOC rather than lignin undergoing complete mineralization to CO_2 could greatly impact models

involving both oceanic DOC as well as atmospheric CO_2 estimates (Bianchi, 2011; Jaffe et al., 2013).

In order to accomplish the goal of tracking the molecular level alterations occurring to lignin upon exposure to the various ROS, a number of advanced analytical techniques including; electrospray ionization Fourier transform ion cyclotron resonance mass spectrometry (ESI-FTICR-MS), ^{1}H nuclear magnet resonance (NMR), one and two dimensional gas chromatography mass spectrometry (GC-MS, GC x GC-MS), and high performance liquid chromatography (HPLC), were utilized both individually and in conjunction with one another throughout the studies presented here. The analysis of highly complex mixtures such as terrestrial DOM present unique analytical challenges, and therefore requires the use of a number of advanced techniques in order to effectively characterize such samples. ESI-FTICR-MS is one of the few techniques capable of additionally tracking molecular level alteration of such complex mixtures following exposure to ROS and was therefore uniquely suited for the studies presented in this work.

The work associated with this dissertation originated from the observation that terrestrial DOM, following extended photoirradiation, was able to form a number of new compounds including aliphatic and alicyclic-like compounds not typically associated with terrestrial DOM, along with condensed aromatic-like compounds previously thought to be predominantly formed through thermogenic processes. From these observations, I hypothesized that the lignin component of DOM could be responsible for the new compounds observed following photoirradiation, and that ROS generated through photochemical processes were responsible for the alterations observed. An alkali isolated sample of lignin was prepared using a brown-rotted Atlantic white cedar (*Chamaecyparis thyoides*) collected from the Great Dismal swamp (DS) in VA and compared to the DOM used in the photoirradiation studies by ESI-FTICR-MS. The results

indicated that the lignin extract and DOM sample had a high degree of similarity between formulas assigned, suggesting there to be a large lignin input in the DOM sample.

Hydroxyl radical ($^{\bullet}OH$) is one of the main ROS present in sunlight waters, and is capable of reacting at near diffusion rates with organic matter. Upon reacting with $^{\bullet}OH$, the lignin extract underwent a number of alterations as determined by ESI-FTICR-MS and NMR, when compared to the initial lignin. Hydroxyl radical treated lignin extract showed the formation of several new compound classes not initially present, including new aliphatic, alicyclic, and condensed aromatic-like formulas in FTICR-MS. ^{1}H NMR data helped support these findings with an increase in aliphatic resonance between 2-3 ppm, as well as a peak at 7.7 ppm indicating the possible presence of multi-ring systems following $^{\bullet}OH$ treatment. From these findings it was concluded that several compound classes not typically attributed to terrestrial organic matter, but which are frequently observed in DOM, could originate from lignin through reactions involving ROS, and in particular $^{\bullet}OH$. This conclusion would additionally suggest that lignin, the commonly used biomarker for the presence of terrestrial organic matter, is likely underestimated in marine systems where lignin can undergo ROS mediated alteration upon export.

As $^{\bullet}OH$ is just one of many ROS present in sunlight waters, additional studies were conducted using singlet oxygen ($^{1}O_2$) and superoxide ($O_2^{-\bullet}$) to obtain a more complete understanding of how ROS may alter lignin in the environment. The study shows that $^{1}O_2$ treatment of lignin results primarily in the formation of oxidized lignin formulas, which plot in the lignin and tannin regions upon analysis with FTICR-MS. Conventional lignin biomarker analysis using GC x GC-MS following tetramethylammonium hydroxide (TMAH) derivatization was additionally performed, and indicated substantial oxidative degradation had occurred as a result of $^{1}O_2$ treatment. These findings indicate that while $^{1}O_2$ appears to degrade lignin based on

conventional analysis of biomarkers, $^1O_2$ alone does not cause sufficient alteration to render lignin unrecognizable for techniques such as FTICR-MS.

Superoxide was shown to result in oxidized lignin formulas similar to those observed in $^1O_2$, and $^{\bullet}OH$, with an additional unique set of formulas at a higher H/C (>1.40) ratio than conventional lignin, as well as a substantially decrease DBE based on data from FTICR-MS analysis. Biomarker analysis using TMAH; however, did not account for this alteration, suggesting minimal oxidative degradation had taken place following $O_2^{-\bullet}$ exposure. Careful analysis of FTICR-MS data resulted in the conclusion that $O_2^{-\bullet}$ was capable of both hydrogenation as well as proton abstraction from lignin. The alteration of lignin through hydrogenation not only results in loss of the phenolic component needed for biomarker analysis, but also makes lignin appear more aliphatic when analyzed by FTICR-MS, thereby making these formulas difficult to attribute to lignin.

Comparing the FTICR-MS results of each ROS treatment with data obtained from a river transect revealed that significant percentages of new formulas generated from lignin were also present in the transect dataset. The prevalence of formulas matching those produced during individual ROS treatment of lignin, particularly the aliphatic formulas commonly attributed to marine DOM, strengthens the conclusion that ROS are important in the alteration of lignin during export to marine systems. An additional major finding came when comparing FTICR-MS data for all three ROS investigated collectively. Comparing the formulas removed following exposure to each ROS, in an effort to gain insight into the relatively reactivity, resulted in the determination that each ROS appears to preferentially react with different formulas present within the lignin sample. Investigation into the selectivity of each ROS revealed that differences in the number of oxygen atoms present in formulas appeared to be responsible for the selective alteration of lignin.

As a result of the extensive alteration seen in the •OH treatment of lignin, the final study discussed in this dissertation attempts to further narrow down the source of new formulas observed with particular interest in the condensed aromatic-like and aliphatic/alicyclic formulas. The observation that •OH selectively reacts with the highest O/C formulas in the lignin sample lead me to the hypothesis that the highest oxygen content, most polar formulas were responsible for a large portion of the new formulas generated. To confirm this theory, HPLC was used to fractionate the lignin sample based on polarity prior to treatment with •OH. FTICR-MS indicated that only polar fractions containing high O/C formulas (>0.60) resulted in the formation of condensed aromatic-like formulas, however no fractions produced the aliphatic/alicyclic formulas observed during •OH treatment of the unfractionated sample. From these results I can draw the conclusion that partially oxidized lignin formulas are responsible for the condensed aromatic-like formulas observed, whereas aliphatic formulas are likely the result of interactions between various polarity fractions.

2. FUTURE WORK

Following the studies outlined in this dissertation there are a number of interesting research directions that could be pursued. A continuation of the HPLC study would be the most logical in an effort to ascertain the origin of aliphatic/alicyclic formulas observed in the •OH treatment of the whole sample. A study recombining various fractions could potentially answer some of the questions about these missing formulas, and also aid in furthering our understanding of the potential mechanisms behind their formation. Attempting to gain more structural information for each of the fractions would additionally be valuable toward understanding the mechanism associated with this process, and structural determination of complex mixtures with ion mobility coupled to FTICR-MS may soon be possible (Ahmed et al., 2014). Because lignin will not be

exposed to only a single ROS in the environment, subjecting a sample to successive treatments with different ROS and monitoring the changes could provide a valuable dataset to compare to DOM and potentially predict formulas originating from lignin as well.

In addition to continuing the work with natural samples, further work with model compounds could be useful in understanding the processes occurring. Lignin model compounds (dehydrogenase polymer, DHP), both isotopically labeled and non-labeled, could be synthesized and reacted with ROS to remove some of the complexity associated with natural samples. Using selectively labeled compounds would enable more detailed NMR studies to be conducted that could better elucidate potential structural alterations occurring to lignin following reaction with ROS. Integration of a label at the C-4 carbon of the aromatic ring for example would allow the reaction pathway proposed in Chapter II to be verified by monitoring for carboxylation at this position. The simplified reactions would then be easier to input into computer models to better predict reaction mechanisms and likely products in more complex natural systems. Working with model compounds would also make the use of tandem mass spectrometry techniques much easier to generate structural information by allowing more precise isolation of masses, which is not currently possible do to the close proximity of other peaks in the mass spectrum.

REFERENCES

Aeschbacher, M., Graf, C., Schwarzenbach, R.P., Sander, M., 2012. Antioxidant Properties of Humic Substances. Environmental Science and Technology 46, 4916-4925.

Aeschbacher, M., Sander, M., Schwarzenbach, R.P., 2009. Novel electrochemical approach to assess the redox properties of humic substances. Environmental Science and Technology 44, 87-93.

Afanas'ev, I.B., 1991. Superoxide Ion: Chemistry and Biological Implications. Taylor & Francis.

Ahmed, A., Cho, Y., Giles, K., Riches, E., Lee, J.W., Kim, H.I., Choi, C.H., Kim, S., 2014. Elucidating Molecular Structures of Nonalkylated and Short-Chain Alkyl (n < 5, (CH2)n) Aromatic Compounds in Crude Oils by a Combination of Ion Mobility and Ultrahigh-Resolution Mass Spectrometries and Theoretical Collisional Cross-Section Calculations. Analytical Chemistry 86, 3300-3307.

Alam, M.S., Rao, B.S.M., Janata, E., 2003. OH reactions with aliphatic alcohols: evaluation of kinetics by direct optical absorption measurement. A pulse radiolysis study. Radiation Physics and Chemistry 67, 723-728.

Andrews, S.S., Caron, S., Zafiriou, O.C., 2000. Photochemical oxygen consumption in marine waters: A major sink for colored dissolved organic matter? Limnology and Oceanography 45, 267-277.

Appiani, E., McNeill, K., 2015. Photochemical Production of Singlet Oxygen from Particulate Organic Matter. Environmental Science and Technology 49, 3514-3522.

Bauer, J.E., 2002. Carbon isotopic composition of DOM, in: Hansell, D.A., Carlson, C.A. (Eds.), Biogeochemistry of Marine Dissolved Organic Matter, pp. 405-453.

Behr, A., Eilting, J., Irawadi, K., Leschinski, J., Lindner, F., 2008. Improved utilisation of renewable resources: New important derivatives of glycerol. Green Chemistry 10, 13.

Bentivenga, G., Bonini, C., D'Auria, M., De Bona, A., 1999. Singlet oxygen degradation of lignin: a GC–MS study on the residual products of the singlet oxygen degradation of a steam exploded lignin from beech. Journal of Photochemistry and Photobiology A: Chemistry 128, 139-143.

Bianchi, T.S., 2011. The role of terrestrially derived organic carbon in the coastal ocean: A changing paradigm and the priming effect. Proceedings of the National Academy of Sciences 108, 19473-19481.

Blough, N.V., Del Vecchio, R., 2002. Chromophoric DOM in the Coastal Environment, in: Carlson, D.A., A., H. (Eds.), Biogeochemistry of Marine Dissolved Organic Matter. Academic Press, San Diego, pp. 509-546.

Bonini, C., D'Auria, M., Mauriello, G., Viggiano, D., Zimbardi, F., 1998. Singlet oxygen degradation of lignin in the pulp. Journal of Photochemistry and Photobiology A: Chemistry 118, 107-110.

Burns, J.M., Craig, P.S., Shaw, T.J., Ferry, J.L., 2010. Multivariate Examination of Fe(II)/Fe(III) Cycling and Consequent Hydroxyl Radical Generation. Environmental Science and Technology 44, 7226-7231.

Candeias, L.P., Folkes, L.K., Porssa, M., Parrick, J., Wardman, P., 1996. Rates of reaction of indoleacetic acids with horseradish peroxidase compound I and their dependence on the redox potentials. Biochemistry 35, 102-108.

Cao, G., Sofic, E., Prior, R.L., 1997. Antioxidant and Prooxidant Behavior of Flavonoids: Structure-Activity Relationships. Free Radical Biology and Medicine 22, 749-760.

Challinor, J.M., 1989. A pyrolysis-derivatisation-gas chromatography technique for the structural elucidation of some synthetic polymers. Journal of Analytical and Applied Pyrolysis 16, 323-333.

Challinor, J.M., 1993. Characterisation of rosin-based commercial resins by pyrolysis— and simultaneous pyrolysis methylation—gas chromatography/mass spectrometry techniques. Journal of Analytical and Applied Pyrolysis 25, 349-360.

Challinor, J.M., 2001. Review: the development and applications of thermally assisted hydrolysis and methylation reactions. Journal of Analytical and Applied Pyrolysis 61, 3-34.

Chang, J.-S., Lee, Y.-D., Chou, L.C.-S., Ling, T.-R., Chou, T.-C., 2012. Methylation of Glycerol with Dimethyl Sulfate To Produce a New Oxygenate Additive for Diesels. Industrial & Engineering Chemistry Research 51, 655-661.

Chefetz, B., Chen, Y., Clapp, C.E., Hatcher, P.G., 2000. Characterization of Organic Matter in Soils by Thermochemolysis Using Tetramethylammonium Hydroxide (TMAH). Soil Science Society of America Journal 64, 583-589.

Chefetz, B., Tarchitzky, J., Deshmukh, A.P., Hatcher, P.G., Chen, Y., 2002. Structural Characterization of Soil Organic Matter and Humic Acids in Particle-Size Fractions of an Agricultural Soil. Soil Science Society of America Journal 66, 129-141.

Chen, H., Abdulla, H.A.N., Sanders, R.L., Myneni, S.C.B., Mopper, K., Hatcher, P.G., 2014. Production of black carbon-like and aliphatic molecules from terrestrial dissolved organic matter in the presence of sunlight and iron. Environmental Science and Technology Letters 1, 399-404.

Cole, J.J., Prairie, Y.T., Caraco, N.F., McDowell, W.H., Tranvik, L.J., Striegl, R.G., Duarte, C.M., Kortelainen, P., Downing, J.A., Middelburg, J.J., Melack, J., 2007. Plumbing the Global Carbon Cycle: Integrating Inland Waters into the Terrestrial Carbon Budget. Ecosystems 10, 172-185.

Cory, R.M., Cotner, J.B., McNeill, K., 2009. Quantifying Interactions between Singlet Oxygen and Aquatic Fulvic Acids. Environmental Science and Technology 43, 718-723.

Cory, R.M., McNeill, K., Cotner, J.P., Amado, A., Purcell, J.M., Marshall, A.G., 2010. Singlet Oxygen in the Coupled Photochemical and Biochemical Oxidation of Dissolved Organic Matter. Environmental Science and Technology 44, 3683-3689.

Cory, R.M., Ward, C.P., Crump, B.C., Kling, G.W., 2014. Sunlight controls water column processing of carbon in arctic fresh waters. Science 345, 925-928.

Crawford, D.L., Crawford, R.L., 1980. Microbial degradation of lignin. Enzyme and Microbial Technology 2, 11-22.

Crawford, R.L., 1981. Lignin Biodegradation and Transformation. Wiley New York.

Crestini, C., D'Auria, M., 1997. Singlet oxygen in the photodegradation of lignin models. Tetrahedron 53, 7877-7888.

Crestini, C., DÁuria, M., 1996. Photodegradation of lignin: the role of singlet oxygen. Journal of Photochemistry and Photobiology A: Chemistry 101, 69-73.

Dasari, M.A., Kiatsimkul, P.-P., Sutterlin, W.R., Suppes, G.J., 2005. Low-pressure hydrogenolysis of glycerol to propylene glycol. Applied Catalysis A: General 281, 225-231.

Davis, M.F., Schroeder, H.A., Maciel, G.E., 1994. Solid-state 13C nuclear magnetic resonance studies of wood decay. III. Decay of Colorado Blue Spruce and Paper Birch by Postia placenta. Holzforschung-International Journal of the Biology, Chemistry, Physics and Technology of Wood 48, 301-307.

del Río, J.C., Hatcher, P.G., 1998. Analysis of aliphatic biopolymers using thermochemolysis with tetramethylammonium hydroxide (TMAH) and gas chromatography–mass spectrometry. Organic Geochemistry 29, 1441-1451.

del Rio, J.C., McKinney, D.E., Knicker, H., Nanny, M.A., Minard, R.D., Hatcher, P.G., 1998. Structural characterization of bio- and geo-macromolecules by off-line thermochemolysis with tetramethylammonium hydroxide. Journal of Chromatography A 823, 433-448.

Devine, P.N., Oh, T., 1992. Asymmetric Diels-Alder reactions of carboxylic ester dienophiles promoted by chiral Lewis acids. The Journal of Organic Chemistry 57, 396-399.

Di Serio, M., Casale, L., Tesser, R., Santacesaria, E., 2010. New Process for the Production of Glycerol tert-Butyl Ethers. Energy & Fuels 24, 4668-4672.

Díaz-Álvarez, A.E., Francos, J., Lastra-Barreira, B., Crochet, P., Cadierno, V., 2011. Glycerol and derived solvents: new sustainable reaction media for organic synthesis. Chemical Communications 47, 6208.

Diaz, J.M., Hansel, C.M., Voelker, B.M., Mendes, C.M., Andeer, P.F., Zhang, T., 2013. Widespread Production of Extracellular Superoxide by Heterotrophic Bacteria. Science 340, 1223.

Diels, O., Alder, K., 1928. Synthesen in der hydroaromatischen Reihe. Justus Liebigs Annalen der Chemie 460, 98-122.

EPA, U.S., 2015. 2014 RIN Generation and Renewable Fuel Volume Production, in: EPA, U.S. (Ed.), 2014 RIN Generation and Renewable Fuel Volume Production

Field, C.B., Behrenfeld, M.J., Randerson, J.T., Falkowski, P., 1998. Primary production of the biosphere: integrating terrestrial and oceanic components. Science 281, 237-240.

Filley, T.R., Cody, G.D., Goodell, B., Jellison, J., Noser, C., Ostrofsky, A., 2002. Lignin demethylation and polysaccharide decomposition in spruce sapwood degraded by brown rot fungi. Organic Geochemistry 33, 111-124.

Fox, L.E., 1983. The removal of dissolved humic acid during estuarine mixing. Estuarine, Coastal and Shelf Science 16, 431-440.

García-Marín, H., van der Toorn, J.C., Mayoral, J.A., García, J.I., Arends, I.W.C.E., 2009. Glycerol-based solvents as green reaction media in epoxidations with hydrogen peroxide catalysed by bis[3,5-bis(trifluoromethyl)-diphenyl] diselenide. Green Chemistry 11, 1605.

García, J.I., García-Marín, H., Mayoral, J.A., Pérez, P., 2010. Green solvents from glycerol. Synthesis and physico-chemical properties of alkyl glycerol ethers. Green Chemistry 12, 426.

García, J.I., García-Marín, H., Pires, E., 2014. Glycerol based solvents: synthesis, properties and applications. Green Chemistry 16, 1007.

Garg, S., Rose, A.L., Waite, T.D., 2011. Photochemical production of superoxide and hydrogen peroxide from natural organic matter. Geochimica et Cosmochimica Acta 75, 4310-4320.

Gerpen, J.V., 2005. Biodiesel processing and production. Fuel Processing Technology 86, 1097-1107.

Goldstone, J.V., Pullin, M.J., Bertilsson, S., Voelker, B.M., 2002. Reactions of hydroxyl radical with humic substances: bleaching, mineralization, and production of bioavailable carbon substrates. Environmental Science and Technology 36, 364-372.

Gonsior, M., Peake, B.M., Cooper, W.T., Podgorski, D., D'Andrilli, J., Cooper, W.J., 2009. Photochemically Induced Changes in Dissolved Organic Matter Identified by Ultrahigh Resolution Fourier Transform Ion Cyclotron Resonance Mass Spectrometry. Environmental Science and Technology 43, 698-703.

Grandbois, M., Latch, D.E., McNeill, K., 2008. Microheterogeneous Concentrations of Singlet Oxygen in Natural Organic Matter Isolate Solutions. Environmental Science and Technology 42, 9184-9190.

Grasset, L., Rovira, P., Amblès, A., 2009. TMAH-preparative thermochemolysis for the characterization of organic matter in densimetric fractions of a Mediterranean forest soil. Journal of Analytical and Applied Pyrolysis 85, 435-441.

Grinhut, T., Hertkorn, N., Schmitt-Kopplin, P., Hadar, Y., Chen, Y., 2011. Mechanisms of humic acids degradation by white rot fungi explored using 1H NMR spectroscopy and FTICR mass spectrometry. Environmental Science and Technology 45, 2748-2754.

Guo, W., Stedmon, C.A., Han, Y., Wu, F., Yu, X., Hu, M., 2007. The conservative and non-conservative behavior of chromophoric dissolved organic matter in Chinese estuarine waters. Marine Chemistry 107, 357-366.

Haag, W.R., Hoigne, J., 1986. Singlet oxygen in surface waters. 3. Photochemical formation and steady-state concentrations in various types of waters. Environmental Science and Technology 20, 341-348.

Haag, W.R., Hoigne´, J.r., Gassman, E., Braun, A.M., 1984. Singlet oxygen in surface waters — Part I: Furfuryl alcohol as a trapping agent. Chemosphere 13, 631-640.

Harris, J.M., Wamser, C.C., 1976. Fundamentals of Organic Reaction Mechanisms. Wiley, New York.

Hartman, B.E., Chen, H., Hatcher, P.G., 2015. A non-thermogenic source of black carbon in peat and coal. International Journal of Coal Geology 144–145, 15-22.

Hatcher, P.G., 1987. Chemical structural studies of natural lignin by dipolar dephasing solid-state 13C nuclear magnetic resonance. Organic Geochemistry 11, 31-39.

Hatcher, P.G., Clifford, D.J., 1994. Flash pyrolysis and in situ methlation of humic acids from soil. Organic Geochemistry 21, 1081-1092.

Hatcher, P.G., Liu, Z., 2009. Direct conversion of biomass to biodiesel fuel. Old Dominion University, USA; Old Dominion University Research Foundation . US.

Hatcher, P.G., Nanny, M.A., Minard, R.D., Dible, S.D., Carson, D.M., 1995. Comparison of two thermochemolytic methods for the analysis of lignin in decomposing gymnosperm wood: the CuO oxidation method and the method of thermochemolysis with tetramethylammonium hydroxide (TMAH). Organic Geochemistry 23, 881-888.

Hedges, J.I., 1992. Global biogeochemical cycles: progress and problems. Marine Chemistry 39, 67-93.

Hedges, J.I., Ertel, J.R., 1982. Characterization of lignin by gas capillary chromatography of cupric oxide oxidation products. Analytical Chemistry 54, 174-178.

Hedges, J.I., Keil, R.G., 1995. Sedimentary organic matter preservation: an assessment and speculative synthesis. Marine Chemistry 49, 81-115.

Hedges, J.I., Keil, R.G., Benner, R., 1997. What happens to terrestrial organic matter in the ocean? Organic Geochemistry 27, 195-212.

Heitmann, T., Goldhammer, T., Beer, J., Blodau, C., 2007. Electron transfer of dissolved organic matter and its potential significance for anaerobic respiration in a northern bog. Global Change Biology 13, 1771-1785.

Helms, J.R., Mao, J., Schmidt-Rohr, K., Abdulla, H., Mopper, K., 2013. Photochemical flocculation of terrestrial dissolved organic matter and iron. Geochimica et Cosmochimica Acta 121, 398-413.

Helms, J.R., Stubbins, A., Ritchie, J.D., Minor, E.C., Kieber, D.J., Mopper, K., 2008. Absorption spectral slopes and slope ratios as indicators of molecular weight, source, and photobleaching of chromophoric dissolved organic matter. Limnology and Oceanography 53, 955.

Hertkorn, N., Benner, R., Frommberger, M., Schmitt-Kopplin, P., Witt, M., Kaiser, K., Kettrup, A., Hedges, J.I., 2006. Characterization of a major refractory component of marine dissolved organic matter. Geochimica et Cosmochimica Acta 70, 2990-3010.

Higuchi, T., 1990. Lignin biochemistry: Biosynthesis and biodegradation. Wood Science and Technology 24, 23-63.

Higuchi, T., 1993. Biodegradation mechanism of lignin by white-rot basidiomycetes. Journal of Biotechnology 30, 1-8.

Higuchi, T., 2004. Microbial degradation of lignin: Role of lignin peroxidase, manganese peroxidase, and laccase. Proceedings of the Japan Academy, Series B 80, 204-214.

Hockaday, W.C., Purcell, J.M., Marshall, A.G., Baldock, J.A., Hatcher, P.G., 2009. Electrospray and photoionization mass spectrometry for the characterization of organic matter in natural waters: a qualitative assessment. Limnology and Oceanography: Methods 7, 81-95.

Ikeya, K., Sleighter, R.L., Hatcher, P.G., Watanabe, A., 2013. Fourier transform ion cyclotron resonance mass spectrometric analysis of the green fraction of soil humic acids. Rapid Communications in Mass Spectrometry 27, 2559-2568.

Jaffe, R., Ding, Y., Niggemann, J., Vahatalo, A.V., Stubbins, A., Spencer, R.G., Campbell, J., Dittmar, T., 2013. Global charcoal mobilization from soils via dissolution and riverine transport to the oceans. Science 340, 345-347.

Johnson, D.T., Taconi, K.A., 2007. The glycerin glut: Options for the value-added conversion of crude glycerol resulting from biodiesel production. Environmental Progress 26, 338-348.

Jovanovic, S.V., Steenken, S., 1992. Substituent effects on the spectral, acid-base, and redox properties of indolyl radicals: a pulse radiolysis study. The Journal of Physical Chemistry 96, 6674-6679.

Kearns, D.R., 1971. Physical and chemical properties of singlet molecular oxygen. Chemical Reviews 71, 395-427.

Khan, A.U., 1981. Direct spectral evidence of the generation of singlet molecular oxygen (1. DELTA. g) in the reaction of potassium superoxide with water. Journal of the American Chemical Society 103, 6516-6517.

Klepáčová, K., Mravec, D., Kaszonyi, A., Bajus, M., 2007. Etherification of glycerol and ethylene glycol by isobutylene. Applied Catalysis A: General 328, 1-13.

Koch, B.P., Dittmar, T., 2006. From mass to structure: an aromaticity index for high-resolution mass data of natural organic matter. Rapid Communications in Mass Spectrometry 20, 926-932.

Koch, B.P., Dittmar, T., 2016. From mass to structure: an aromaticity index for high-resolution mass data of natural organic matter. Rapid Communications in Mass Spectrometry 30, 250-250.

Kopáček, J., Marešová, M., Norton, S.A., Porcal, P., Veselý, J., 2006. Photochemical source of metals for sediments. Environmental Science and Technology 40, 4455-4459.

Kujawinski, E.B., Behn, M.D., 2006. Automated Analysis of Electrospray Ionization Fourier Transform Ion Cyclotron Resonance Mass Spectra of Natural Organic Matter. Analytical Chemistry 78, 4363-4373.

Kujawinski, E.B., Del Vecchio, R., Blough, N.V., Klein, G.C., Marshall, A.G., 2004. Probing molecular-level transformations of dissolved organic matter: insights on photochemical degradation and protozoan modification of DOM from electrospray ionization Fourier transform ion cyclotron resonance mass spectrometry. Marine Chemistry 92, 23-37.

Lalonde, K., Vähätalo, A.V., Gélinas, Y., 2014. Revisiting the disappearance of terrestrial dissolved organic matter in the ocean: a δ13C study. Biogeosciences 11, 3707-3719.

Lam, B., Baer, A., Alaee, M., Lefebvre, B., Moser, A., Williams, A., Simpson, A.J., 2007. Major Structural Components in Freshwater Dissolved Organic Matter. Environmental Science and Technology 41, 8240-8247.

Lam, B., Simpson, A.J., 2008. Direct 1H NMR spectroscopy of dissolved organic matter in natural waters. Analyst 133, 263-269.

Latch, D.E., McNeill, K., 2006. Microheterogeneity of singlet oxygen distributions in irradiated humic acid solutions. Science 311, 1743-1747.

Latch, D.E., Stender, B.L., Packer, J.L., Arnold, W.A., McNeill, K., 2003. Photochemical Fate of Pharmaceuticals in the Environment: Cimetidine and Ranitidine. Environmental Science and Technology 37, 3342-3350.

Lee-Ruff, E., Lever, A.B.P., Rigaudy, J., 1976. The reaction of catechol and derivatives with potassium superoxide. Canadian Journal of Chemistry 54, 1837-1839.

Leonowicz, A., Cho, N., Luterek, J., Wilkolazka, A., Wojtas-Wasilewska, M., Matuszewska, A., Hofrichter, M., Wesenberg, D., Rogalski, J., 2001. Fungal laccase: properties and activity on lignin. Journal of Basic Microbiology 41, 185-227.

Liu, Z., Sleighter, R.L., Zhong, J., Hatcher, P.G., 2011. The chemical changes of DOM from black waters to coastal marine waters by HPLC combined with ultrahigh resolution mass spectrometry. Estuarine, Coastal and Shelf Science 92, 205-216.

Martin, J.G., Hill, R.K., 1961. Stereochemistry of the Diels-Alder reaction. Chemical Reviews 61, 537-562.

Matsumoto, A., Matsumura, T., Aoki, S., 1996. Stereospecific polymerization of dialkyl muconates through free radical polymerization: Isotropic polymerization and topochemical polymerization. Macromolecules 29, 423-432.

Matsumoto, A., Yokoi, K., Aoki, S., Tashiro, K., Kamae, T., Kobayashi, M., 1998. Crystalline-state polymerization of diethyl (Z,Z)-2,4-hexadienedioate via a radical chain reaction mechanism to yield an ultrahigh-molecular-weight and stereoregular polymer. Macromolecules 31, 2129-2136.

Maurer, F., Christl, I., Kretzschmar, R., 2010. Reduction and reoxidation of humic acid: Influence on spectroscopic properties and proton binding. Environmental Science and Technology 44, 5787-5792.

McKinney, D.E., Carson, D.M., Clifford, D.J., Minard, R.D., Hatcher, P.G., 1995. Off-line thermochemolysis versus flash pyrolysis for the in situ methylation of lignin: Is pyrolysis necessary? Journal of Analytical and Applied Pyrolysis 34, 41-46.

McNally, A.M., Moody, E.C., McNeill, K., 2005. Kinetics and mechanism of the sensitized photodegradation of lignin model compounds. Photochemical & Photobiological Sciences 4, 268-274.

Miles, C.J., Brezonik, P.L., 1981. Oxygen consumption in humic-colored waters by a photochemical ferrous-ferric catalytic cycle. Environmental Science and Technology 15, 1089-1095.

Miller, A.-F., Padmakumar, K., Sorkin, D.L., Karapetian, A., Vance, C.K., 2003. Proton-coupled electron transfer in Fe-superoxide dismutase and Mn-superoxide dismutase. Journal of Inorganic Biochemistry 93, 71-83.

Miller, J.S., 2005. Rose bengal-sensitized photooxidation of 2-chlorophenol in water using solar simulated light. Water Research 39, 412-422.

Miller, W.L., Zepp, R.G., 1995. Photochemical production of dissolved inorganic carbon from terrestrial organic matter: Significance to the oceanic organic carbon cycle. Geophysical Research Letters 22, 417-420.

Mopper, K., Kieber, D.J., 2000. Marine photochemistry and its impact on carbon cycling, in: Mora, S.D., Demers, S., Vernet, M. (Eds.), The effects of UV radiation in the marine environment. Cambridge University Press, pp. 101-129.

Mopper, K., Kieber, D.J., 2002. Photochemistry and the Cycling of Carbon, Sulfur, Nitrogen and Phosphorus, in: Carlson, D.A.H.A. (Ed.), Biogeochemistry of Marine Dissolved Organic Matter. Academic Press, San Diego, pp. 455-507.

Opsahl, S., Benner, R., 1997. Distribution and cycling of terrigenous dissolved organic matter in the ocean. Nature 386, 480-482.

Opsahl, S., Benner, R., 1998. Photochemical reactivity of dissolved lignin in river and ocean waters. Limnology and Oceanography 43, 1297-1304.

Page, S.E., Kling, G.W., Sander, M., Harrold, K.H., Logan, J.R., McNeill, K., Cory, R.M., 2013. Dark formation of hydroxyl radical in arctic soil and surface waters. Environmental Science and Technology 47, 12860-12867.

Page, S.E., Logan, J.R., Cory, R.M., McNeill, K., 2014. Evidence for dissolved organic matter as the primary source and sink of photochemically produced hydroxyl radical in arctic surface waters. Environmental Science: Processes & Impacts 16, 807-822.

Page, S.E., Sander, M., Arnold, W.A., McNeill, K., 2011. Hydroxyl radical formation upon oxidation of reduced humic acids by oxygen in the dark. Environmental Science and Technology 46, 1590-1597.

Pagliaro, M., Ciriminna, R., Kimura, H., Rossi, M., Della Pina, C., 2007. From Glycerol to Value-Added Products. Angewandte Chemie International Edition 46, 4434-4440.

Pariente, S., Tanchoux, N., Fajula, F., 2009. Etherification of glycerol with ethanol over solid acid catalysts. Green Chemistry 11, 1256-1261.

Peterson, B.M., McNally, A.M., Cory, R.M., Thoemke, J.D., Cotner, J.B., McNeill, K., 2012. Spatial and temporal distribution of singlet oxygen in Lake Superior. Environmental Science and Technology 46, 7222-7229.

Porcal, P., Dillon, P.J., Molot, L.A., 2013. Photochemical production and decomposition of particulate organic carbon in a freshwater stream. Aquatic sciences 75, 469-482.

Powers, L.C., Miller, W.L., 2014. Blending remote sensing data products to estimate photochemical production of hydrogen peroxide and superoxide in the surface ocean. Environmental Science: Processes & Impacts 16, 792-806.

Pullin, M.J., Bertilsson, S., Goldstone, J.V., Voelker, B.M., 2004. Effects of sunlight and hydroxyl radical on dissolved organic matter: Bacterial growth efficiency and production of carboxylic acids and other substrates. Limnology and Oceanography 49, 2011-2022.

Ralph, J., Marita, J.M., Ralph, S.A., Hatfield, R.D., Lu, F., Ede, R.M., Peng, J., Quideau, S., Helm, R.F., Grabber, J.H., Kim, H., Jimenez-Monteon, G., Zhang, Y., Jung, H.-J.G., Landucci, L.L., MacKay, J.J., Sederoff, R.R., Chapple, C., Boudet, A.M., 1999. Solution-state NMR of lignins, in: Argyropoulos, D.S. (Ed.), Advances in Lignocellulosic Characterization. Tappi Press, Atlanta, pp. 55-108.

Rose, A.L., Godrant, A., Furnas, M., Waite, T.D., 2010. Dynamics of nonphotochemical superoxide production in the Great Barrier Reef lagoon. Limnology and Oceanography 55, 1521-1536.

Sawyer, D.T., Valentine, J.S., 1981. How super is superoxide? Accounts of Chemical Research 14, 393-400.

Schlesinger, W.H., Melack, J.M., 1981. Transport of organic carbon in the world's rivers. Tellus 33, 172-187.

Scully, N.M., Cooper, W.J., Tranvik, L.J., 2003. Photochemical effects on microbial activity in natural waters: the interaction of reactive oxygen species and dissolved organic matter. FEMS Microbiology Ecology 46, 353-357.

Shadkami, F., Helleur, R., 2010. Recent applications in analytical thermochemolysis. Journal of Analytical and Applied Pyrolysis 89, 2-16.

Sholkovitz, E., 1976. Flocculation of dissolved organic and inorganic matter during the mixing of river water and seawater. Geochimica et Cosmochimica Acta 40, 831-845.

Sleighter, R.L., Chen, H., Wozniak, A.S., Willoughby, A.S., Caricasole, P., Hatcher, P.G., 2012. Establishing a Measure of Reproducibility of Ultrahigh-Resolution Mass Spectra for Complex Mixtures of Natural Organic Matter. Analytical Chemistry 84, 9184-9191.

Sleighter, R.L., Hatcher, P.G., 2007. The application of electrospray ionization coupled to ultrahigh resolution mass spectrometry for the molecular characterization of natural organic matter. Journal of Mass Spectrometry 42, 559-574.

Sleighter, R.L., Hatcher, P.G., 2008. Molecular characterization of dissolved organic matter (DOM) along a river to ocean transect of the lower Chesapeake Bay by ultrahigh resolution electrospray ionization Fourier transform ion cyclotron resonance mass spectrometry. Marine Chemistry 110, 140-152.

Sleighter, R.L., Hatcher, P.G., 2011. Fourier transform mass spectrometry for the molecular level characterization of natural organic matter: Instrument capabilities, applications, and limitations, in: Nikolic, G. (Ed.), Fourier Transforms –Approach to Scientific Principles. InTech, Rijeka, Croatia, pp. 295–320.

Sleighter, R.L., Liu, Z., Xue, J., Hatcher, P.G., 2010. Multivariate Statistical Approaches for the Characterization of Dissolved Organic Matter Analyzed by Ultrahigh Resolution Mass Spectrometry. Environmental Science and Technology 44, 7576-7582.

Søndergaard, M., Stedmon, C.A., Borch, N.H., 2003. Fate of terrigenous dissolved organic matter (DOM) in estuaries: Aggregation and bioavailability. Ophelia 57, 161-176.

Southworth, B.A., Voelker, B.M., 2003. Hydroxyl Radical Production via the Photo-Fenton Reaction in the Presence of Fulvic Acid. Environmental Science and Technology 37, 1130-1136.

Spencer, R.G.M., Stubbins, A., Hernes, P.J., Baker, A., Mopper, K., Aufdenkampe, A.K., Dyda, R.Y., Mwamba, V.L., Mangangu, A.M., Wabakanghanzi, J.N., Six, J., 2009. Photochemical degradation of dissolved organic matter and dissolved lignin phenols from the Congo River. Journal of Geophysical Research 114.

Stenson, A.C., Marshall, A.G., Cooper, W.T., 2003. Exact masses and chemical formulas of individual suwannee river fulvic acids from ultrahigh resolution electrospray ionization Fourier transform ion cyclotron resonance mass spectra. Analytical Chemistry 75, 1275-1284.

Stevenson, F.J., 1994. Humus Chemistry: Genesis, Composition, Reactions. Wiley, New York.

Stubbins, A., Spencer, R.G.M., Chen, H., Hatcher, P.G., Mopper, K., Hernes, P.J., Mwamba, V.L., Mangangu, A.M., Wabakanghanzi, J.N., Six, J., 2010. Illuminated darkness: molecular signatures of Congo River dissolved organic matter and its photochemical alteration as revealed by ultrahigh precision mass spectrometry. Limnology and Oceanography 55, 1467-1477.

Sutter, M., Pehlivan, L., Lafon, R., Dayoub, W., Raoul, Y., Métay, E., Lemaire, M., 2013. 1,2,3-Trimethoxypropane, a glycerol-based solvent with low toxicity: new utilization for the reduction of nitrile, nitro, ester, and acid functional groups with TMDS and a metal catalyst. Green Chemistry 15, 3020.

Thevenot, M., Dignac, M.-F., Rumpel, C., 2010. Fate of lignins in soils: A review. Soil Biology and Biochemistry 42, 1200-1211.

Tremblay, L.B., Dittmar, T., Marshall, A.G., Cooper, W.J., Cooper, W.T., 2007. Molecular characterization of dissolved organic matter in a North Brazilian mangrove porewater and mangrove-fringed estuaries by ultrahigh resolution Fourier Transform-Ion Cyclotron Resonance mass spectrometry and excitation/emission spectroscopy. Marine Chemistry 105, 15-29.

Umezawa, T., Higuchi, T., 1987. Formation of a muconate in aromatic ring cleavage of a β-O-4 lignin substructure model by lignin peroxidase. Agricultural and Biological Chemistry 51, 2281-2284.

Umezawa, T., Nakatsubo, F., Higuchi, T., 1983. Degradation pathway of arylglycerol-beta-aryl ethers by phanerochaete chrysosporium. Agricultural and Biological Chemistry 47, 2677-2681.

Valentine, J.S., Curtis, A.B., 1975. Convenient preparation of solutions of superoxide anion and the reaction of superoxide anion with a copper(II) complex. Journal of the American Chemical Society 97, 224-226.

Vaughan, P.P., Blough, N.V., 1998. Photochemical Formation of Hydroxyl Radical by Constituents of Natural Waters. Environmental Science and Technology 32, 2947-2953.

Vermilyea, A.W., Voelker, B.M., 2009. Photo-Fenton reaction at near neutral pH. Environmental Science and Technology 43, 6927-6933.

von Wachenfeldt, E., Sobek, S., Bastviken, D., Tranvik, L.J., 2008. Linking allochthonous dissolved organic matter and boreal lake sediment carbon sequestration: The role of light-mediated flocculation. Limnology and Oceanography 53, 2416.

Waggoner, D.C., Chen, H., Willoughby, A.S., Hatcher, P.G., 2015. Formation of black carbon-like and alicyclic aliphatic compounds by hydroxyl radical initiated degradation of lignin. Organic Geochemistry 82, 69-76.

Waggoner, D.C., Wozniak, A.S., Cory, R.M., Hatcher, P.G., 2017. The role of reactive oxygen species in the degradation of lignin derived dissolved organic matter. Geochimica et Cosmochimica Acta 208, 171-184.

Walling, C., 1975. Fenton's reagent revisited. Accounts of Chemical Research 8, 125-131.

Wang, H., Cao, G., Prior, R.L., 1997. Oxygen Radical Absorbing Capacity of Anthocyanins. Journal of Agricultural and Food Chemistry 45, 304-309.

Ward, C.P., Cory, R.M., 2016. Complete and Partial Photo-oxidation of Dissolved Organic Matter Draining Permafrost Soils. Environmental Science and Technology 50, 3545-3553.

Ward, C.P., Sleighter, R.L., Hatcher, P.G., Cory, R.M., 2014. Insights into the complete and partial photooxidation of black carbon in surface waters. Environmental Science Processes & impacts 16, 721-731.

Wenk, J., von Gunten, U., Canonica, S., 2011. Effect of Dissolved Organic Matter on the Transformation of Contaminants Induced by Excited Triplet States and the Hydroxyl Radical. Environmental Science and Technology 45, 1334-1340.

Williams, P.M., Druffel, E.R.M., 1987. Radiocarbon in dissolved organic matter in the central North Pacific Ocean. Nature 330, 246-248.

Wolfson, A., Dlugy, C., Shotland, Y., 2007. Glycerol as a green solvent for high product yields and selectivities. Environmental Chemistry Letters 5, 67-71.

Wolfson, A., Dlugy, C., Tavor, D., 2011. Glycerol-based solvents in organic synthesis. Trends in Organic Chemistry 15, 41-49.

APPENDIX A

COPYRIGHT PERMISSIONS

Permission for Chapter II, which contains the Org. Geochem. article, published by Elsevier. Permission was obtained from Rightslink

This Agreement between Derek C Waggoner ("You") and Elsevier ("Elsevier") consists of your license details and the terms and conditions provided by Elsevier and Copyright Clearance Center.

License Number	4073150375848
License date	
Licensed Content Publisher	Elsevier
Licensed Content Publication	Organic Geochemistry
Licensed Content Title	Formation of black carbon-like and alicyclic aliphatic Compounds by hydroxyl radical initiated degradation of lignin
Licensed Content Author	Derek C. Waggoner,Hongmei Chen,Amanda S. Willoughby, Patrick G. Hatcher
Licensed Content Date	May 2015
Licensed Content Volume	82
Licensed Content Issue	n/a
Licensed Content Pages	8
Start Page	69
End Page	76
Type of Use	reuse in a thesis/dissertation
Portion	full article
Format	both print and electronic
Are you the author of this Elsevier article?	Yes
Will you be translating?	No
Title of your thesis/dissertation	LIGNIN CONTRIBUTION TO THE GLOBAL CARBON POOL:INVESTIGATING THE ABIOTIC MODIFICATION OF LIGNIN BY REACTIVE OXYGEN SPECIES
Expected completion date	Aug 2017
Estimated size (number of pages)	150
Elsevier VAT number	GB 494 6272 12
Requestor Location	Derek C Waggoner 4402 Elkhorn Ave Norfolk, VA 23529

Permission for Chapter III, which contains the GCA article, published by Elsevier. Permission was obtained from Rightslink.

This Agreement between Derek C Waggoner ("You") and Elsevier ("Elsevier") consists of your license details and the terms and conditions provided by Elsevier and Copyright Clearance Center.

License Number	4091981173829
License date	
Licensed Content Publisher	Elsevier
Licensed Content Publication	Geochimica et Cosmochimica Acta
Licensed Content Title	The role of reactive oxygen species in the degradation of lignin derived dissolved organic matter
Licensed Content Author	Derek C. Waggoner,Andrew S. Wozniak,Rose M. Cory, Patrick G. Hatcher
Licensed Content Date	1 July 2017
Licensed Content Volume	208
Licensed Content Issue	n/a
Licensed Content Pages	14
Start Page	171
End Page	184
Type of Use	reuse in a thesis/dissertation
Portion	full article
Format	both print and electronic
Are you the author of this Elsevier article?	Yes
Will you be translating?	No
Title of your thesis/dissertation	LIGNIN CONTRIBUTION TO THE GLOBAL CARBON POOL: INVESTIGATING THE ABIOTIC MODIFICATION OF LIGNIN BY REACTIVE OXYGEN SPECIES
Expected completion date	Aug 2017
Estimated size (number of pages)	150
Elsevier VAT number	GB 494 6272 12
Requestor Location	Derek C Waggoner 4402 Elkhorn Ave Norfolk, VA 23529

Permission for Apendix B, which contains the JAAP article, published by Elsevier. Permission was obtained from Rightslink.

This Agreement between Derek C Waggoner ("You") and Elsevier ("Elsevier") consists of your license details and the terms and conditions provided by Elsevier and Copyright Clearance Center.

License Number	4073150469737
License date	
Licensed Content Publisher	Elsevier
Licensed Content Publication	Journal of Analytical and Applied Pyrolysis
Licensed Content Title	Thermally assisted methylation of glycerol by tetramethylammonium hydroxide thermochemolysis
Licensed Content Author	Derek C. Waggoner,Patrick G. Hatcher
Licensed Content Date	November 2016
Licensed Content Volume	122
Licensed Content Issue	n/a
Licensed Content Pages	5
Start Page	289
End Page	293
Type of Use	reuse in a thesis/dissertation
Intended publisher of new work	other
Portion	full article
Format	both print and electronic
Are you the author of this Elsevier article?	Yes
Will you be translating?	No
Order reference number	
Title of your thesis/dissertation	LIGNIN CONTRIBUTION TO THE GLOBAL CARBON POOL: INVESTIGATING THE ABIOTIC MODIFICATION OF LIGNIN BY REACTIVE OXYGEN SPECIES
Expected completion date	Aug 2017
Estimated size (number of pages)	150
Elsevier VAT number	GB 494 6272 12
Requestor Location	Derek C Waggoner 4402 Elkhorn Ave Physical Sciences building rm 3100 Norfolk, VA 23529

APPENDIX B

THERMALLY ASSISTED METHYLATION OF GLYCEROL BY TETRAMETHYLAMMOIUM HYDROXIDE THERMOCHEMOLYSIS

PREFACE

The contents of this Chapter was published in 2016 in Analytical and Applied Pyrolysis as part of a previous research project, and below is the full citation. See Appendix A for copyright permission.

Waggoner, D.C. and Hatcher, P.G. (2016). Thermally assisted methylation of glycerol by tetramethylammonium hydroxide thermochemolysis. *Journal of Analytical and Applied. Pyrolysis* 122, 289-293.

1. INTRODUCTION

Glycerol, or 1,2,3-propanetriol, is a chemical used in a wide variety of fields including the pharmaceutical, food, and cosmetics industries (Johnson and Taconi, 2007). Until recently the demand for glycerol was largely satisfied using glycerol generated from propene and other non-renewable petrochemical starting materials (García et al., 2014). The sources and availability of glycerol have since changed due to the growth of the biodiesel industry. With the dramatic increase in the price of petroleum on world markets, biodiesel production has experienced a steady increase worldwide (EPA, 2015). Conventional commercial biodiesel production mainly employs a transesterification process to convert a triacylglyceride (TAG) source, often vegetable oil, into

fatty acid methyl esters or FAME's, which can be used as diesel fuel (Gerpen, 2005). The major by-product of the commercial biodiesel production process is glycerol, obtained in roughly 10% wt yields from the TAG source (Dasari et al., 2005). As biodiesel production soars into the billions of gallons annually, a large supply of glycerol has been generated and is due to increase significantly (Johnson and Taconi, 2007). A fast approaching problem will be finding a use for the ever-growing production of glycerol generated from the biodiesel industry.

Because of the large volume of available glycerol, one growing area of interest is investigating the viability of glycerol and related derivatives for use as possible renewable sourced solvents. Glycerol itself as a solvent has been previously studied and found to be useful in a number of applications, however, the low solubility of hydrophobic compounds in glycerol limits its widespread use (Wolfson et al., 2007; Wolfson et al., 2011). To address the issue of solubility, many groups have derivatized glycerol to generate products with physical and chemical properties that make them more favorable as solvents. There currently exist a number of glycerol-based chemical processes that convert glycerol into higher value derivatives (Behr et al., 2008; Chang et al., 2012; Dasari et al., 2005; Di Serio et al., 2010; Díaz-Álvarez et al., 2011; García et al., 2010; Johnson and Taconi, 2007; Klepáčová et al., 2007; Pagliaro et al., 2007; Pariente et al., 2009) that could generate a higher commercial value. An approach used by several groups for the generation of useful solvents is alkylation to glycerol ethers, which have been shown to be useful in a number of oxidation and reduction reactions, as well as in biphasic catalytic systems (García-Marín et al., 2009; García et al., 2010; García et al., 2014; Sutter et al., 2013). One method described by García et al. (2010) alkylates glycerol using methanol to produce a series of mono, di, and trimethoxy ethers of glycerol to test their use as green solvent alternatives. The alkylation described by Garcia utilizes an autoclave at autogenic pressure to carry out the reaction between glycerol and a variety

of alcohols. The alcohol used determines the alkyl chain length added to the glycerol backbone in the formation of the ether. An alternative method by Chang et al. (2012) recently described the methylation of glycerol using dimethyl sulfate to produce mono, di, and trimethoxy ethers for use as possible new fuel oxygenates. The method used by Chang et al. (2012) is a stirred tank reaction where dimethyl sulfate and sodium hydroxide are added to glycerol to produce methoxylated glycerols. While the stirred tank method lends itself well to large-scale use, the reactants are added over the course of several (5) hours followed by a lengthy workup to separate the desired methoxylated glycerols.

In the current paper, a new approach is described, shown below in Scheme 1, for the thermally assisted methylation of glycerol using tetramethylammonium hydroxide (TMAH). TMAH is the most commonly used thermochemolysis reagent, accounting for roughly 90% of thermochemolysis publications (Shadkami and Helleur, 2010). Thermally assisted methylation, sometimes referred to as thermochemolysis, has previously been used to examine polymers (Challinor, 1989, 1993), lignin (Hatcher and Clifford, 1994; McKinney et al., 1995), soil organic matter (Chefetz et al., 2000; Chefetz et al., 2002; Grasset et al., 2009), cuticular material (del Río and Hatcher, 1998; del Rio et al., 1998), and other forms of macromolecular natural organic matter (Challinor, 2001; Shadkami and Helleur, 2010). In these previous studies, the TMAH served to methylate polar pyrolysis products or to assist with the chemical degradation of natural and synthetic polymers to produce suites of methylated compounds amenable to gas chromatographic analysis. In the current study, we show that it can effectively methylate polar residues generated from transesterification processes used in the biofuel industry to render them volatile enough for the gas chromatography. Unlike other processes currently used to alkylate glycerol, methylation using TMAH can be accomplished rapidly and on a large scale using continuous flow reactors,

making it ideally suited to generating large quantities of products for use as solvents (Hatcher and Liu, 2009).

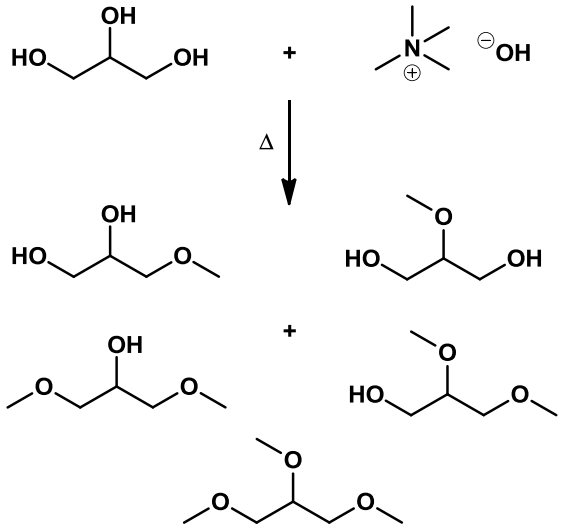

Scheme A1. Production of mono, di, and trimethoxy glycerol ether products from glycerol.

2. MATERIALS AND METHODS

2.1. Pilot Scale reactors and operating procedures

Two continuous flow reactors were employed to evaluate the action of TMAH with glycerol. One was a fluidized bed reactor operated in the laboratory and the other was a horizontal wiped film reactor operated at a facility known as the ODU algal farm. The fluidized bed reactor, a home-built device, provided much of the quantitative recovery information for this report while the pilot-scale thin film reactor provided the proof of concept for scaling up of the process.

A schematic diagram for the fluidized bed reactor is shown in Figure A1. The major component of the reactor is a Barnstead Thermolyne tube furnace model 21100. The reactor tube and connections were homemade and attached to a cold trap condenser from ACE glass incorporated. The reactor is prepared by adding ~ 30 grams of clean sand (US Silica) to the reaction tube and assembling the reactor. The temperature of the tube furnace is set and is held constant at 330°C throughout each run. Nitrogen gas is passed through the reaction tube (approximately 60mL/min) to fluidize the sand before injecting the sample. The sample is prepared by mixing TMAH (25% in methanol) with glycerol in various molar ratios with a slight excess of TMAH. Once mixed, sample can be injected in a continuous feed mode using a peristaltic pump (Fischer Scientific variable flow mini pump model 3389). Products are volatilized and carried through the reactor before being collected in the cold trap condenser.

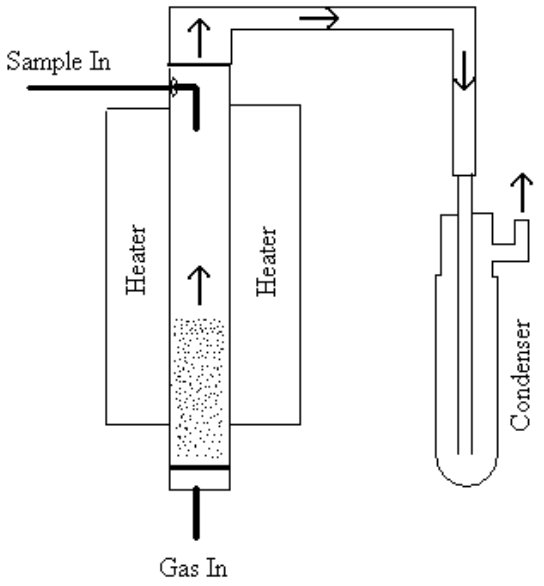

Fig. A1. Schematic diagram of fluidized bed reactor displaying configuration and collection point.

A horizontal thin film reactor, Rototherm© model E, purchased from Artisan Industries, Inc. was used for pilot-scale testing. The reactor consists of a hot oil jacketed 1 ft^2 contact area reaction chamber with rotating blades, refrigerated condenser, and liquid nitrogen cold trap all connected serially to vacuum pumps as shown in Figure A2. The trial reactions are prepared by mixing glycerol with TMAH (25% in methanol) in various molar ratios with a slight excess of TMAH. This mixture is injected in a continuous feed mode using a peristaltic pump at a rate of 3.8 gallons/hr at 200 torr and a hot oil temperature of 330°C that provides the required heat for the reaction zone. The mono, di, and trimethoxy glycerols are collected at the condenser trap along with the majority of methanol. Following thermochemolysis, the TMAH consumed in the reaction forms trimethyl amine (TMA), which is highly volatile and is collected mainly in the cold trap along with excess methanol. The resulting product mixture is then purified to individual compounds using distillation.

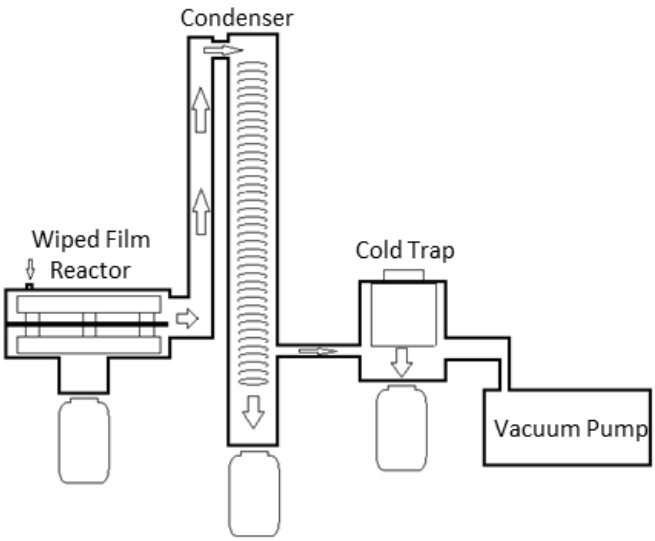

Fig. A2. Schematic diagram of Rototherm model E reactor displaying configuration and sample collection points.

2.1.1 Reagent ratio impact on continuous flow reactors

Several tests were conducted to evaluate the influence of reagent ratios on product distributions. Two approaches were employed, one involving variations in the molar ratio of TMAH to glycerol by adjustment to the amounts of TMAH, and the other involving a multi-step serial addition of TMAH to glycerol. Our objective was to determine conditions that might be employed to select higher proportions of one methoxylated glycerol over the others in the process. In the case of the serial addition strategy, feedstocks were prepared by mixing TMAH with glycerol in a 1:1 molar ratio and injected into the reactors using the same conditions as described above. Products trapped in the condensers of both the fluidized bed reactor and thin film reactor were then mixed with another molar equivalent of TMAH in methanol based on the original feed amount of glycerol and reprocessed through the reactors . This strategy was repeated for a third time only on

the fluidized bed reactor to effectively represent the equivalent of adding a 3:1 molar ratio of TMAH to glycerol. Single pass experiments for 1:1, 2:1 and 3:1 molar ratios of TMAH to glycerol were also prepared and processed through the reactors. The products trapped in the condenser from each trial are analyzed via GC x GC-MS as described below.

2.1.2 Performance of the reaction with crude glycerol

Crude glycerol obtained directly from an operating biodiesel facility contains variable amounts of free fatty acids, TAGs and fatty acid methyl esters because the refinery operators utilize the crude glycerol as a scrubber to remove free fatty acids from the vegetable oil feedstock prior to transesterification. This crude glycerol also contains fatty acid methyl esters due to the incomplete phase separation of glycerol from biodiesel following transesterification in the refinery. Experiments were performed to determine the applicability of the methylation reaction for treating crude glycerol. TMAH was mixed with unrefined crude glycerol in a 3:1 molar ratio and injected into the horizontal thin film reactor under identical conditions as for pure glycerol. Samples were analyzed using GC x GC-MS as described below. It is important to mention that without prior knowledge of the amounts of glycerol in the crude glycerol we cannot fully evaluate the efficiency for methylation. Our purpose was mainly to determine if crude glycerol could be processed without problems.

2.2 Laboratory-scale sealed tube reactions.

Additional thermochemolysis reactions were performed on a small scale in custom made glass tubes to qualitatively establish the validity of our hypothesis that glycerol can be methylated using TMAH. TMAH was mixed with Glycerol in a 3:1 molar ratio. Using a micropipette, 100μL of the glycerol-TMAH solution was added to glass reaction tubes, which were then connected to

a vacuum line where any excess vapor was removed. Under vacuum the tubes were then flame sealed using a propane-oxygen torch before being placed in an oven at temperature to induce reaction, which was complete within 2 minutes. The tubes were removed from the oven and allowed to cool before being opened using a glass file. The sample was then taken up using methanol for analysis on GC x GC-MS. Temperatures at 50ºC increments ranging from 300-500°C were tested to find the optimal conditions for the reaction in sealed tubes. All tubes were prepared using the same mixture of TMAH-glycerol in a 3:1 molar ratio.

To test the need for methanol in the reaction, sealed tube experiments were also conducted using glycerol and solid TMAH pentahydrate (Acros). Solid TMAH pentahydrate was added to glycerol in a 3:1 molar ratio and warmed to dissolve. The mixture was vortexed to homogenize before pipetting into glass tubes. The tubes were sealed and let stand at 350°C for 2 minutes prior to analysis described below.

2.3 Product Analysis

The products collected from the fluidized bed reactor, horizontal thin film reactor, and sealed tube experiments were injected, using the split mode, into a GC x GC coupled to a time of flight mass spectrometer (LECO Pegasus 4D). The analyses were carried out with an autosampler (CTC Analytics) integrated to the GC system (Agilent Technologies, 6890N) fitted with a thermal modulation assembly. The columns used were a 30m x 0.25 mm i.d. RTX-5 first dimension column, and 1m x 0.1 mm i.d. RXI-17 second dimension column. Helium was used as a carrier gas and adjusted for constant flow throughout the run. The temperature program used consisted of an initial temperature of 40°C ramping to 200°C at 10°C min^{-1} followed by a 30°C min^{-1}ramp to a final temperature of 280°C after a 1 µL sample injection. Peak areas were measured by the

Pegasus software and identification of the products was via mass spectral comparisons to NIST library spectra.

Fractional distillation was used to purify each of the methoxylated glycerols to generate internal mass spectral libraries in cases where the NIST library was ineffective. These authentic standards were confirmed by both ^{1}H and ^{13}C NMR using a 400 MHz NMR system located in the College of Sciences Major Instrumentation Cluster (COSMIC) at ODU.

3. RESULTS AND DISCUSSION

Thermochemolysis of glycerol with TMAH in 3:1 molar ratios using the pilot-plant thin film reactor, fluidized bed reactor, and the laboratory-scale sealed tube reactors, leads to the production of 4 ethers, as shown in Figure 3, including one mono-methylated glycerol, 3-methoxy-1,2-propanediol (3-MDP), two di-methylated glycerols, 1,3-dimethoxy-2-propanol (1,3-DMP) and 1,2-dimethoxy-3-propanol (1,2-DMP), and one tri-methylated ether, 1,2,3-trimethoxy propane (TMP). Other structural isomers are possible but not observed or recognized.

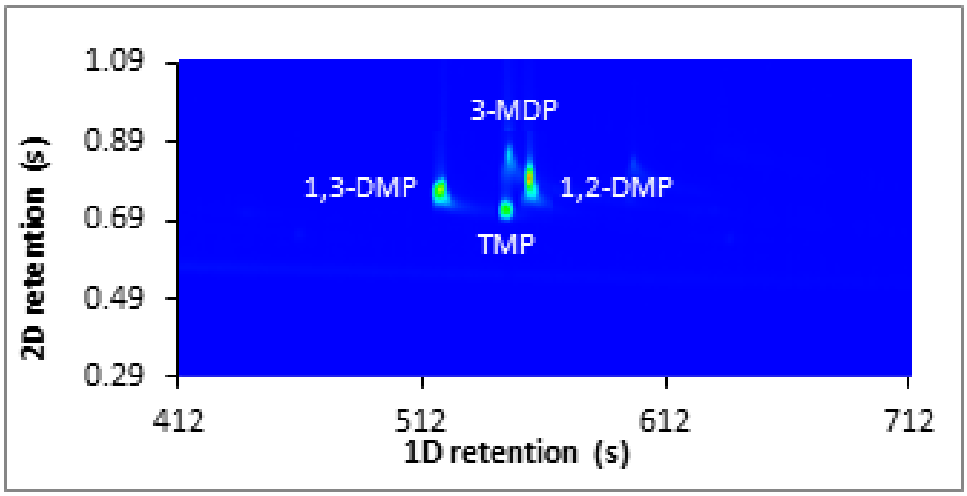

Fig. A3. GC x GC-MS total ion current plot of TMAH reacted with glycerol in 2:1 molar ratio showing presence of methoxylated glycerols. The abscissa scale is seconds of elution time on the primary column while the ordinate is elution time on the more polar column.

3.1 Effect of Temperature

As shown in Figure A4, the product distribution for the thermally assisted methylation of glycerol using TMAH is relatively constant over the temperature range tested. GC x GC-MS shows the percentage of reactant glycerol converted to glycerol ethers to be approximately 60% of the glycerol input for each temperature point, suggesting that temperature variation has a minimal influence on the reaction process. Temperatures below the set point of the GC injection port (280°C) are not included as additional reaction could potentially occur, thereby invalidating any data obtained. It is important to mention that the yields in sealed tubes are systematically lower than we observe in the pilot-scale reactor discussed below. We believe that this is attributable to a less efficient mass transfer in sealed tubes. The sealed tubes are none-the-less useful for rapid laboratory-scale testing of the reaction.

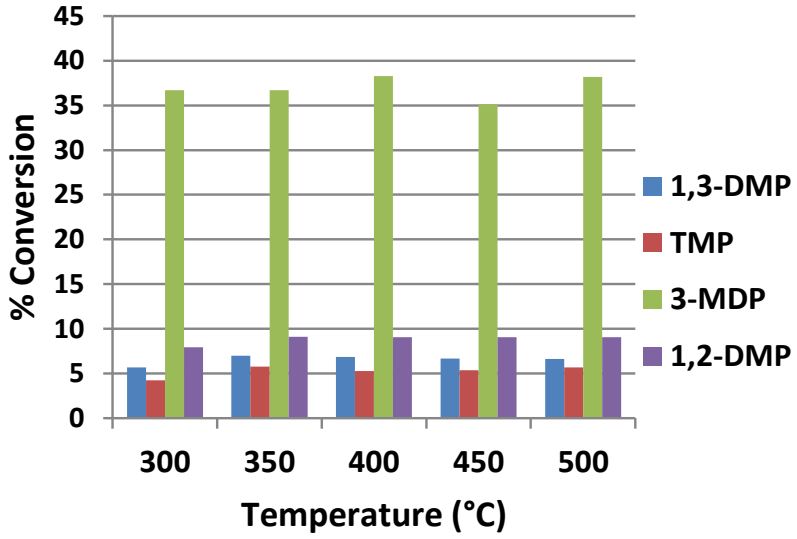

Fig. A4. Percent of glycerol converted to 1,3-dimethoxy-2-propanol (1,3-DMP), 1,2,3-trimethoxy propane (TMP), 1,2-dihydroxy-3-methoxy propane (3-MDP), and 1,2-dimethoxy-3-propanol (1,2-DMP) from sealed tube experiments over temperature range.

3.2 Need for Methanol

While the majority of methanol was removed via vaccuum line to conduct the sealed tube reactions, residual methanol was still present. To verify that methanol is not integral to the methylation of glycerol, sealed tube experiments using methanol free solid TMAH pentahydrate were performed to generate glycerol ethers. The resulting data (Figure A5) shows the production of 3-MDP, 1,2-DMP, 1,3-DMP, and TMP. The generation of glycerol ethers in a methanol free system supports the fact that TMAH is methylating glycerol directly, and that methanol is not required or directly involved in the methylation process.

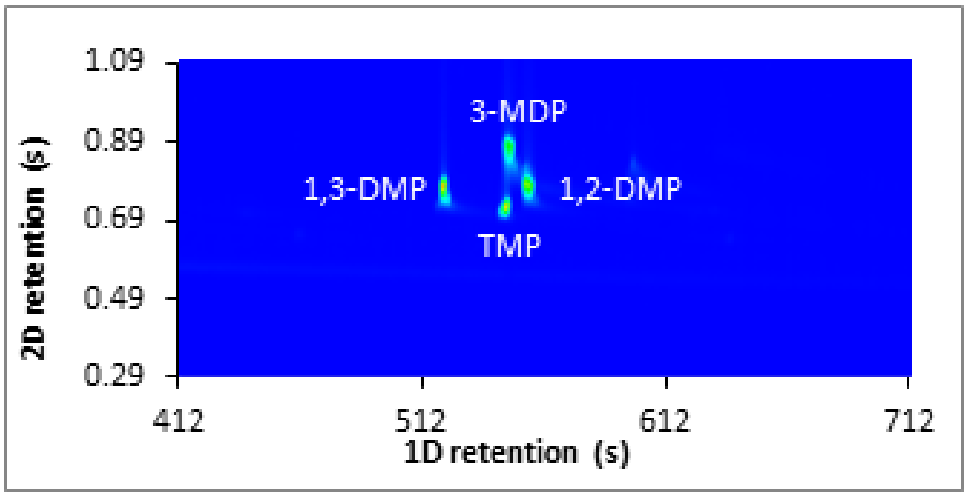

Fig. A5. GC x GC-MS total ion current plot of glycerol reacted with solid TMAH in 1:3 molar ratio showing presence of methoxylated glycerols. The abscissa scale is seconds of elution time on the primary column while the ordinate is elution time on the more polar column.

3.3 Effects of Varying Amounts of TMAH and Serial Addition.

In an effort to determine if the reaction could be tuned to favor one product, various molar ratios of reactants were tested in both the fluidized bed and thin film reactors. Due to the proximity of the fluidized bed reactor to the laboratory we found it more convenient to show quantitative results from this reactor system, even though the same type of testing was done on the thin film reactor at a larger scale. Reliable product yields could be better controlled with the fluidized bed reactor compared with the thin-film reactor where significant dead volumes limit the measurement accuracy for product recoveries on small-scale trials. Figure A6 shows the resulting product distribution when TMAH was reacted with glycerol in a 1:1, 2:1, and 3:1 molar ratio fashion in the fluidized bed reactor. As expected, the more highly substituted glycerol ethers are produced to a greater extent as the ratio of TMAH to glycerol increases. The product distribution however,

does not considerably favor one product over another for the molar ratios tested, but rather shows a mixture of the mono,di, and tri-substituted products. The lack of complete conversion to the fully substituted TMP product, even in the presence of a stochiometric excess of TMAH, suggested insufficient contact time between reagents during thermochemolysis.

To increase the contact time between reagents without significantly increasing the amount of TMAH used, serial addition experiments were conducted utilizing the same overal ratio of TMAH to glycerol as the single pass runs. Figure A6 shows the diffences in product distribution between serial and batch additon of TMAH under the same run condition. As anticipated, adding TMAH in a serial manner greatly influenced the distribution of products when compared to the same amount of TMAH for a single pass run. The result of adding a 2:1 molar ratio of TMAH in a serial fashion for example, generates products with a similar composition to that of the 3:1 batch addition while using one third less TMAH. The sucsessive 3:1 serial addition results in the desired production of predominately TMP with only small amounts of less substituted products. This data would suggest that if so desired, exclusively TMP could potentially be produced if TMAH were added in a serial fashion, without using large excesses of reagents.

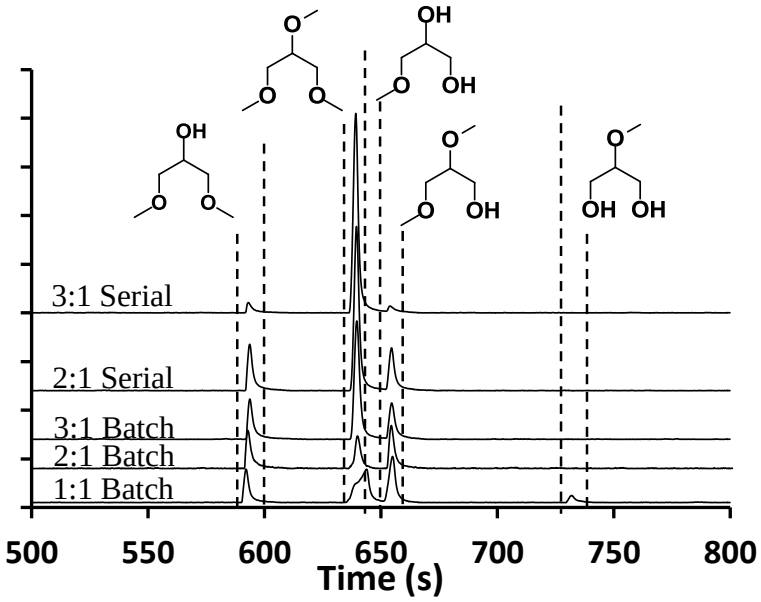

Fig. A6. GC-MS total ion current chromatograms depicting product distribution for various TMAH to glycerol ratios and feed methods. Products generated via serial addition of TMAH to glycerol are labeled as serial, while products from single pass runs are indicated as batch. The 1:1 batch and serial runs are represented by one chromatogram as the run conditions used for both are the same.

The specific product distribution for the run conditions depicted in Figure A6 can be seen in Table A1 below. While the overall conversion for the serial addition experiments appears to be low, it should be noted that after rinsing the reactor with methanol, an additional 29% of products were recovered. It is likely that similar results would be obtained after the first and second serial additions, however this was not performed, as the primary purpose of this experiment was to form the fully substituted TMP product. The overall yield for the 3:1 serial addition of TMAH to glycerol is therefore 82.5%, with TMP accounting for 75.7% of converted glycerol. The 2:1 and

3:1 batch addition experiments on the other hand produced 15% and 30% TMP respectively, confirming that serial addition does generate more TMP without using excess amounts of reagents.

Table A1. Percentage of glycerol input converted to each of the methoxylated glycerol products for the molar ratios and reagent addition methods tested using the fluidized bed reactor.

	% Conversion of Glycerol to Methoxylated Glycerol Products				
	1,3-DMP	TMP	1-MDP	1,2-DMP	Conversion (%)
1:1 Serial addition	3.63	1.36	25.32	5.64	35.94
2:1 Serial addition	4.70	31.73	0.00	6.87	43.30
3:1 Serial addition	2.16	49.36	0.00	2.26	53.78
Reactor rinse following 3:1	0.86	26.36	0.00	1.49	28.71
2:1 Batch addition	31.18	15.56	12.06	35.93	94.73
3:1 Batch addition	18.24	30.36	7.49	22.58	78.66

The overall conversion efficiency of the continuous feed reactors is also greater than that seen in the sealed tube experiments described earlier. While the sealed tube reactions resulted in glycerol conversion of approximately 60%, the continuous feed reactors have conversions of roughly 80-90%. The larger reagent volumes, presence of solvent, and the reactor design in the larger reactor experiments are credited with the significant increase in the conversion process.

3.4 Crude Glycerol Reaction

Unrefined glycerol was tested to determine if the presence of impurities from a biodiesel product stream would influence the ability of TMAH to generate methoxylated glycerols. As

illustrated in Figure A7, TMAH effectively converts crude glycerol into methoxylated glycerol ethers. The additional peaks present are those of FAME's remaining in the glycerol after preliminary separation during the biodiesel production process. Comparing these results to those of pure glycerol under the same reaction conditions, it is noteworthy that the product distribution of methoxylated glycerols is found to be very similar using crude glycerol; indicating impurities (free fatty acids, TAGs, and any other possible impurities) have little to no effect on the reaction.

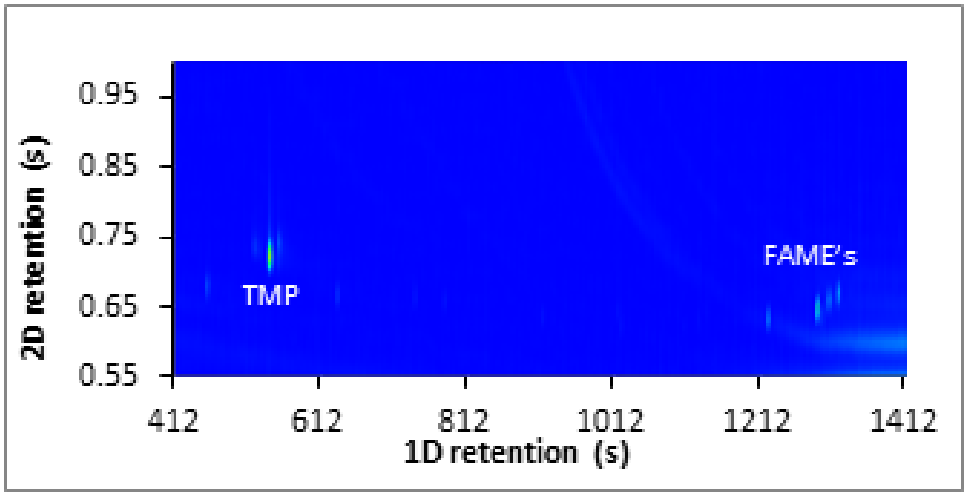

Fig. A7. GC x GC-MS total ion current plot of crude glycerol reacted with TMAH in a 1:3 molar ratio showing the presence of methoxylated glycerol ethers as well as fatty acid methyl esters.

4. CONCLUSIONS

While analytical pyrolysis is most frequently used for the structural characterization of hard to analyze compounds, here TMAH thermochemolysis has been demonstrated to be capable of rapidly methylating glycerol to produce a mixture of mono, di, and tri-methoxylated products that can be used as potential renewable solvents. The methoxylated glycerols obtained in this reaction have previously been demonstrated to be useful in a variety of applications and are therefore considered to be of greater value than glycerol. The efficient conversion (80-90%) of glycerol to higher value products in a continuous flow thermochemolysis process was readily achieved at temperatures greater than 250ºC and a 3:1 molar ratio of TMAH to glycerol. It has also been demonstrated that the distribution of methoxylated products can be roughly controlled through alteration of reagent ratios and introduction methods. While other methods exist to produce methoxylated glycerol ethers, the continuous flow process described here is ideally suited for the commercial scale production of solvents needed to meet current demand.

VITA

Derek Charles Waggoner
Dwagg002@odu.edu

Department of Chemistry and Biochemistry
Old Dominion University

Education

August 2017 ..... Ph.D. Chemistry, Old Dominion University
Norfolk, VA

May 2009 ..... B.S. Biochemistry, Old Dominion University
Norfolk, VA

Selected Publication

Waggoner, Derek C.; Chen, Hongmei; Hatcher, Patrick G. Formation of black carbon like compounds by hydroxyl radical initiated degradation of lignin. Organic Geochemistry, 2015, 82, (0), 69-76.

Waggoner, Derek C.; Hatcher, Patrick G. Thermally assisted methylation of glycerol by tetramethylammonium hydroxide thermochemolysis. Journal of Analytical and Applied Pyrolysis, 2016, 122, 289-293.

Waggoner, Derek C.; Wozniak, Andrew s.; Cory, Rose M.; Hatcher, Patrick G. The role of reactive oxygen species in the degradation of lignin derived dissolved organic matter. Geochimica et Cosmochimica Acta, 2017, 208, 171-184.

DiDonato, Nicole; Chen, Hongmei; Waggoner, Derek; Hatcher, Patrick G. Potential origin and formation for molecular components of humic acids in soils. Geochimica et Cosmochimica Acta 2016, 178, 210-222.

Jiménez-Morillo, Nicasio T.; de la Rosa, José M.; Waggoner, Derek C.; Almendros, Gonzalo; González-Vila, Francisco J.; González-Pérez, José A. Fire effects in the molecular structure of soil organic matter fractions under Quercus suber cover. Catena, 2016, 145, 266-273.

Awards

Summer 2014 ..... *CIBA Fellowship* Department of Chemistry and Biochemistry

Spring 2013 ..... Outstanding Chemistry prep Teaching Assistant